

Universidade de São Paulo

Instituto de Física

# Termodinâmica e eficiência de sistemas coletivos

Felipe Hawthorne Gomes da Costa

Orientador: Prof. Dr. Carlos Eduardo Fiore dos Santos

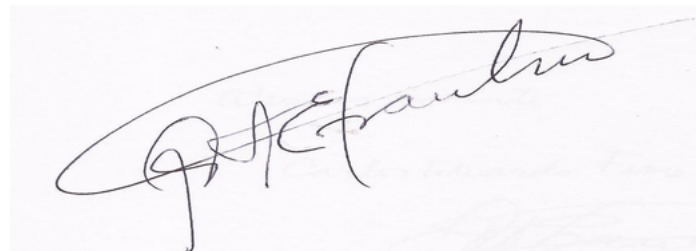
Dissertação de mestrado apresentada ao Instituto de Física da Universidade de São Paulo, como requisito parcial para a obtenção do título de Mestre em Ciências.

Banca avaliadora:

Prof. Dr. Carlos Eduardo Fiore dos Santos

Prof. Dr. Jeferson Jacob Arenzon

Profa. Dra. Lucimara Stolz Roman

A handwritten signature in black ink, appearing to read 'C. E. Fiore dos Santos', written over a light blue horizontal line.

São Paulo

2024

**FICHA CATALOGRÁFICA**  
**Preparada pelo Serviço de Biblioteca e Informação**  
**do Instituto de Física da Universidade de São Paulo**

Costa, Felipe Hawthorne Gomes da

Termodinâmica e eficiência de sistemas coletivos /  
.Thermodynamics and efficiency of collective systems São Paulo, 2024.

Dissertação (Mestrado) – Universidade de São Paulo. Instituto de  
Física. Departamento de Física Geral.

Orientador(a): Prof<sup>o</sup> Dr<sup>o</sup> Carlos Eduardo Fiore dos Santos

Área de Concentração: Mecânica Estatística

Unitermos: 1. Entropia; 2. Mudança de fase; 3. Teorias da  
termodinâmica; 4. Física computacional.

USP/IF/SBI-003/2024

University of São Paulo

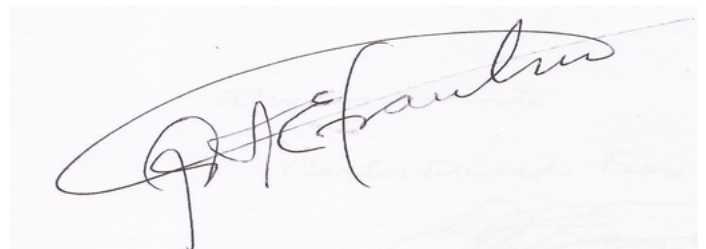
Physics Institute

# Thermodynamics and efficiency of collective systems

Felipe Hawthorne Gomes da Costa

Supervisor: Prof. Dr. Carlos Eduardo Fiore dos Santos

Dissertation submitted to the Physics Institute of the University of São Paulo in partial fulfillment of the requirements for the degree of Master of Science

A handwritten signature in black ink, appearing to read 'C. E. Fiore dos Santos', is written over a light blue horizontal line on a white background.

Examining Committee:

Prof. Dr. Carlos Eduardo Fiore dos Santos

Prof. Dr. Jeferson Jacob Arenzon

Profa. Dra. Lucimara Stolz Roman

São Paulo

2024

*A minha família, pela fé e apoio incondicionais.*

# Acknowledgements

The two years of work that went into this dissertation would not have been possible without the support and patience of the many people who entered this journey with me, or whom I've met throughout it. First, and foremost, I would like to thank my wife, **Ideusuita Krishna**, for the constant showing of love and support throughout the last two years. While in the subject of family, the proper thanks need to be given to my mother, **Eliana Hawthorne**, father, **Ademir Costa**, and sister, **Polyanna**, who have supported by throughout my entire life.

Finally, I would like to thank **Carlos Fiore**, for the patience, friendship, and honesty that helped me grow as a physicist during our time working together, and **José Freire**, for being a friend and a mentor.

Thank you!

The present work was done thanks to the financial support of **CAPES**, under grant 88887.816488/2023-00.

# Resumo

A termodinâmica estocástica tornou-se um dos principais pilares da mecânica estatística moderna, e uma atenção especial tem sido dada a sistemas que apresentam comportamento coletivo. Neste projeto de mestrado, investigamos aspectos distintos em duas classes de sistemas que exibem comportamento coletivo. O primeiro é um sistema de opinião que mostra uma variedade de transições de fase, dependendo dos detalhes do modelo (topologia, inércia e vizinhança). Investigamos em detalhes suas propriedades, formulando uma abordagem termodinâmica consistente, relacionando calor com dissipação. O último sistema estudado aqui é um protótipo mínimo de um modelo de motor fora do equilíbrio que exibe comportamento coletivo, composto por duas nanomáquinas interagentes. Investigamos suas propriedades termodinâmicas, como eficiência, potência, o design do motor e rotas distintas para melhorar seu desempenho. Os resultados mostram que uma escolha adequada de parâmetros e design do sistema pode resultar em uma melhoria notável, incluindo eficiências máximas se aproximando de valores ideais e eficiências em potência máxima maiores do que os limites conhecidos na literatura.

**Palavras-chave:** Termodinâmica estocástica; transições de fase fora do equilíbrio; máquinas térmicas; mecânica estatística.

# Abstract

Stochastic thermodynamics has become one of the main cornerstones of modern statistical mechanics and special attention has been given to systems presenting collective behavior. In this master project, we have investigated distinct aspects in two classes of systems exhibiting collective behavior. The former is an opinion system displaying a variety of phase transitions depending on the model details (topology, inertia, and neighborhood). We have investigated in detail its properties by formulating a consistent thermodynamics approach by relating heat with dissipation. The latter system studied here is a minimal prototype of a nonequilibrium engine model displaying collective behavior, composed of two interacting nanomachines. We investigated its thermodynamic properties, such as efficiency, power, engine design, and distinct routes for improving its performance. Results show that a suitable choice of parameters and design can result in a remarkable improvement, including maximum efficiencies approaching ideal values and efficiencies at maximum power greater than known bounds in the literature.

**Keywords:** Stochastic thermodynamics; out-of-equilibrium phase transitions; heat engines; statistical mechanics.

# Contents

<b>1</b>	<b>Introduction</b>	<b>3</b>
<b>2</b>	<b>Fundamental Concepts</b>	<b>7</b>
2.1	Non-Equilibrium Statistical Physics . . . . .	8
2.1.1	Markov Chains . . . . .	8
2.2	The master equation . . . . .	10
2.2.1	Solution via Eigendecomposition . . . . .	12
2.3	Stochastic Thermodynamics . . . . .	14
2.3.1	The Collisional Approach . . . . .	17
2.4	Overview about Phase Transitions . . . . .	21
2.4.1	Mean-Field Theory for Phase Transitions . . . . .	22
<b>3</b>	<b>Non-Equilibrium Thermodynamics of the Majority Vote Model</b>	<b>25</b>
3.1	Overview of the Majority Vote Model . . . . .	25
3.1.1	Majority Vote Model without Inertia . . . . .	26
3.1.2	Majority Vote Model with Inertia . . . . .	26
3.1.3	Entropy Production . . . . .	31



# CONTENTS

---

3.1.4	Finite-Size Scaling for the Entropy Production . . . . .	33
3.2	Thermodynamics of The Majority Vote Model . . . . .	35
3.2.1	Fluctuation theorems . . . . .	39
3.2.2	Heat fluxes at phase transitions . . . . .	40
3.2.3	Contributions to dissipation . . . . .	41
3.2.4	Concluding Remarks . . . . .	43
<b>4</b>	<b>Stochastic Heat Engines</b>	<b>46</b>
4.1	Minimal Collective Model: 3 states and 2 strokes . . . . .	47
4.2	General Thermodynamic Properties . . . . .	50
4.3	Applications . . . . .	52
4.3.1	Distinct Interactions between units . . . . .	52
4.3.2	Distinct Non-conservative Drivings . . . . .	59
4.3.3	The fast time switchings $\tau \rightarrow 0$ and the two reservoirs case . . . . .	63
4.3.4	Concluding Remarks . . . . .	65
<b>5</b>	<b>Conclusion</b>	<b>67</b>
<b>A</b>	<b>Finished and submitted Papers</b>	<b>79</b>

# Chapter 1

## Introduction

The ambition to build efficient engines is not only prominent, but also pressing in thermodynamics since the pioneering work by Sadi Carnot [1, 2], having gained new momentum with the development of nonequilibrium thermodynamics of small-scale systems [3–5]. Unlike classical thermodynamics, fluctuations become fundamental at the nanoscopic scale, and the study about their role has attracted large attention both theoretically [6–8] and experimentally [9, 10]. As irreversibility is unavoidable, the search for new strategies to satisfactorily characterize it in the realm of nonequilibrium thermodynamics is crucial and strongly desirable. With this in mind, several distinct approaches have been proposed. Among them, we highlight the study of the maximum attainable power and efficiency [11–14] and the modulation of the system-bath interaction time control via shortcuts to adiabaticity [15–17] or isothermality [17, 18]. The thermodynamic description of nonequilibrium systems is done thanks to the stochastic thermodynamics for both master equation and Fokker-Planck systems, and can be understood as an enlargement of the statistical mechanics for systems out of thermodynamic equilibrium. In addition, this approach provides an expression for the production of entropy (a keystone quantity that characterizes systems out of thermodynamic equilibrium) and a suited formulation of the first law of thermodynamics.

More recently, the properties of systems operating under collective rules have attracted much attention, not only for understanding their thermodynamic properties but also for using them as a reliable setup for many distinct applications [10, 19]. The best-known example of collective behavior in equilibrium systems is the ferromagnetism phenomenon, in which systems become polarized due to a particular external influence (*e.g.*, magnetic

fields or temperature changes). In the last years, equilibrium models have had long-standing importance in the context of collective effects and are at the heart of numerous theoretical and experimental advances, presenting distinct models (*e.g.*, Ising, Potts, XY, and Heisenberg) as ideal platforms for describing ferromagnetism. Among the distinct examples of collective behavior existing in out of equilibrium, we cite the synchronization and swarming phenomena. While both can be observed in insects, the former is mainly associated with the species of synchronous fireflies *P. carolinus* that have been shown to flash in sync under certain conditions [20–23], while the latter has been documented in distinct biological collectives such as bacterial colonies performing chemotaxis [24, 25] and the migration of schools of fish, flights of birds and cells [26–28]. It then becomes clear that collective effects are present in many aspects of nature and physics and are prime subjects to investigate under the stochastic thermodynamics framework.

This master dissertation investigates the thermodynamics of two models presenting collective effects. The first is the majority vote model, one of the simplest nonequilibrium up-down symmetric systems exhibiting an order-disorder phase transition [4, 29]. Extensive studies of this model in distinct lattice topologies have shown that the symmetry-breaking phase transition is not affected by the kind of underlying networks, even though the critical behavior results in an entirely different set of critical exponents. However, in the last years, recent works verified that the usual second-order phase transition in the majority vote model (MV) becomes first-order upon the inclusion of a term that adds competition between local neighborhood and individual opinion (inertia) [29, 30]. The behavior of entropy production as a tool for characterizing phase transition has attracted great and recent interest, as it discerns equilibrium from nonequilibrium systems, such as the latter one characterized by a positive entropy production rate in the nonequilibrium steady state regime (NESS) [31, 32]. Despite previous works investigating the main properties of the MV through the entropy production signatures, other thermodynamic quantities have yet to be defined to establish a firm link between voter models and stochastic thermodynamics' framework. Aimed at partially overcoming such drawbacks, a thermodynamic description for opinion models is proposed in this work, in which the idea of a distinct thermal reservoir per neighborhood opinion configuration was introduced. Such a framework allows one to associate the dynamics with well-defined temperatures and reconciles the relationship between entropy production and heat flux [33]. More concretely, a general and unambiguous temperature definition is derived, providing a way to properly investigate the behavior of entropy production and heat fluxes in distinct phases

and continuous and discontinuous transition regimes [34].

In the second part of this work, we investigate another aspect of collective effects, considering a comparison between distinct engine designs for a minimal setup for a collective engine. Under a generic point of view, stochastic engines are classified into three categories, stemming from fixed thermodynamic forces [7, 8], from the time-periodic variation of external parameters [5, 35] and via sequential/collisional approach [36–38], in which at each stroke/stage, the system is subjected to a different condition (held fixed along the stage). Each one has been considered as a reliable approach in distinct contexts, such as the last one encompassing the presence of distinct drivings over each member of the system, a weak coupling between the system and the reservoir, or even for mimicking the environment for quantum systems. As stated before, the thermodynamics of systems exhibiting collective effects have received considerable recent attention as an alternative strategy for improving the system’s performance. Among the distinct examples, we cite a system of interacting Brownian particles [32, 39–42], work-to-work transducers [43, 44] and heat engines [32, 45–48]. All of them are restricted to cases of systems operating at equal temperatures and fixed parameters. Our study will investigate a simpler case, dealing with a minimal collective effect system composed of two interacting units beyond the fixed forces context. Hence, its simplicity constitutes an ideal laboratory for comparing three fundamental aspects of nanoscopic engines: the kind of design (sequential versus fixed thermodynamic forces), distinct approaches for the work source (not considered previously) and under situations collective effects can improve the system’s performance when compared with its interactionless version. The former goal has been inspired from previous contributions [5, 7, 49]. Our findings reveal that collective effects, along with a suited design of parameters (energy, period, duration of each stage) at each stroke can significantly enhance the system’s performance. Such remarkable improvement can result in optimal power outputs and efficiencies at maximum a power greater than known bounds or even efficiencies approaching the ideal (Carnot) limit. As a side result, our study shows the simultaneous contact between two thermal baths case [7] as the ideal limit of fast switching times.

This work is organized as follows: in Chapter 2, a general theory behind the work presented is shown. Starting from the usual Markov Chain, we move on to master equations, showing that different formalisms (in the context of thermodynamics and lattice models) can be helpful to describe different physical phenomena. Then, a brief descrip-

tion of Stochastic Thermodynamics and Active Matter is presented. In Chapter 3, we present the work performed to derive general relationships for the majority vote model's thermodynamic heat flux and entropy productions. Chapter 4 contains the work made to idealize and explore a minimal 3-state model, obtaining its complete solution in the collisional approach and then showcasing two distinct applications for the general Quantum Dot engine. Finally, conclusions are drawn in Chapter 5, and Appendixes show the published/submitted papers.

# Chapter 2

## Fundamental Concepts

One of the earliest documented observations of random motion at the microscopic scale was made by the botanist Robert Brown [50]. Upon introducing pollen grains into a water container, he noticed that they would "jiggle" and disperse throughout the water, eventually occupying a space resembling a sphere. This unique movement dynamic, coined *Brownian Motion*, coupled with its macroscopic manifestation, known as *diffusion*, would later be rigorously studied by Paul Langevin [51, 52] and Albert Einstein [53]. Their groundbreaking work laid the foundations for what would eventually be named "Stochastic Physics", and set the stage for many years to come. Beyond the confines of pure physics, these dynamic behaviors found applicability in a plethora of scientific areas. Notably, they offered insights into phenomena ranging from public opinion formation to the motility of microscopic biological collectives, including bacteria and cells [25, 54–56].

The modification of Newton's second law to include a random force for a particle subject to a dissipative force leads to what is commonly known as Brownian motion [4, 57],

$$m\dot{v}(t) = -\alpha v(t) + \mathcal{F}_\ell(t). \quad (2.1)$$

In Eq.(2.1),  $v(t)$  denotes the particle's velocity and  $\mathcal{F}_\ell(t)$  is known as the *Markov propagator*, a random variable with dimensions of force that, in the absence of temporal correlation, that is,  $\langle \mathcal{F}_\ell(t) \rangle = 0$ ,  $\langle \mathcal{F}_\ell(t) \mathcal{F}_\ell(t') \rangle = \mathcal{D}_T \delta(t-t')$ , defined the equation presented above as a *Langevin Equation*. In this context,  $\mathcal{D}_T$  is defined as the translation diffusion

coefficient.

The inherent randomness of the Langevin equation paves the way for the three primary tools employed in Stochastic Physics and throughout this work: the derivation of probability distribution, averages, and their respective connection with thermodynamics. The absence of temporal correlation in the stochastic variable ensures that the system's state at a given time step,  $t$ , is solely influenced by its previous state. Such class of systems, known as Markovian, can be studied by either obtaining the *average behavior over a specific duration*—especially in the non-equilibrium steady state,  $t \rightarrow \infty$ , effectively mitigates the impact of random fluctuations—or by deducing the probability density function describing the system's average temporal evolution [3, 58]. While these two theoretical frameworks are intrinsically connected with each other, a strategic tackling of each base concept is essential for the full understanding of the three distinct projects presented in this work.

## 2.1 Non-Equilibrium Statistical Physics

Imagine you dine at the same breakfast spot every day. This establishment offers only three different meals: avocado toast ( $A$ ), breakfast burritos ( $B$ ), and cereal ( $C$ ). One of their unique rules is that they rarely serve the same meal on consecutive days. Moreover, the probability of serving a particular meal next depends solely on what was served the day before. Now, if they served avocado toast ( $A$ ) today, is it possible to determine the probability that the sequence of meals over the next four days will be  $C$ ,  $A$ ,  $B$ , and  $C$  respectively?

### 2.1.1 Markov Chains

A Markov chain characterizes the probability dynamics of a sequence of events unfolding in discrete time space. When this evolution is purely stochastic within a discrete time space, the transition of states between steps remains temporally uncorrelated, except for the correlation between the current step and the immediately previous one [3, 4, 52].

Consider a system whose state at step  $\ell$  is described by the variable  $s_\ell$ . At each step, the transitions between states are random. Consequently, the probability that the system

will be in state  $s_\ell$  at step  $\ell$ , after following a specific stochastic trajectory starting at  $\ell = 0$ , is described by the usual Kolmogorov relation [59] for the conditional probability  $\mathcal{P}_\ell(s_\ell|s_0, s_1, \dots, s_{\ell-1})$ . This system is said to be *Markovian* as long as this conditional probability is *equivalent* to the probability of the system being in state  $s_\ell$  given *only* that it was in state  $s_{\ell-1}$  in previous step,

$$\mathcal{P}_{\ell+1}(s_{\ell+1}|s_\ell) = \mathcal{P}_\ell(s_\ell|s_{\ell-1}) \mathcal{P}_{\ell-1}(s_{\ell-1}|s_{\ell-2}) \dots \mathcal{P}_1(s_1|s_0) \mathcal{P}_0(s_0). \quad (2.2)$$

In other words: a system is said to be Markovian if its evolution on the state space can be entirely described by the information of the previous state and the initial condition [4, 57]. Using Eq.(2.2), we can then define the probability of the system being in the state  $s_\ell$  regardless of any specific trajectory,  $P_\ell(s_\ell)$ . This is achieved by summing over all possible trajectories up until  $\ell - 1$ ,

$$P_\ell(s_\ell) = \sum_{s_{\ell-1}} \mathcal{P}_\ell(s_\ell|s_{\ell-1}) P_{\ell-1}(s_{\ell-1}).$$

In the cases where the conditional probability has no temporal dependence, *i.e.*, the transition between states occurs at a constant rate, one can express said probability as the matrix containing all the information of every possible transition between states, coined *Stochastic Matrix*,  $\mathcal{P}_\ell(s_\ell|s_{\ell-1}) := T(s_\ell, s_{\ell-1})$ , and obtain the probability at time  $\ell$ ,

$$P_\ell = T P_{\ell-1}, \quad (2.3)$$

that can be expressed in the equivalent form, using the simplified notation for states,

$$P_{\ell+1}(n) = \sum_{m(\neq n)} T(n, m) P_{\ell-1}(m) + T(n, n) P_\ell(n). \quad (2.4)$$

where  $P_\ell$  now represents a probability vector of dimensions equivalent to the number of states,  $S$ , and  $T$  is the stochastic matrix of dimensions  $S \times S$  with properties  $T(n, m) > 0$ ,  $\sum_n T(n, m) = 1$ . An intuitive way to represent a Markov chain is through the diagram presented in Fig. (2.1).

In essence, the equation for a Markov chain allows for the description of possible steady states of any stochastic model, given its restrictions. In simple systems like the one described by Ehrenfest model, a diffusion model describing the resulting dynamics of a set of  $N$  balls hopping between two containers, the solution of the adequate form of



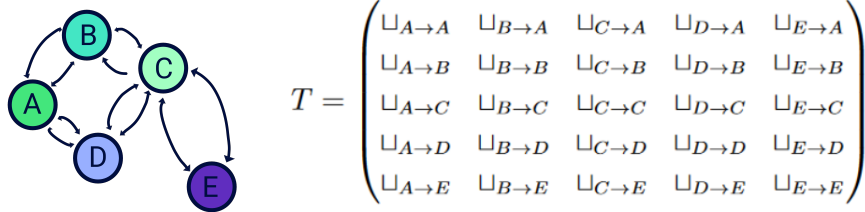


Figure 2.1: Illustration of a Markov chain (left) and its respective Stochastic Matrix (right). Each entry on the  $T_{i,j}$  matrix represents the transition rate at which the system goes **from**  $j$  **to**  $i$ . In the case of the illustration on the left, every entry on the last row is zero except from  $\sqcup_{C \rightarrow E}$  and  $\sqcup_{E \rightarrow E}$ . It follows that  $\sqcup_{C \rightarrow E} + \sqcup_{E \rightarrow E} = 1$ .

Eq. (2.3) can predict the existence of multiple phases and, in the case of a simple Random Walk, where the underlying mechanism behind the dynamics is also diffusion, lead to more robust results, *e.g.* the Central Limit Theorem [3, 4, 52, 57]. While this might suffice for the macroscopic description of inorganic matter and simple stochastic models, the transition from discrete to a continuous temporal space will allow for a more elegant and intricate investigation in more complex dynamics, such as in biological systems, opinion models, or out-of-equilibrium thermodynamic heat engines. The description of systems evolving at continuous time, however, is done by means of the *master equation* formalism.

## 2.2 The master equation

The continuous time limit of Eq. (2.4) is obtained by assuming that transitions between different states occur at a time instant,  $\tau \rightarrow 0$ , in such a way that the probability of remaining at the same state is close to 1. More specifically, we express transition probabilities in the following way

$$\begin{aligned} T(n, m) &= \tau W(n, m), \quad n \neq m \\ T(n, n) &= 1 - \tau \Theta(n), \end{aligned}$$

where  $\Theta(n) = \sum_{m(\neq n)} W(m, n)$  Now, the dynamics are entirely expressed in terms of transition rates  $W(n, m)$ , and due to the property

$$\sum_m T(m, n) = 1,$$

the  $\Theta(n)$  term must obey the relation

$$\Theta(n) = \sum_{m(\neq n)} W(m, n).$$

We can then rewrite Eq.(2.4), including the  $\tau$  dependence,

$$p(n, t + \tau) = \tau \sum_{m(\neq n)} W(n, m)p(m, t) + [1 - \tau\Theta(n)]p(n, t), \quad (2.5)$$

where  $p(n, t)$  denotes the probability of the system being in state  $n$  at time  $t$ , and the change in notation is simply a visual choice to indicate the transition from Markov chains to master equation formalisms.

That, after some manipulation, assumes the usual derivative form

$$\frac{p(n, t + \tau) - p(n, t)}{\tau} = \sum_{m(\neq n)} W(n, m)p(m, t) - \Theta(n)p(n, t),$$

and, by taking the limit  $\tau \rightarrow 0$ , we obtain

$$\frac{dp(n, t)}{dt} = \sum_{m(\neq n)} [W(n, m)p(m, t) - W(m, n)p(n, t)], \quad (2.6)$$

where  $W(n, m)$  accounts for the transition *from* state  $m$  *to* state  $n$ . In *all* of these constructions and solutions, some properties of the master equation must remain the same [4, 60]. The transition matrices must have only *real* eigenvalues, and the probability *must* converge at the limit  $t \rightarrow \infty$ . Both of these requirements are fulfilled in the normalization of  $W$ , namely

$$\sum_n W(n, m) \geq 0 \quad n \neq m, \quad (2.7)$$

where  $W(n, m) > 0$ . From now on, transition rates  $W(n, m)$  will be expressed in the form  $\omega_{nm}$ .

In principle, the probability distribution can be found by solving the master equation at the steady state, as  $dp(n, t)/dt = 0$ . However, in many cases (*e.g.*, systems with a large number of configurations), it can become quite cumbersome to find a steady state solution. For this reason, alternative techniques, such as perturbative methods [61] or

eigendecomposition [4] have been considered. Conversely, solutions via mean-field theory and numerical integrations/simulations are also remarkable, and also will be mentioned in the following sections [30, 62, 63]. The following section shows one of the exact solutions, via eigendecomposition.

### 2.2.1 Solution via Eigendecomposition

This method of solving the master equation relies on the algebraic properties of the transition matrix [4]. First, by defining the vectors  $\vec{\phi}_\mu$  and  $\vec{\psi}_\mu$  as the respective *left* and *right* eigenvectors of the  $\mu$ -th state of the transition matrix,  $W$ , it follows that

$$\vec{\phi}_\mu W = \vec{\phi}_\mu \lambda_\mu \quad (2.8a)$$

$$W \vec{\psi}_\mu = \lambda_\mu \vec{\psi}_\mu \quad (2.8b)$$

where  $\lambda_\mu$  is the  $\mu$ -th eigenvalue of  $W$ . The associate master equation, in this notation, reads

$$\frac{d\vec{p}(t)}{dt} = W\vec{p}(t). \quad (2.9)$$

Given that the general solution of this ODE is

$$\vec{p}(t) = e^{W(t-t_0)}\vec{p}(0),$$

it is possible to perform an expansion using the aforementioned quantities in the following way

$$e^{W(t-t_0)} = e^{\lambda_0(t-t_0)}\vec{\psi}_0\vec{\phi}_0 + e^{\lambda_1(t-t_0)}\vec{\psi}_1\vec{\phi}_1 + e^{\lambda_2(t-t_0)}\vec{\psi}_2\vec{\phi}_2\dots$$

up to the  $\mu$ -th state, allowing for the general solution for  $\vec{p}(t)$  in terms of the eigenvectors and eigenvalues,

$$\vec{p}(t) = \sum_{\mu}^N e^{\lambda_\mu(t-t_0)}\vec{\psi}_\mu\vec{\phi}_\mu\vec{p}(0)$$

that we can promptly rewrite in terms of the operator resulting of the product of the left and right eigenvectors,  $\Gamma_\mu = \vec{\psi}_\mu \vec{\phi}_\mu$ ,

$$\vec{p}(t) = \sum_{\mu}^N e^{\lambda_\mu(t-t_0)} \Gamma_\mu \vec{p}(0). \quad (2.10)$$

Now, it is interesting to make a few observations about this matrix. First, due to general linear algebra, we can safely write, using matrix diagonalization,

$$\begin{aligned} W &= \psi \Lambda \phi \\ &= \begin{pmatrix} \psi_{0,0} & \psi_{1,0} & \dots & \psi_{N,0} \\ \psi_{0,1} & \psi_{1,1} & \dots & \psi_{N,1} \\ & \dots & & \\ \psi_{0,N} & \psi_{1,N} & \dots & \psi_{N,N} \end{pmatrix} \begin{pmatrix} \lambda_0 & 0 & \dots & 0 \\ 0 & \lambda_1 & \dots & 0 \\ & \dots & & \\ 0 & 0 & \dots & \lambda_N \end{pmatrix} \begin{pmatrix} \phi_{0,0} & \phi_{0,1} & \dots & \phi_{0,N} \\ \phi_{1,0} & \phi_{1,1} & \dots & \phi_{1,N} \\ & \dots & & \\ \phi_{N,0} & \phi_{N,1} & \dots & \phi_{N,N} \end{pmatrix} \\ &= \vec{\psi}_0 \lambda_0 \vec{\phi}_0 + \vec{\psi}_1 \lambda_1 \vec{\phi}_1 + \dots + \vec{\psi}_N \lambda_N \vec{\phi}_N \\ &= \sum_{\mu}^N \lambda_\mu \vec{\psi}_\mu \vec{\phi}_\mu \\ &= \sum_{\mu}^N \lambda_\mu \Gamma_\mu, \end{aligned}$$

where  $\Lambda = \phi W \psi$  is the eigenvalue matrix that comes from the diagonalization of  $W$  and  $\phi_{\mu,i}$  is the  $i$ -th component of the  $\mu$ -th eigenvector. Using the fact that, due to the imposed normalization of the transition matrix,  $\lambda_0 = 0$ , we find that

$$\begin{aligned} W &= \sum_{\mu}^N \lambda_\mu \Gamma_\mu \\ &= \lambda_0 \Gamma_0 + \lambda_1 \Gamma_1 + \dots + \lambda_N \Gamma_N \\ &= 0 + \lambda_1 \Gamma_1 + \dots + \lambda_N \Gamma_N \\ &= \sum_{\mu \neq 0}^N \lambda_\mu \Gamma_\mu, \end{aligned}$$

which we can then sum over *rows*, knowing that  $\sum_m W_{m,n} = 0$ ,

$$\begin{aligned} \sum_m W_{m,n} &= \sum_m \left( \sum_{\mu \neq 0} \lambda_\mu^N \Gamma_\mu \right)_{m,n} \\ 0 &= \sum_{\mu \neq 0} \lambda_\mu^N \sum_m \Gamma_{\mu,m,n}, \end{aligned}$$

implying that this operator carries the normalization of the transition matrix,

$$\sum_m \Gamma_{\mu,m,n} = 0. \quad (2.11)$$

Furthermore, by taking advantage of the trace property,  $\text{Tr}\{W\} = \sum_\mu \lambda_\mu$ , and proceeding analogously,

$$\begin{aligned} \text{Tr}\{W\} &= \text{Tr} \left\{ \sum_\mu^N \lambda_\mu \Gamma_\mu \right\}, \\ \sum_\mu^N \lambda &= \sum_\mu^N \text{Tr}\{\lambda_\mu \Gamma_\mu\}, \\ \sum_\mu^N \lambda &= \sum_\mu^N \lambda_\mu \text{Tr}\{\Gamma_\mu\}, \end{aligned}$$

and we see that  $\text{Tr}\{\Gamma_\mu\} = 1$ . Finally, the solution for the master equation considered in Chapter 4 assumes the form

$$\vec{p}(t) = \vec{p}^{(eq)} + [e^{\lambda_1(t-t_0)}\Gamma_1 + e^{\lambda_2(t-t_0)}\Gamma_2] \vec{p}(0) \quad (2.12)$$

where  $\vec{p}^{(eq)} = \Gamma_0 \vec{p}(0) = \Gamma_0(\mathbf{1}/3)$ , and it becomes clear that in the limit  $t \rightarrow \infty$ , that is, in the stationary state, the probability distribution evolves to a time-independent value, that will be one of equilibrium or nonequilibrium depending on the specifications of each problem. On the other hand, in the cases where the transition matrix changes periodically, the steady state will also be periodic.

## 2.3 Stochastic Thermodynamics

To contextualize the stochastic thermodynamics framework, let us consider a simple example [57]. A system of interacting Brownian particles will dissipate heat at each collision,

but the random nature of Brownian motion implies that the dissipated heat is also a stochastic quantity. They show us that, unlike the standard thermodynamics, dealing with macroscopic systems operating at the quasi-static limit, several (most of) systems in nature operate far from equilibrium [3]. Stochastic thermodynamics corresponds to a unified theory combining the theory of stochastic processes (*e.g.* master equation or Fokker-Planck) with thermodynamic considerations. At a fundamental level, stochastic thermodynamics is aimed at reformulating the first and second laws in a representation of average fluxes in the non-equilibrium steady state and using these average quantities to provide a satisfactory description of the system being investigated [3, 4, 56].

However, reliably defining these quantities requires some assumptions about the system being studied to be made. First, when the system is placed in contact with a single thermal reservoir without time variation of parameters nor nonconservative forces, it will evolve to its (equilibrium) steady state being (Boltzmann-Gibbs) in which transition rates between any microscopic states,  $n$  and  $m$ , and, after sufficiently long times, obey the detailed balance condition,

$$\omega_{m,n}p_n^{(eq)} - \omega_{n,m}p_m^{(eq)} = 0. \quad (2.13)$$

Once detailed balance is followed, we can define the stationary probability as the *thermodynamic equilibrium probability*,  $\mathbf{p}^{(eq)}$ . In general, the detailed balance will be fulfilled if transition rates are defined in such a way that they obey

$$\frac{\omega_{n,m}}{\omega_{m,n}} = \exp[-\beta(\epsilon_n - \epsilon_m)], \quad (2.14)$$

where  $\epsilon_n$  is the energy level of state  $n$ , and does not explicitly depend on the time. In the case at which Eq. (2.13) is not satisfied (*e.g.*, systems placed in contact with distinct thermal baths or whose parameters are time-dependent), the system will evolve to a nonequilibrium steady state regime. However, one can use Eq. (2.13) as a starting point for deriving a thermodynamical approach, in which one relates quantities with macroscopic variables using Eq. (2.14), in many situations referred to as *local* detailed balance [64, 65]. Along this work, we shall consider transition rates defined according to the local detailed balance. Second, the stochastic approach for thermodynamics consists

of defining the entropy as a function of time,  $S(t)$ , using the Boltzmann-Gibbs form,

$$S(t) = -k_B \sum_n p_n(t) \ln p_n(t), \quad (2.15)$$

whose time derivative reads

$$\frac{dS(t)}{dt} = -k_B \sum_n \left[ \frac{dp_n(t)}{dt} \ln p_n(t) + \frac{dp_n(t)}{dt} \right].$$

Due to the normalization of the probability,  $\sum_n p_n(t) = 1$ , the second term on the right side of Eq. (2.16) vanishes. Using the master equation, the first term can be rewritten in terms of the rates,

$$\frac{dS(t)}{dt} = -k_B \sum_{(n,m)} \ln p_n(t) [\omega_{n,m} p_m(t) - \omega_{m,n} p_n(t)]. \quad (2.16)$$

This change in entropy must correspond to the difference between the entropy that is produced internally by the system and the entropy that is exchanged between the system and the environment. Defining the former as the *entropy production rate*,  $\sigma(t)$ , and the latter and the entropy flux from the system,  $\Phi(t)$ , we can rewrite the previous expression simply as

$$\frac{dS(t)}{dt} = \sigma(t) - \Phi(t).$$

The next step for a thermodynamic approach consists of assuming that the entropy production can be written according to the Schakenberg formula [66],

$$\sigma(t) = \frac{k_B}{2} \sum_{(n,m)} [\omega_{m,n} p_n(t) - \omega_{n,m} p_m(t)] \ln \frac{\omega_{m,n} p_n(t)}{\omega_{n,m} p_m(t)}. \quad (2.17)$$

Having  $dS/dt$  and  $\sigma$ , it follows that  $\Phi$  reads

$$\Phi(t) = -\frac{k_B}{2} \sum_{(n,m)} [\omega_{m,n} p_n(t) - \omega_{n,m} p_m(t)] \ln \frac{\omega_{m,n}}{\omega_{n,m}}. \quad (2.18)$$

Note that  $\sigma(t)$  is strictly non-negative, while  $\Phi(t)$  depends on the heat flow exchanged between the system and the thermal bath. Also, in the *NESS* (nonequilibrium steady state regime),  $\sigma = \Phi$ . In the equilibrium state (detailed balance fulfilled)  $\sigma = 0$ , whereas  $\sigma = \Phi > 0$  in the *NESS*.

Third and last, the first law of (stochastic) thermodynamics can be set in a similar way. Starting from the mean energy definition,  $U(t) = \sum_n \epsilon_n(t)p_n(t)$ , and taking the time derivative,

$$\frac{dU(t)}{dt} = \sum_n \left[ \frac{d\epsilon_n(t)}{dt} p_n(t) + \epsilon_n(t) \frac{dp_n(t)}{dt} \right], \quad (2.19)$$

where the first and second terms of the right side can be identified as direct work,  $\dot{W}_d$  and heat fluxes,  $\dot{Q}$ , respectively. Since  $U(t)$  is a state function, it follows that, in the *NESS*,  $dU/dt = 0$ , and, consequently,

$$\dot{W}_d = \sum_n \dot{\epsilon}_n p_n^{st}, \quad (2.20)$$

$$\dot{Q} = \sum_{m,n} \epsilon_n \omega_{m,n} p_n^{st}, \quad (2.21)$$

where the superscript *st* indicates the steady state. It follows that  $\dot{W}_d + \dot{Q} = 0$ , consistent with the first law of thermodynamics.

As a closing remark, it is important to point out that, in the case of some protocol promoting the time variation of energy levels,  $\dot{W}_d$  is associated with the variation of energy levels with respect to a given protocol (*e.g.*, time variations, changes in the magnetic field), while the heat flux, in turn, is related to the variation of the probability distribution.

### 2.3.1 The Collisional Approach

In classical thermodynamics, a certain worksource, such as water put into a furnace to boil and generate vapor, placed in contact with both hot and cold thermal baths, can operate as a thermal engine or as a pump, according to the work generated along the cyclic process being positive or negative [1, 67]. Recently, these thermal engines have been reproduced via stochastic models depicting nonequilibrium systems [36, 48, 68]. In this section, we focus on a second framework to design out-of-equilibrium systems as thermodynamic machines, namely, the *collisional approach*.

In this approach, we define a certain time period,  $\tau$ , in which our setup evolves in time [61]. At  $t = 0$ , the dynamic starts and the system is placed in contact with a thermal reservoir of inverse temperature  $\beta^{(1)}$  and transition rates  $\omega_{m,n}^{(1)}$ , for a total time



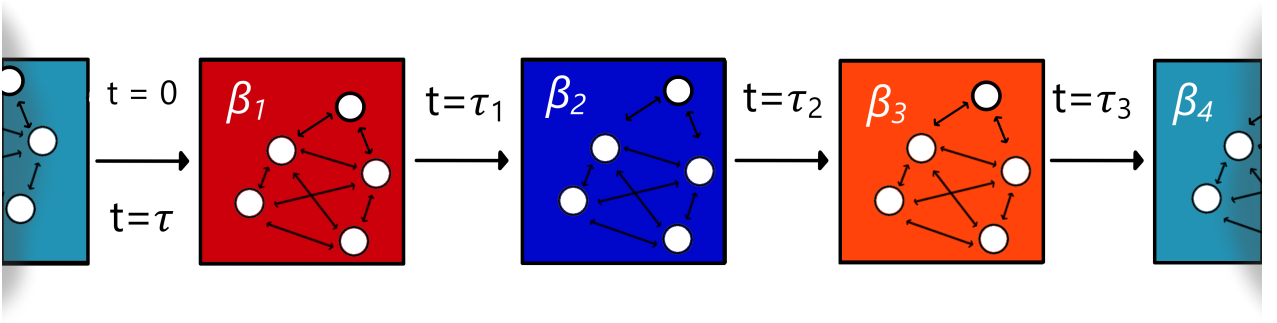


Figure 2.2: Simple illustration of the idea behind the collisional approach. At every  $\tau_\nu$ , a certain interacting system is placed in contact with a distinct thermal bath, and, after the period ( $t = \tau$ ) is complete, the system is then returned to its original position.

$\tau_1$ . Afterward, the system is then switched and placed in contact with a second reservoir, giving rise to another set of parameters characterized by the  $\omega_{m,n}^{(2)}$ , for a total time of  $\tau_2$ . *e.g.*, if the application is constrained to  $N$  reservoirs, when  $t = \sum_\nu \tau_\nu = \tau$ , the system is then returned to its initial state. Since probabilities are continuous functions, the probabilities associated with each stage must obey periodic boundary conditions,

$$p_\mu^{(\nu)}(t = \tau_{\nu-1}) = p_\mu^{(\nu+1)}(t = \tau_\nu), \quad (2.22)$$

where,  $\nu = N + 1 = 1$ . Naturally, this also implies that the fluxes will also vanish when summed over  $\tau$ .

In general, the number of reservoirs and the relationship between the periods of each switching are parameters to be considered in each framework [32, 36, 38, 69, 70]. The properties of the system at the *NESS* are obtained by averaging each quantity over an entire period,  $\tau$ . Therefore, the probability fluxes are in general defined as

$$\langle \mathbf{J}^{(\nu)} \rangle = \frac{1}{\tau} \int_{\tau_{\nu-1}}^{\tau_\nu} \omega^{(\nu)} \mathbf{p}^{(\nu)}(t) dt, \quad (2.23)$$

where each flux component corresponds to the probability *from* a certain state *to* another, and can be individually written as

$$\langle J_{ij}^{(\nu)} \rangle = \frac{1}{\tau} \int_{\tau_{\nu-1}}^{\tau_\nu} \left[ \omega_{i,j}^{(\nu)} p_j^{(\nu)}(t) - \omega_{j,i}^{(\nu)} p_i^{(\nu)}(t) \right] dt. \quad (2.24)$$

Similarly, quantities associated with the entire duration of the dynamic can be expressed

as the sum of each contribution at each state,

$$\langle \sigma \rangle = \sum_{\nu} \langle \sigma^{(\nu)} \rangle, \quad (2.25a)$$

$$\langle \dot{W}_d \rangle = - \sum_{\nu} \langle \dot{Q}^{(\nu)} \rangle, \quad (2.25b)$$

where both entropy production and heat flux can be obtained using the proceedings presented in the previous section. These quantities, when averaged over the entire period, become equivalent to the values assumed in the *NESS*. The following section presents a simple application of the collisional approach for a system with 2 states.

### Simple Example: the 2 states and 2 reservoirs case

As a brief "case study", imagine a simple stochastic system of 2 states,  $n = 0, 1$ , that stay in a cold thermal bath for a total time period of  $\tau/2$ , and afterward, it's moved to a hot reservoir until  $t = \tau$ . The results presented here will be used to draw comparisons with the model presented in Chapter 4, and were inspired in Ref. [7]. At each stage, we consider the transition rates defined by  $\omega_{0,1}^{(\nu)} = \exp[\epsilon^{(\nu)}\beta^{(\nu)}/2]$ ,  $\omega_{1,0}^{(\nu)} = \exp[-\epsilon^{(\nu)}\beta^{(\nu)}/2]$ . By using the eigendecomposition of the evolution matrix,  $\omega$ , presented previously, alongside the boundary conditions to obtain the initial condition for the probabilities, we see that

$$\mathbf{p}^{(\nu)}(t) = \mathbf{p}^{(eq,\nu)} - \exp[\lambda^{(\nu)}[t - (\nu - 1)\tau/2]] \frac{(e^{\lambda^{(\nu+1)}\tau/2} - 1) (\mathbf{p}^{(eq,\nu)} - \mathbf{p}^{(eq,\nu+1)})}{e^{[\lambda^{(1)} + \lambda^{(2)}]\tau/2} - 1} \quad (2.26)$$

where  $\lambda^{(\nu)} = -\cosh[\epsilon^{(\nu)}\beta^{(\nu)}/2]$  and, subsequently, the single probability flux takes the form

$$\langle J_1^{(\nu)} \rangle = (-1)^{\nu} \frac{(e^{\lambda^{(1)}\tau/2} - 1) (e^{\lambda^{(2)}\tau/2} - 1) [p_1^{(eq,1)} - p_1^{(eq,2)}]}{\tau [e^{[\lambda^{(1)} + \lambda^{(2)}]\tau/2} - 1]}. \quad (2.27)$$

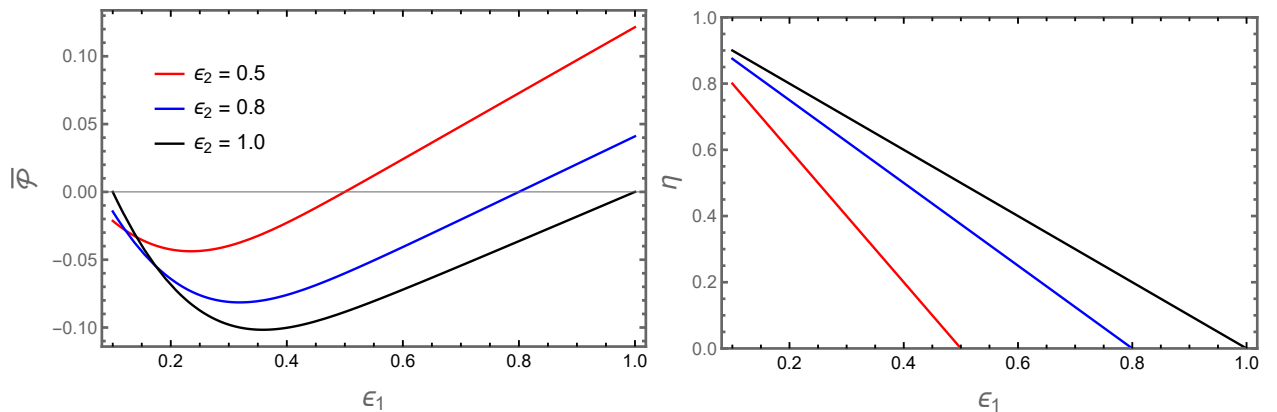


Figure 2.3: Curves of power, given by Eq.(2.31) and efficiency,  $\eta = 1 - \epsilon^{(1)}/\epsilon^{(2)}$  for different values of  $\epsilon^{(2)}$  and  $\beta^{(1)} = 10, \beta^{(2)} = 1, \tau = 1$ .

With this, using the relationships previously shown for entropy production, one can see that this quantity, for each stage, can be expressed simply as

$$\begin{aligned} \langle \sigma^{(\nu)} \rangle &= \frac{1}{2} \left\{ \ln \left[ \frac{\omega_{\omega_{0,1}^{(\nu)}}}{\omega_{1,0}^{(\nu)}} \right] \langle J_{0,1}^{(\nu)} \rangle + \ln \left[ \frac{\omega_{\omega_{1,0}^{(\nu)}}}{\omega_{0,1}^{(\nu)}} \right] \langle J_{1,0}^{(\nu)} \rangle \right\} \\ &= \ln \left[ \frac{\omega_{\omega_{0,1}^{(\nu)}}}{\omega_{1,0}^{(\nu)}} \right] \langle J_{0,1}^{(\nu)} \rangle \end{aligned}$$

that, when summed over both strokes, yields

$$\langle \sigma \rangle = X \langle J \rangle_1^{(1)} \quad (2.28)$$

where  $\langle \sigma \rangle$  assumes the usual flux times thermodynamic force form, and  $X$  plays the role of a thermodynamic force, given by

$$X = \left[ \frac{\epsilon^{(1)}}{T^{(1)}} - \frac{\epsilon^{(2)}}{T^{(2)}} \right]. \quad (2.29)$$

The heat fluxes at each stroke are obtained in a similar manner, yielding

$$\langle \dot{Q}^{(\nu)} \rangle = (-1)^{\nu+1} \langle J_1^{(1)} \rangle \epsilon^{(\nu)}, \quad (2.30)$$

that corresponds to power of the form

$$\mathcal{P} = \langle J_1^{(1)} \rangle [\epsilon^{(2)} - \epsilon^{(1)}]. \quad (2.31)$$

Given that the hot reservoir is defined to correspond to  $\nu = 2$ , efficiency is expressed as  $\eta = -\mathcal{P}/\langle\dot{Q}^{(2)}\rangle = 1 - \epsilon^{(1)}/\epsilon^{(2)}$ . The curves for both of these quantities are shown in Fig. (2.3). As it will become clear in Chapter 4, one can then explore the optimal relations between parameters for obtaining maximum power and maximum efficiency, as well as remarkable optimization routes and extensions for such model, taking into account collective effects [7, 8, 71].

## 2.4 Overview about Phase Transitions

Phase transitions in equilibrium systems are very well documented and sufficiently described via rigorous [67, 72, 73] results and mean-field frameworks like the Landau or Ginzburg-Landau functionals [1, 2, 4, 57, 73]. As mentioned in the introduction, equilibrium models have been considered ideal platforms for verifying the universal aspects of phase transitions. As an example, we cite the Ising and the Blume-Emery-Griffiths (BEG) models phase diagrams (disordered, ferromagnetic, and staggered quadrupolar, in the latter case) is sufficiently described with the Landau theory with single and coupled ordered parameters, respectively [74]. In this case, the transition between phases will be either of first/discontinuous or second/continuous order, depending on the free energy having a discontinuity in its first or second thermodynamic derivative, respectively [67]. Out-of-equilibrium phase transitions, in general, observed in systems with different types of interactions, such as the Kinetic Ising, opinion, and the Vicsek models [29, 75–77] are not satisfyingly described via the framework of classical statistical mechanics, since one has not a free energy to decide in which phase the system will be. Also, the absence of an exact solution in most cases prevents some analytical treatments. However, in the last years the general concepts about second/continuous and first/discontinuous for nonequilibrium phase transitions have been proposed/extended with respect to equilibrium ones [62, 78–80].

In order to illustrate the main ideas behind nonequilibrium phase transitions, we shall consider a mean-field-like treatment.

### 2.4.1 Mean-Field Theory for Phase Transitions

The idea behind opinion systems is to provide an insight into general phenomena observed in many different aspects of life, such as elections, propagation of information, diseases, and general consensus formation. Aside from this, opinion models are also able to provide valuable contributions about out-of-equilibrium transitions. One approach to investigate the phase transitions generally associated with these types of models is through the use of mean-field theory, where one is able to obtain a reasonable description of for both continuous and discontinuous transitions, albeit missing the characterization of the steady state nature (equilibrium or nonequilibrium) of these phenomena [4].

#### Order Parameter

Like the equilibrium Ising model, nonequilibrium systems with  $\mathbb{Z}_2$  (up-down) symmetry, are described using spin variables [60]. Given a certain topology, described either by a regular square lattice or a complex network, each site (or node) will be described by a spin variable  $\sigma_i = \pm 1$  and the system ordering can be characterized via the (order parameter) magnetization:

$$\langle m \rangle = \left\langle \left| \frac{1}{N} \sum_i \sigma_i \right| \right\rangle. \quad (2.32)$$

Given that the average value of the magnetization will be restrained between 0 and 1, these types of systems will present two distinct phases: ordered, when  $m \neq 0$ , and disordered, when  $m = 0$ . By varying a given control parameter, the system behavior is changed, from an ordered (ferromagnetic) phase to a disordered (paramagnetic) phase, respectively.

For the description of *continuous* phase transitions, the general mean-field-like approximation for the behavior of the order parameter is obtained in a similar way to the proceedings presented in "Landau" theory for equilibrium transitions [4, 60, 75]. Assuming the magnetization has translational invariance, so that  $m = \langle \sigma_i \rangle$ , this approximation can be written accordingly to Ref. [4]

$$\frac{dm}{dt} = -rm - \frac{u}{2}m^3 \quad (2.33)$$

Since  $m = 0$  is the trivial solution, the parameters at which Eq. (2.33) presents another

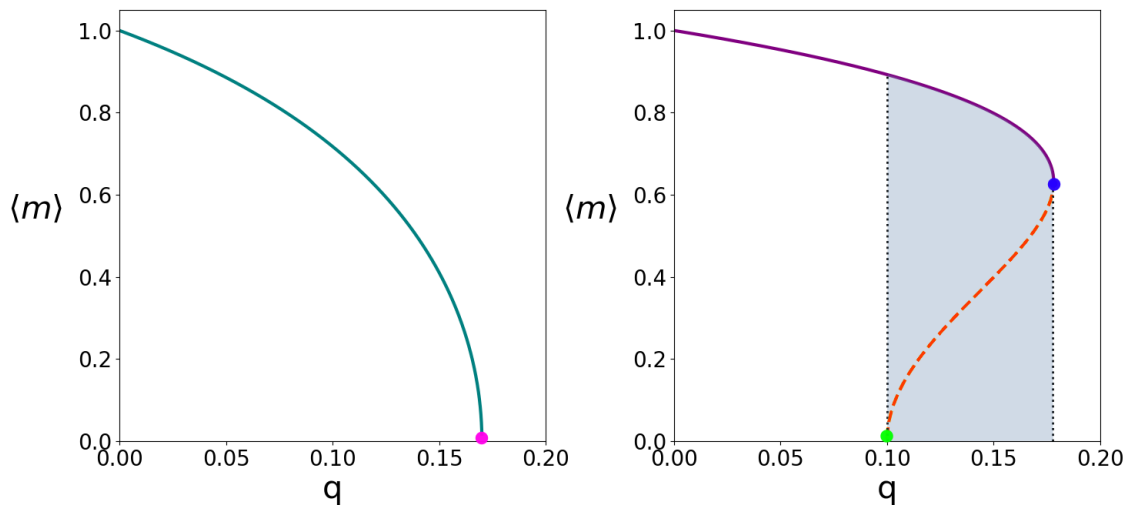


Figure 2.4: Behavior of the order parameter,  $\langle m \rangle$  for the continuous (left) and discontinuous (right) phase transitions. In the left, the  $\bullet$  indicates the critical point,  $q_C$ . In the right, the symbols  $\bullet$  and  $\bullet$  pertains to the critical points in the backwards and forwards transitions, respectively. The darkened region in the right panels indicates the bistability region.

(non-trivial) solution, given by  $m = m_C \neq 0$ ,

$$[m_C(t)]^2 = \frac{2m_0^2 r}{[2r + m_0^2 u] e^{2rt} - m_0^2 u}. \quad (2.34)$$

and it becomes clear that, when  $t \rightarrow \infty$ , the possible solutions will be  $m_C^2 = 0$  or  $m_C^2 = -r/2u$ , meaning that the only possible way to  $m \neq 0$  to exist is when  $r < 0$ . A more intuitive way to write  $r$ , then, is as  $r \sim q - q_c$ , where  $q$  is the control parameter. If  $q \geq q_c$ , the only possible phase predicted will be the disordered one, whereas when  $q < q_c$ , we'll find the system in the ferromagnetic phase [4, 74]. Furthermore, it is possible to see that the critical exponent of the order parameter as we approach the critical point,  $m_C \sim (q - q_c)^{1/2}$  places this type of transitions in the same universality class of the classical ferromagnetic model ( $\beta = 1/2$ ). As can be seen in Fig. (2.4), the order parameter in this case will continuously decrease until reaching zero, at  $q_c$ , indicating a smooth transition between ordered and disordered phases.

In order to reproduce discontinuous, or first-order, phase transitions, one can simply add an extra term in Eq.(2.33),

$$\frac{dm}{dt} = -rm + \frac{u}{2}m^3 - cm^5, \quad (2.35)$$

where  $c > 0$ . Solving this problem in the steady state,  $dm/dt = 0$ , shows that we have now 2 possible steady solutions aside from the trivial one, given by

$$m_{D,1} = \pm \frac{1}{2} \sqrt{\frac{u - \sqrt{u^2 - 16rc}}{c}}, \quad (2.36a)$$

$$m_{D,2} = \pm \frac{1}{2} \sqrt{\frac{u + \sqrt{u^2 - 16rc}}{c}}. \quad (2.36b)$$

As long as  $r < u^2/(16c)$ , both solutions will be real, consistent with the spontaneous symmetry breaking. Conversely, for the solution  $m_{D,1}$ , the transition point will occur when  $r_1 = u^2/(16c)$ , and the system will evolve to the solution  $m = 0$  irrespective of the initial condition. By increasing  $r$  by a sufficiently small amount, the order parameter will present a jump and vanish in a discontinuous way. The solution  $m_{D,2}$  will present the same behavior at a second critical point,  $r_2$ . The region of  $r_2 < r < r_1$  is then marked by bistability, *i.e.*, the system evolves to one of the two possible stable solutions ( $m = 0$  or  $m \neq 0$ ), depending on the initial conditions, which is a trademark of discontinuous phase transitions.

As a final remark, although such a heuristic description is able to capture the transition behavior, it fails to characterize the thermodynamics and nonequilibrium aspects of these systems. Such issues will be addressed in Chapter 3.

# Chapter 3

## Non-Equilibrium Thermodynamics of the Majority Vote Model

The original majority vote model is one of the simplest and most representative nonequilibrium systems exhibiting a continuous phase transition belonging to the same universality class of the Ising model, irrespective of the lattice topology and system neighborhood. More recently [29, 79, 81, 82], it has been shown that the inclusion of an inertial term can shift the phase transition, from continuous to discontinuous. Since these models are irreversible and produce entropy in the (nonequilibrium) steady state regime, a question that naturally arises concerns a thermodynamic description in order to relate the production of entropy with heat as well as to associate a temperature to its dynamics. The central goal of this chapter is to address such points.

### 3.1 Overview of the Majority Vote Model

While the proposition of the majority vote model presented in this dissertation contains the inertial term, it is interesting to make a few comments about the previous work done on the inertia-less case [4].



### 3.1.1 Majority Vote Model without Inertia

The majority vote model is a simple out-of-equilibrium opinion system with  $\mathbb{Z}_2$  (up-down) symmetry whose system's state is described by the configuration given by the collection of  $N$  individual opinion variables (*i.e.*, spins),  $\sigma \equiv \{\sigma_1, \sigma_2, \sigma_3, \dots, \sigma_N\}$ , where  $\sigma_i = \pm 1$  [4, 34]. At any time, each site will be randomly chosen and change its spin to be aligned with the average spin of its  $k$ -neighbours with probability  $1 - f$ , and with complementary probability  $f$ , the spin does not follow the majority rule, and remains unchanged. More specifically, the transition rate from  $\sigma_i$  to  $-\sigma_i$  is given by

$$\omega_i(\sigma) = \frac{1}{2} [1 - (1 - 2f)\sigma_i \text{sgn}(\ell)], \quad (3.1)$$

where  $\text{sgn}(\bullet)$  is the sign function and  $\ell = \sum_{\delta} \sigma_{i+\delta}^k$  is the sum over the spins of the  $k$  neighbors of site  $i$ .

The model dynamics are governed by the following master equation,

$$\dot{P}(\sigma, t) = \sum_i^N \{ \omega_i(\sigma^i) P(\sigma^i, t) - \omega_i(\sigma) P(\sigma, t) \}, \quad (3.2)$$

where  $\omega(\sigma)$  denotes the transition rate. From the configuration in which the  $i$ -th site flips its spin from  $\sigma_i$  to  $-\sigma_i$  and  $\sigma^i \equiv (\sigma_1, \dots, -\sigma_i, \dots, \sigma_N)$ . Although such a master equation is not exactly solvable, through mean-field theory it is possible to obtain remarkable insight about its phase dynamics.

### 3.1.2 Majority Vote Model with Inertia

While the original majority vote model doesn't present discontinuous transitions [4], the introduction of an inertial term so each site under the possibility of transition has a certain "resistance" to flipping its own spin, together with the variation of the connectivity number, gives rise to discontinuous phase transitions both on regular and complex networks. Aside from the misalignment parameter,  $f$ , and from the number of site connections per site (*e.g.* Euclidean neighbors in a square lattice or number of nodes in a random graph),  $k$ , these transitions will also be influenced by the parameter representing transition inertia,

$\theta$ , making it so the transitions of the spin of site  $i$  from  $\sigma_i$  to  $-\sigma_i$  is given by

$$\omega_i(\sigma) = \frac{1}{2} \{1 - [1 - 2f] \sigma_i \text{sgn}[X_i(\theta, \ell, k)]\}, \quad (3.3)$$

where  $\ell = \sum_{j=1}^k \sigma_j$  represents the sum of the nearest  $k$  spins, *i.e.*, the majority's spin,  $\text{sgn}(X)$  is the sign function, and  $X_i = (1 - \theta)\ell + k\theta\sigma_i$  attempts to the competition between local and majority opinions, through the connectivity. In the case of  $\theta = 0$ , the model is reduced to the original formulation presented previously [29]. When  $\theta > 0$ , depending on the topology and connectivity (illustrated in Fig.3.1), the model can predict a shift in the nature of the phase transitions (from continuous to discontinuous) [4, 83–88].

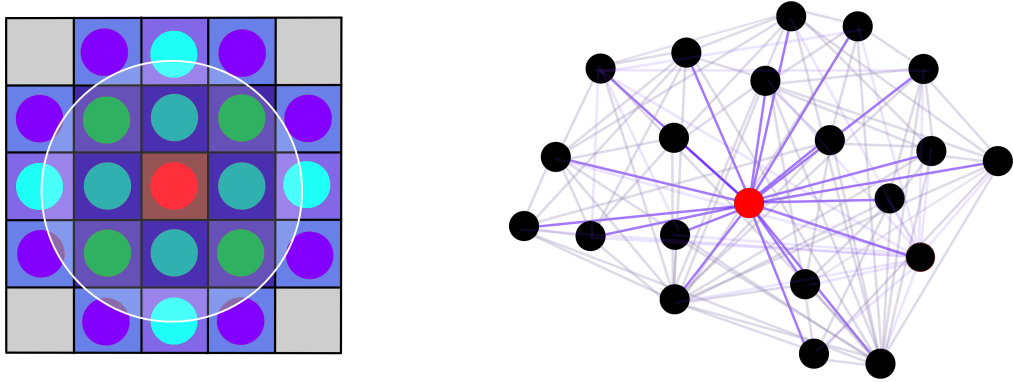


Figure 3.1: Illustration of the topologies studied in this work. The left panel shows a regular square lattice in which each site has  $k = 20$  neighbors. The right panel presents a (simplified) illustration of a random regular network where each node has  $k = 20$  connections.

In configurations described by the latter condition, the inertia will effectively control the minimum value of  $\ell$  for which transitions occur with rate  $1 - f$ . In the case of  $\sigma_i = 1$ , the site will present the transition  $\sigma_i \rightarrow -\sigma_i$  with probability  $1 - f$  if  $\text{sgn}(X) < 0$ , *i.e.*, if  $X < 0$ , and, naturally,  $\ell > \frac{k\theta}{\theta-1}$ . In the opposite case, when  $\sigma_i = -1$ , the favored transition will happen when  $\text{sgn}(X) > 0$ , for  $X > 0$ , and  $\ell < \frac{k\theta}{\theta-1}$ . For both cases, when  $\ell = \frac{k\theta}{\theta-1}$ ,  $\text{sgn}(X) = 0$  and, therefore, the transitions will be simply  $\frac{1}{2}$ .

From the master equation, together with the magnetization relations  $m = \langle \sigma_i \rangle$  and  $dm/dt = -2\langle \sigma_i \omega_i(\sigma) \rangle$ , the general expression for the magnetization in the *NESS* simply reads

$$m = (1 - 2f) \langle \text{sgn}(X) \rangle. \quad (3.4)$$

As stated before, the above expression can not be exactly solved and for this reason, we are going to perform an approximate treatment, based on a mean-field-analysis. By assuming that the probabilities associated with each site's spin are independent, irrespective of topology, it becomes possible to rewrite the average in Eq.(3.4) as a combination of conditional probabilities,

$$\begin{aligned} \langle \text{sgn}(X) \rangle &= P(X > 0 | \sigma_i = 1) P(\sigma_i = 1) + P(X > 0 | \sigma_i = -1) P(\sigma_i = -1) \\ &\quad - P(X < 0 | \sigma_i = 1) P(\sigma_i = 1) + P(X < 0 | \sigma_i = -1) P(\sigma_i = -1), \end{aligned}$$

where each conditional probability is approximated via a product of a constant belonging to the connectivity and the number of spins, in the mean-field hypothesis, that are pointing up,  $n_1 = k(1 - 2\theta)/(2(1 - \theta))$ , or down,  $n_2 = k/(2(1 - \theta))$  and

$$P(X > 0 | \sigma_i = 1) = \sum_{n=n_1}^k C_n^k p_+^n p_-^{k-n}, \quad (3.5a)$$

$$P(X > 0 | \sigma_i = -1) = \sum_{n=n_2}^k C_n^k p_+^n p_-^{k-n}, \quad (3.5b)$$

$$P(X < 0 | \sigma_i = 1) = \sum_{n=n_2}^k C_n^k p_-^n p_+^{k-n}, \quad (3.5c)$$

$$P(X < 0 | \sigma_i = -1) = \sum_{n=n_1}^k C_n^k p_-^n p_+^{k-n}. \quad (3.5d)$$

Note that  $\text{sgn}(X)$  is solely expressed in terms of  $m$ ,  $k$ ,  $\theta$  and  $f$ . Furthermore, these results, together with the numerical ones, show the existence of a hysteresis loop (as mentioned in Chapter 2 and in agreement with general theory for discontinuous phase transitions) for the random regular topology, as  $\theta$  and  $k$  are increased, as shown in Figure 3.2, in the forward and backward changing of the control parameter,  $f$ . In the regime of large  $k$ , the above summations can be replaced for Gaussian integrals, in which one can obtain a simplified expression for  $m$ . As can be seen in Ref.[31], this results in the transcendental equation for the order parameter,

$$m = \frac{(1 - 2f)(\text{erf}(a) - \text{erf}(b))}{2 - (1 - 2f)(\text{erf}(a) + \text{erf}(b))}, \quad (3.6)$$

where

$$a = \sqrt{\frac{k}{2}} \left[ \frac{\theta}{1-\theta} + m \right]$$

$$b = \sqrt{\frac{k}{2}} \left[ \frac{\theta}{1-\theta} - m \right].$$

For  $k \rightarrow \infty$ , Eq.(3.6) simplifies to

$$m = \frac{(1-2f)(1 + \text{sgn}[m - \theta/(1-\theta)])}{2 - (1-2f)(1 - \text{sgn}[m - \theta/(1-\theta)])}. \quad (3.7)$$

In order to proceed beyond the mean-field theory, we resort to numerical simulations in

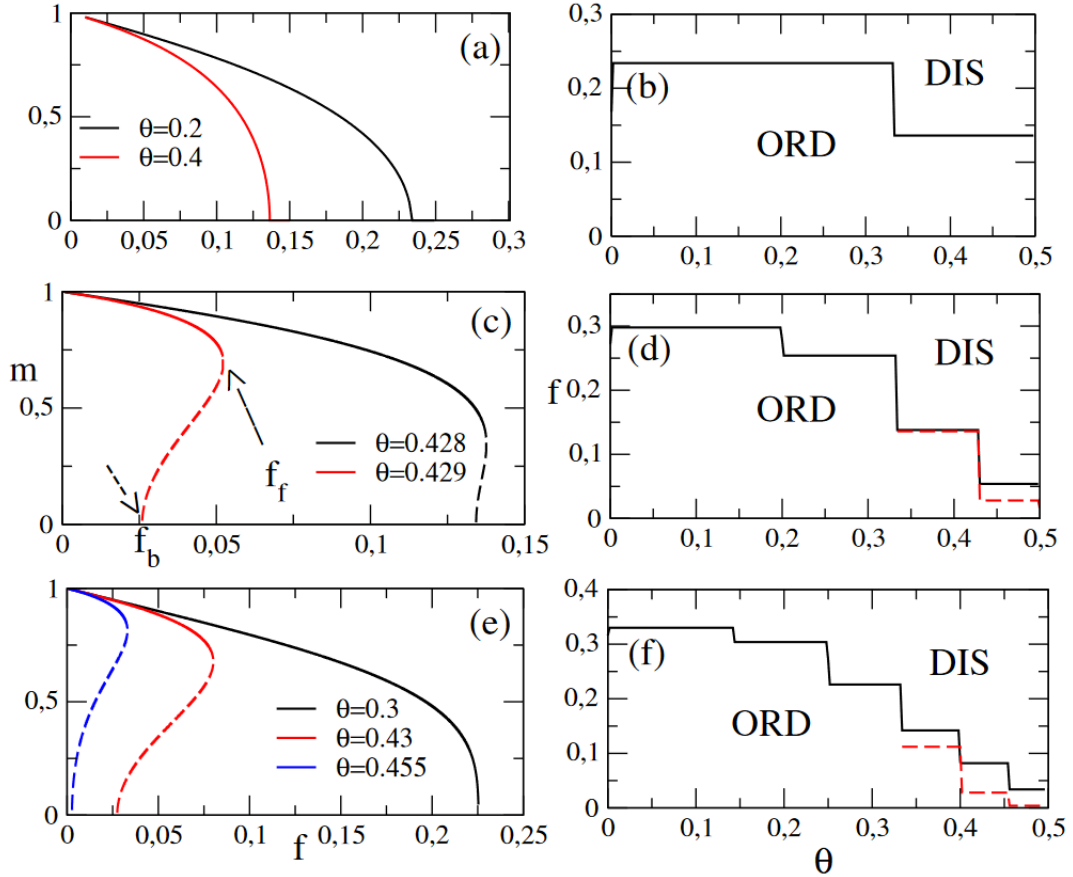


Figure 3.2: From top to bottom, mean-field results for regular networks for  $k = 4$ ,  $k = 8$  and  $k = 12$ , respectively. Left panels show the behaviour of magnetization, whereas right panels shows the respective phase diagrams. Figure adapted from [31]

which a spin flip is performed according to the transition rates given by Eq. (3.3). For the sake of illustration, we plot the behavior of the magnetization for regular lattices and random regular graphs in Fig.(3.3) for different system sizes.

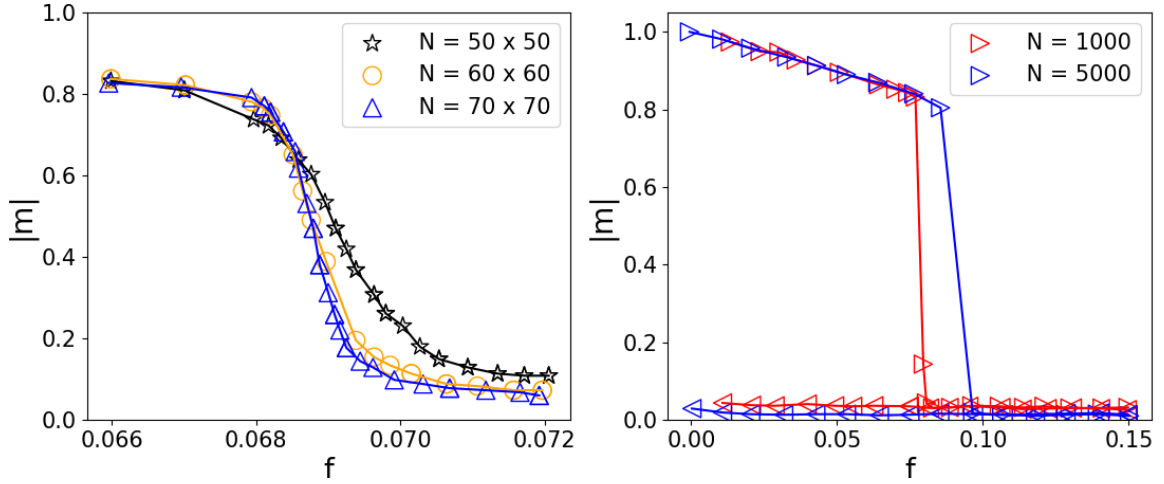


Figure 3.3: Behavior of magnetization for (left) the regular square lattice and (right) random regular topology, with forwards and backwards trajectories indicated via the  $\triangleright$  and  $\triangleleft$  symbols, respectively. For both panels,  $\theta = 3/8$  and  $k = 20$ . It's interesting to note that as  $N \rightarrow \infty$ , for the complex topology, the behavior of magnetization approaches the one expected for the mean-field results, showing an increasing abrupt drop at the critical point.

The above findings highlight the role of inertia in order to shift the phase transition. In order to describe it in more detail, as well as its influence on the model thermodynamics (to be described further), we can resort again, for a given  $\theta$  and  $k$ , to the threshold value,  $\ell^* = \frac{\sigma k \theta}{\theta - 1}$ , that will define the minimum majority configuration of (for simplicity),  $|\ell|$ , for the spin flip to occur with probability  $1 - f$ . In other words, the transition rate will be given by the complementary probability  $f$  as long as  $|\ell| < |\ell^*|$ . The consequence of these competing dynamics will directly affect the nature of the transitions predicted by the model, the phase diagrams, and thermodynamic quantities [30, 85–87]. The threshold inertia,  $\theta^*$ , given by  $\theta^* = \frac{2\ell}{k+2\ell}$ , marks the existence of plateaus in the phase diagram (see, *e.g.* Fig 3.4), in which transition rate reads  $1 - f$  for  $\theta < \theta^*$  and  $f$  otherwise. For example, for  $k = 20$ , the plateau positions occur at the following values of inertia

$$\theta^* = \left\{ \frac{1}{11}, \frac{1}{6}, \frac{3}{13}, \frac{2}{7}, \frac{1}{3}, \frac{3}{8}, \frac{7}{17}, \frac{4}{9}, \frac{9}{19}, \frac{1}{2} \right\}. \quad (3.8)$$

whose effect on the phase diagram is shown in Fig.(3.4). Note that plateau's positions do not depend on the lattice topology.

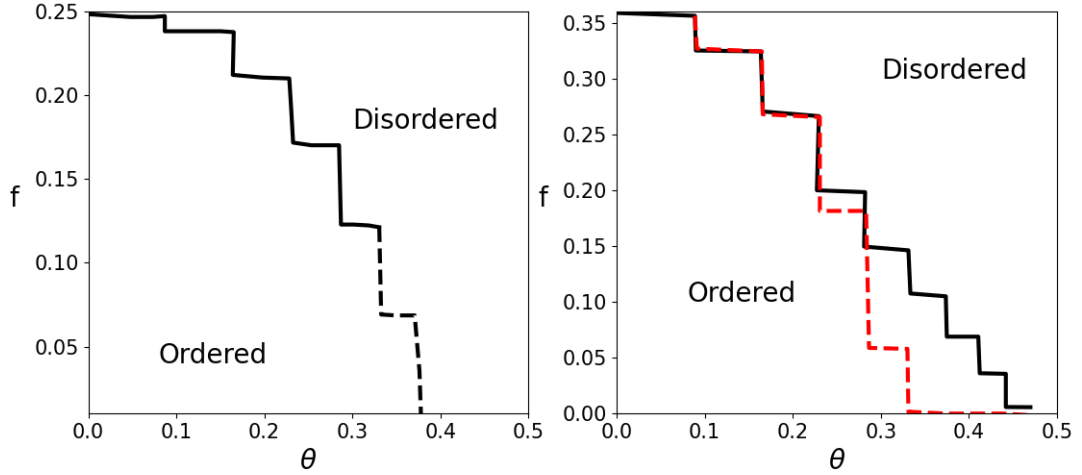


Figure 3.4: Phase diagrams in the  $f \times \theta$  plane for (left) a regular square lattice and (right) a random regular network, for connectivity  $k = 20$ . Solid lines represent continuous transitions, whereas dashed lines indicate discontinuous transitions. The colors black and red on the right panel indicate the forwards and backwards changing of the misalignment parameter,  $f$ , being respectively increased or decreased for the same initial condition.

### 3.1.3 Entropy Production

As mentioned previously in Chapter 2, the model description in terms of the magnetization does not characterize the nonequilibrium feature of such systems. In Ref. [31], the irreversible feature of such systems is characterized in terms of entropy production at the steady state, given by,

$$\langle \sigma \rangle = k_B \sum_i \left\langle \omega_i(\sigma) \ln \frac{\omega_i(\sigma)}{\omega_i(\sigma^i)} \right\rangle. \quad (3.9)$$

Using the transition rates from Eq.(3.1), the ratio inside the  $\ln(\bullet)$  term can be rewritten as

$$\frac{\omega_i(\sigma)}{\omega_i(\sigma^i)} = \sigma |\ell| \operatorname{sgn}(\ell) \ln \frac{1 - (1 - 2f)|\ell|}{1 + (1 - 2f)|\ell|},$$

so the average entropy production becomes

$$\langle \sigma \rangle = \sum_i \frac{1}{2} \left\langle \left[ \sigma \operatorname{sgn}(X) - |\ell|(1 - 2f) \operatorname{sgn}^2(X) \right] \ln \frac{1 - (1 - 2f)|\ell|}{1 + (1 - 2f)|\ell|} \right\rangle. \quad (3.10)$$

Using the one-site approximation and following the procedures presented in Ref.[31], this simplifies to

$$\langle \sigma \rangle = \frac{N}{2} \ln \frac{1 + (1 - 2f)|\ell|}{1 - (1 - 2f)|\ell|} \left[ \frac{m^2}{(1 - 2f)|\ell|} - (1 - 2f)|\ell| \right]. \quad (3.11)$$

It is now important to draw a few comments about this result. First, for continuous transitions, Eq. (3.11) is continuous at the vicinity of the critical point, where  $m \sim (f - f_c)^{1/2}$ , but its derivative in respect to  $f$  presents a discontinuity at  $f_c$ . Second, this behavior, characterized via the mean-field exponent  $\alpha = 0$ , together with the previously calculated  $\beta = 1/2$  and (obtained via the variance of the order parameter)  $\gamma = 3/2$ , shows that the critical point,  $f_c$ , is characterized via the aforementioned discontinuity of  $d\sigma/df$  (see Section 3.1.4 for a more detailed discussion), reinforced by the fact that the critical exponents follow the hyperscaling relation,  $\alpha + \beta + \gamma = 2$ . It then becomes possible to characterize both types of transitions, continuous or not, using the entropy production and its first derivative with respect to the control parameter [29, 62].

Finally, proceeding analogously, it's possible to define the entropy production for this system in the presence of inertia. The ratio of the transition rate and its inverse then reads,

$$\frac{w_i(\sigma)}{w_i(\sigma^i)} = \frac{1 - (1 - 2f)\sigma_i \text{sgn}[(1 - \theta)\ell + k\theta\sigma_i]}{1 + (1 - 2f)\sigma_i \text{sgn}[(1 - \theta)\ell - k\theta\sigma_i]}. \quad (3.12)$$

As previously stated, the argument of the  $\text{sgn}$ , for a given  $k$  and  $\theta$ , will be non-zero only for certain values of  $\ell$ . This indicates that only certain local configurations will contribute to the production of entropy [31, 34]. For  $\ell \neq k\theta/(1 - \theta)$ , Eq. (3.12) can be conveniently rewritten as

$$\ln \frac{w_i(\sigma)}{w_i(\sigma^i)} = -\sigma_i \text{sgn}(\ell) H \left[ \left| \ell - \frac{k\theta}{1 - \theta} \right| \right] \ln \left( \frac{1 - f}{f} \right), \quad (3.13)$$

where  $H(\bullet)$  is the Heaviside theta function. However, for  $\ell = k\theta/(1 - \theta)$ , Eq. (3.13) acquires a distinct value given by  $\ln(w_i(\sigma)/w_i(\sigma^i)) = \sigma_i \text{sgn}(\ell) \ln(2f)$ . Finally, by substituting Eq.(3.3) and Eq.(3.13) in Eq.(3.12), we obtain an expression for the entropy production in terms of the misalignment parameter,

$$\langle \sigma \rangle = \frac{1}{2} \ln \frac{1 - f}{f} \left\{ (1 - 2f) \left\langle \text{sgn}^2(\ell) H \left[ \left| \ell - \frac{k\theta}{1 - \theta} \right| \right] \right\rangle - \left\langle \sigma_i \text{sgn}(\ell) H \left[ \left| \ell - \frac{k\theta}{1 - \theta} \right| \right] \right\rangle \right\}, \quad (3.14)$$

An illustration of the relationship between  $\theta$  and  $\ell/k$  that allows for the contribution to

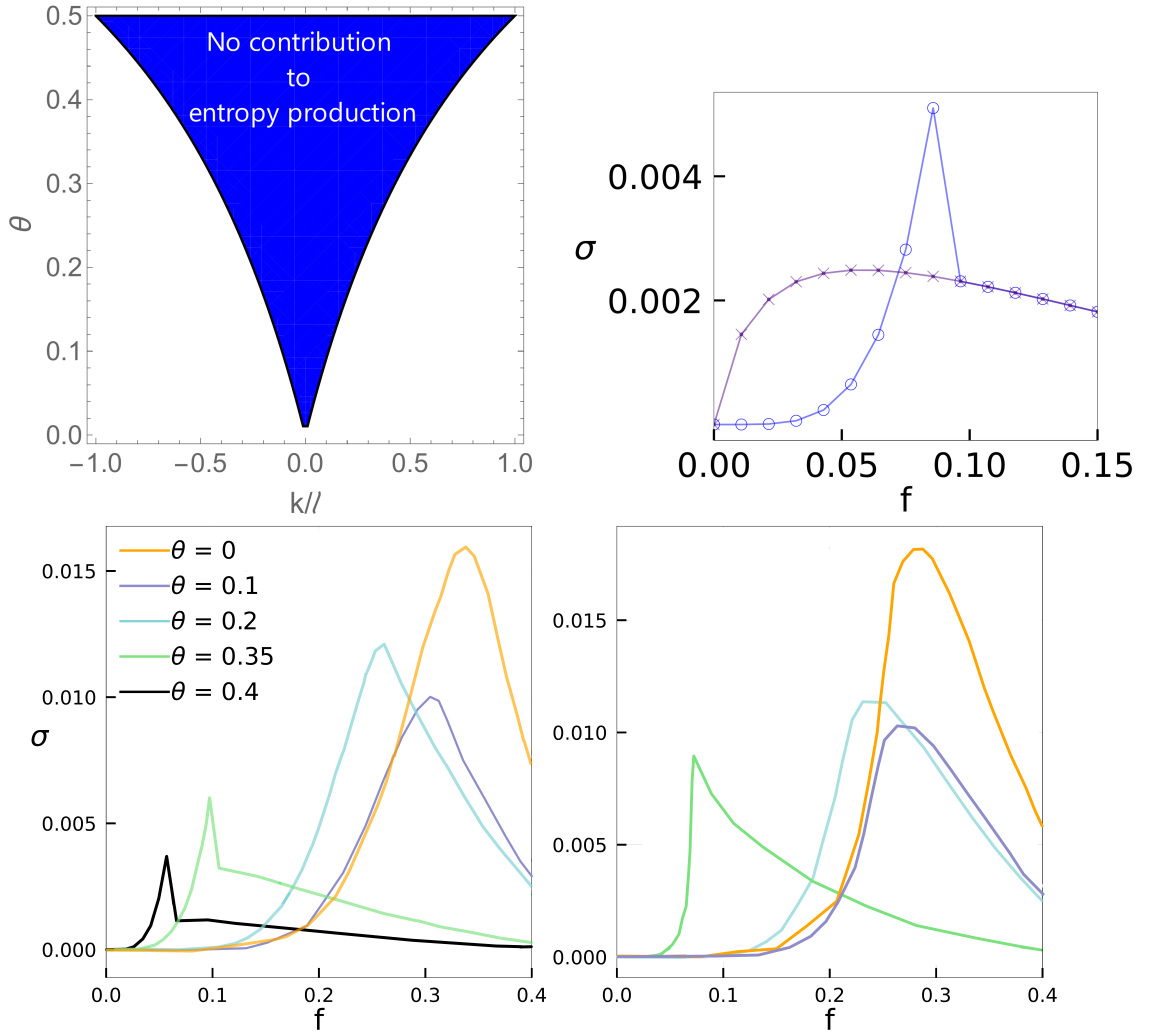


Figure 3.5: Top left: Scheme representing the values of  $\ell^*$  for  $\eta_i = \pm 1$  corresponding to the plateaus. In the shaded area, where  $|\ell| < |\ell^*|$ , the neighborhoods do not contribute to the entropy production. Dashed lines indicate the values of  $\theta^*$ . Top right: hysteresis loop for entropy production on a random graph for  $k = 20$  and  $\theta = 3/8$ . Bottom: entropy production obtained via numerical simulations for different values of  $\theta$ ,  $k = 20$ ,  $N = 1600$ , and a (left) random regular network and a (right) regular lattice.

entropy production, alongside the curves of said thermodynamic quantity for different configurations is presented in Fig.(3.5).

### 3.1.4 Finite-Size Scaling for the Entropy Production

According to finite-size scaling (FSS) theory, at the vicinity of the critical point,  $f_c$ , a given quantity  $X$  [ $X \in (|m|, \chi$  and  $\sigma' \equiv d\sigma/df$ )] will behave as  $X = N^{y_x/\nu} f_x(N^{1/\nu}|\epsilon|)$ , where  $f_x$  is a scaling function,  $\epsilon = (f - f_c)/f_c$  is the distance to the criticality and  $y_x$  is the critical exponent obtained from ( $y_x = -\beta, \gamma$  and  $\alpha$ )[89]. The last exponent is similar



to the relationship between the thermal derivative of the entropy,  $S$ , and specific heat,  $C$ , in equilibrium phase transitions (recalling that  $C = N^{\alpha/\nu} f_c(N^{1/\nu}|\epsilon|)$  [89], illustrating that the connection between entropy production and exchanged heat presented here introduces a physical argument for such scaling behavior.

In this work, we focus on its relationship with discontinuous phase transitions (for continuous phase transitions, see Ref.[33]). For a generic ensemble average  $X$ , the starting point consists of assuming a bimodal Gaussian distribution, centred at  $\mu_o$  and  $\mu_d$  (with associated variances  $\chi_o$  and  $\chi_d$ ). In the case of the steady entropy production at the vicinity of  $\epsilon = f - f_c$ , a bimodal entropy production probability distribution centered at  $\mu_o$  and  $\mu_d$  (with associate variances  $\chi_d$  and  $\chi_o$ ) leads to the approximate expression for  $\sigma$ :

$$\langle \sigma \rangle \approx \frac{\mu_o + \bar{\alpha}\mu_d e^{-N[(\mu_o - \mu_d)\epsilon]}}{1 + \bar{\alpha}e^{-N[(\mu_o - \mu_d)\epsilon]}}, \quad (3.15)$$

where  $\bar{\alpha} = \sqrt{\chi_d/\chi_o}$ . We note that the ordered and disordered phases are favored as  $\epsilon < 0$  and  $\epsilon > 0$  (assuming that  $\mu_o < \mu_d$ ), respectively, and  $\sigma = (\mu_o + \bar{\alpha}\mu_d)/(1 + \bar{\alpha})$  at  $\epsilon = 0$ , indicating that all entropy production curves, simulated for distinct  $N$ 's, will cross at the transition point  $f_c$ . Having  $\sigma$ , its derivative in respect to  $f$  behaves at the vicinity of  $f_c$  as:

$$\langle \sigma' \rangle \approx \frac{N(\mu_o - \mu_d)^2 e^{N(\mu_o - \mu_d)\epsilon}}{\bar{\alpha}(1 + \bar{\alpha}e^{N(\mu_o - \mu_d)\epsilon})^2}, \quad (3.16)$$

showing that  $\sigma'$  scales with  $N$  at the coexistence  $\epsilon = 0$ , in agreement with the above finite size expression for the quantity  $X$ . Alternatively (and analogously), Eq. (3.15) is obtained by resorting to the ideas presented in [90–92], where coexisting phases are treated via a two-state model in which ordered and disordered phases are given by transition rates exhibiting an exponential dependence on the system size  $N$  and proportionality to the distance  $\epsilon$  to the transition point:

$$a \sim k\sqrt{\chi_a}e^{-N(c_0 - c_a\epsilon)}, \quad b \sim k\sqrt{\chi_b}e^{-N(c_0 + c_b\epsilon)}, \quad (3.17)$$

where  $k, c_0, c_a, c_b > 0$  are constants. "Ordered" and "disordered" probabilities,  $p$  and  $q$  respectively, are related to rates  $a$  and  $b$  by means of relations  $p = b/(a+b)$  and  $q = 1 - p$ , given by  $p = \sqrt{\chi_b}(\sqrt{\chi_b} + \sqrt{\chi_a}e^{cN\epsilon})^{-1}$ , where  $c = c_a + c_b > 0$ . As shown in Ref. [91], a given ensemble average (including the entropy production  $\sigma = \langle \sigma_\tau \rangle / \tau$  averaged over a sufficiently long time  $t \rightarrow \infty$  and over many independent stochastic trajectories has its

average given by  $\sigma = \mu_a p + \mu_b b$ , where

$$\langle \sigma \rangle \approx \frac{\mu_b \sqrt{\chi_b} + \mu_a \sqrt{\chi_a} e^{cN\epsilon}}{\sqrt{\chi_b} + \sqrt{\chi_a} e^{cN\epsilon}}, \quad (3.18)$$

which has precisely the form of Eq. (3.15).

The main features of discontinuous phase transitions are summarized in Fig. 3.6. From now on we shall consider  $k = 20$  again, which exhibits a discontinuous phase transition for  $\theta > 1/3$ , as depicted in panel Fig.3.6(a). Aforementioned portraits are exemplified in panels (b) – (d) for  $\theta = 3/8$ . We remark that continuous lines, given by Eq. (3.15), describe very well the behavior of the entropy production and its derivative, the latter presenting a maximum at  $f_c^*$  scaling with  $N^{-1}$ , whose value as  $N \rightarrow \infty$  agrees very well with those obtained from the crossing among curves.

## 3.2 Thermodynamics of The Majority Vote Model

Historically, the properties of the majority vote model have been studied without thermodynamic consideration, mostly due to its inherent inconsistency in this regard. In other words, the MV is a model defined by probabilistic rules in such a way that no energy has been associated with transitions nor connection with temperature has been considered previously [4, 33]. To tackle this issue, our approach consists of assuming that the one-site transition rate,  $\omega_i(\sigma)$ , can be decomposed in  $\ell$  distinct components, each component as being associated with a given thermal bath, with reciprocal inverse temperature,  $\beta_\ell$ , as illustrated in Fig. (3.7). Note that such assumption (transition decomposed as a sum of mutually excludent transition rates) can be performed since at each time the site  $i$  has solely a given specific neighborhood (ranging from  $-\ell$  to  $\ell$ ). However, due to the  $\mathbb{Z}_2$  symmetry, transitions with  $\ell$  and  $-\ell$  nearest neighbor sites can be associated to the same reservoir. We then represent the one-site transition rate,  $\omega_i(\sigma)$ , as the total sum of the  $k/2$  unique contributions associated with the distinct thermal baths of each  $|\ell|$ -th reservoir, allowing for the definition of each rate using mutually excludent Glauber-form rates,

$$\omega_i(\sigma) = \sum_{\ell} \omega_{\ell i}(\sigma) = \sum_{\ell} \frac{\alpha_{\ell}}{2} [1 - \tanh(\beta_{\ell} \Delta E / 2)], \quad (3.19)$$

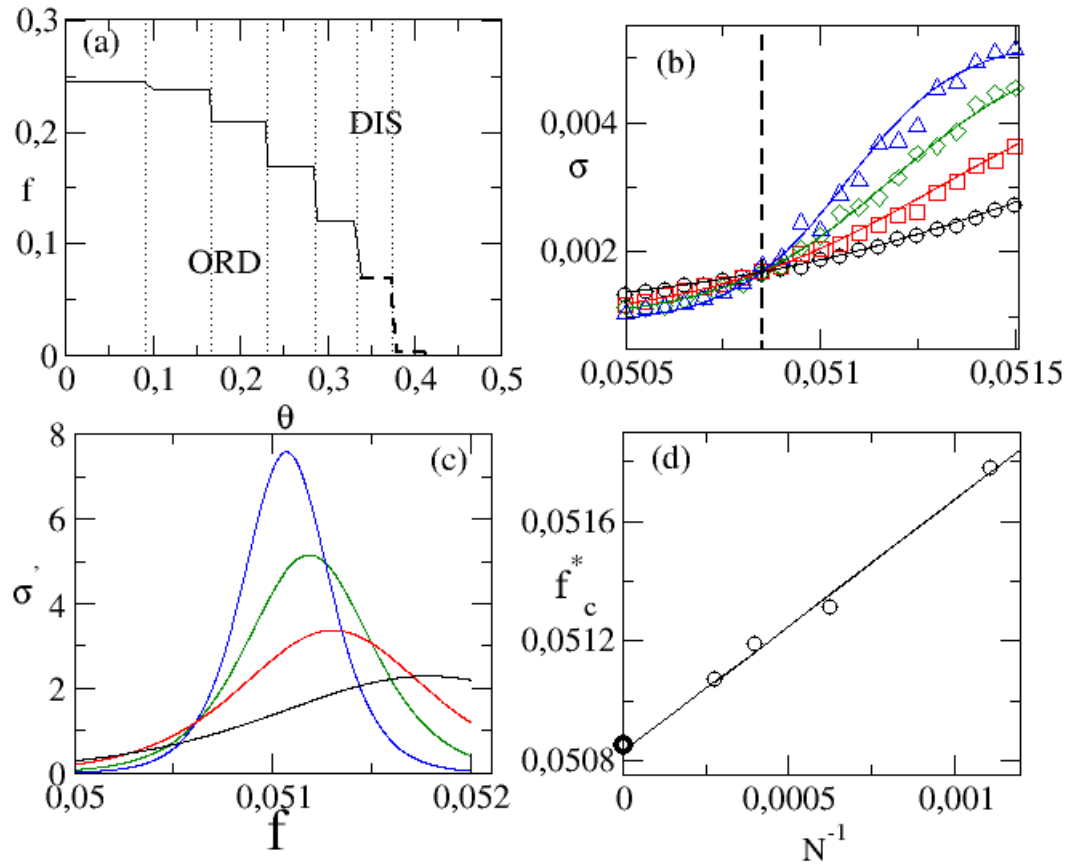


Figure 3.6: In (a), the phase diagram of the inertial majority model for a regular lattice for  $k = 20$ . Panel (b) depicts the entropy production  $\sigma$  for distinct system sizes  $N = L^2$ . Continuous lines denote the phenomenological description from Eq. (3.15) and vertical line corresponds to the crossing among entropy production curves at  $f_c = 0.05085(2)$ . In (c), the derivative  $\sigma' \equiv d\sigma/df$  versus  $f$  obtained from continuous lines in (b). Panel (d) show the position  $f_c^*$  of maximum of  $\sigma'$  versus  $N^{-1}$  and its accordance with the crossing among entropy production curves yielding (symbol  $\bullet$ ) as  $N \rightarrow \infty$ .

where  $\alpha_\ell$  is a constant and  $\Delta E$  denotes the energy to "flip" a site's opinion, that, due to the model's  $Z_2$  symmetry, can be written in an Ising-like form,  $E(\sigma) = -J \sum_{\langle ij \rangle} \sigma_i \sigma_j - h \sum_i \sigma_i$ , where  $J$  stands for the interaction strength between sites and  $h$  would be an analogous to the magnetic field [72]. Note that for a generic  $Z_2$  dynamics, the energy of the system being expressed according to the Ising form is the most general form accounting the interaction between nearest neighbor spins. In the present case, due to  $Z_2$  symmetry, we set  $h = 0$  for all values of  $\theta$ .

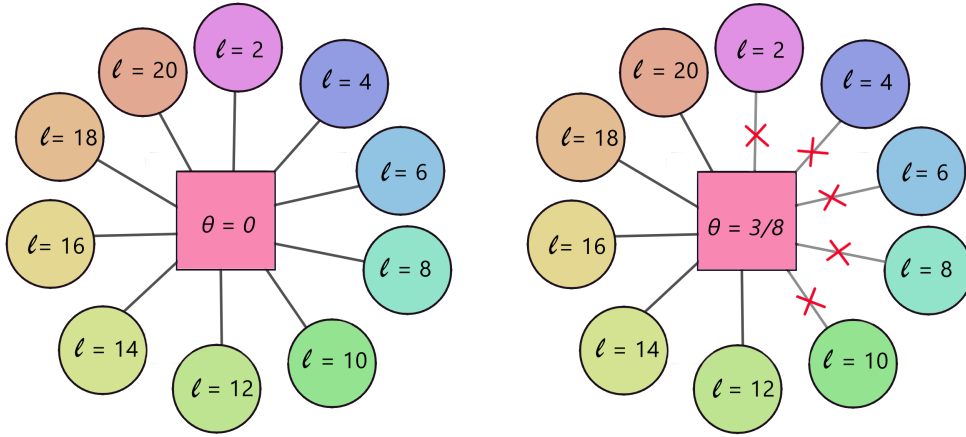


Figure 3.7: Simple illustration of the approach proposed: a given system with  $k$  connectivity and a certain value of  $\theta$  is assumed to be in contact with  $k/2$  thermal baths, each one associated with a distinct local configurations  $\ell$ . For a given  $\theta$ , the number of baths is either kept at  $k/2$  or reduced, according to  $|\ell^*|$ .

From Eq.(3.19), the ratio between each component  $\omega_{\ell i}(\sigma)$  in the right side and its reverse,  $\omega_{\ell i}(\sigma^i)$ , is given by

$$\frac{w_{\ell i}(\sigma)}{w_{\ell i}(\sigma^i)} = e^{-\beta_\ell [E(\sigma^i) - E(\sigma)]}. \quad (3.20)$$

Once a relationship between transition rates and difference of energy and temperature was introduced, we can obtain the model's thermodynamic properties. As shown in Chapter 2, the mean energy flux,  $d\langle U \rangle/dt$ , can be expressed via the sum of the contributions of each thermal reservoir's heat exchange. By inserting the above energy definition into the master equation, it follows that  $d\langle U \rangle/dt = \Phi_\ell$ , where

$$\Phi_\ell = \sum_i \langle [E(\sigma^i) - E(\sigma)] \omega_{\ell, i}(\sigma) \rangle \quad (3.21)$$

implying that  $\sum_\ell \Phi_\ell = 0$  at the *NESS*, consistent with the first law of thermodynamics. Similarly, both entropy production and flux will also be decomposed according to the  $\ell$ -th thermal reservoir. Since the entropy change vanishes at the *NESS*,  $dS/dt = \sum_\ell (\Pi_\ell - \sigma_\ell)$ ,

the entropy production and entropy flux can be identified by Eq. (3.22):  $\Pi = \sum_{\ell} \Pi_{\ell} = \sum_{\ell} \sigma_{\ell} = \sigma$ . The expressions above are consistent with Refs. [40, 93]. Finally, by inserting Eq. (3.20) into Eq. (3.14), each entropy flux component  $\sigma_{\ell}$  is related with exchanged heat  $\Phi_{\ell}$  by a Clausius-like form  $\sigma_{\ell} = -\beta_{\ell}\Phi_{\ell}$ , where  $\Phi_{\ell}$  is given by Eq. (3.21). Alternatively,  $\sigma$  can also be written in the usual thermodynamics form as a sum of thermodynamic fluxes times forces:

$$\sigma = - \sum_{\ell} \beta_{\ell} \Phi_{\ell} \quad \text{or} \quad \sigma = \sum_{\ell \neq 2} X_{\ell} \Phi_{\ell}, \quad (3.22)$$

where the second temperature was set as a reference to define all  $(k/2) - 1$  thermodynamic forces  $X_{\ell} \equiv \beta_2 - \beta_{\ell}$ , associated with its respective flux,  $\Phi_{\ell}$ . For simplicity, we set the Ising interaction parameter to  $J = 1$ . The relationship between the temperature and the model parameters is obtained as follows. From the expression for  $E(\sigma)$ , it follows that  $\Delta E = 2\sigma_i \ell$ , which can be rewritten as  $\Delta E = 2\sigma_i |\ell| \text{sgn}(\ell)$ . By taking the logarithm of Eq. (3.20), it follows that

$$\ln \frac{w_{\ell i}(\sigma)}{w_{\ell i}(\sigma^i)} = -2\beta_{\ell} |\ell| \sigma_i \text{sgn}(\ell). \quad (3.23)$$

Since the rates associated with each thermal bath are mutually excludent, from the direct comparison with Eq. (3.13) for a given  $\ell$  provides to obtain each (reciprocal inverse) temperature  $\beta_{\ell}$  given by

$$\beta_{\ell} = \frac{1}{2|\ell|} H \left[ |\ell| - \frac{k\theta}{1-\theta} \right] \ln \left( \frac{1-f}{f} \right), \quad (3.24)$$

where  $\beta_2 = 2\beta_4 = 3\beta_6 \dots = k\beta_k/2$  in the inertialess case. We pause to make a few comments. First, Eq. (3.24) is one of the main results of this chapter. It extends the calculation of temperatures for a given neighborhood and inertia, and reduces to the expression from Ref. [33] as  $\theta = 0$ . Second,  $\beta_{\ell}$  vanishes for large enough values of inertia  $\theta > \theta_p$ , illustrating that despite a heat flux associated with the  $\ell$ -th reservoir being well-defined, it does not produce entropy. Third and last, the temperature assumes a different value for  $\theta = \theta^*$  given by

$$\beta_{\ell} = -\frac{1}{2|\ell|} \ln(2f). \quad (3.25)$$

This completes our description of the temperature definitions for the MV as well as the influence of inertia. Now we turn to unravel the role of each  $\ell$  to the fluxes of heat and entropy production.

Starting with the inertialess case, where  $\beta_2 > \beta_4 > \dots > \beta_k$ , we argue that the

heat fluxes associated with the states in contact with the coldest and hottest baths are always positive and negative, respectively:  $\Phi_2 < 0$  and  $\Phi_k > 0$ , whose a (non-rigorous) argument is present as follows. Starting with the two thermal baths case ( $k = 4$ ), it is straightforward to verify that, since  $\sigma$  acquires the simple form  $\sigma = (\beta_2 - \beta_4)\Phi_4 > 0$ . Given that  $\beta_2 - \beta_4 > 0$  [cf. Eq. (3.24)], it follows that  $\Phi_4 \geq 0$  and hence  $\Phi_2 = -\Phi_4 \leq 0$ . The case of more than two reservoirs is more intriguing, since intermediate fluxes can be positive, negative, or even change their sign upon  $f$  being varied [see e.g. Fig. 4.3 (d)]. For  $k = 6$ , one has  $\sigma = -(\beta_2 - \beta_6)\Phi_2 - (\beta_4 - \beta_6)\Phi_4 \geq 0$  and three possibilities for  $\Phi_2$  and  $\Phi_4$ . The former, in which both are negative, promptly implies  $\sigma \geq 0$ , whereas the second case,  $\Phi_2 \leq 0$  and  $\Phi_4 \geq 0$ , is also consistent since  $-(\beta_2 - \beta_6)\Phi_2 \geq (\beta_4 - \beta_6)\Phi_4$  and hence  $\Phi_6 \geq 0$  (recalling that  $\Phi_6 = -(\Phi_2 + \Phi_4)$ ). The third possibility, in which  $\Phi_2 \geq 0$  and  $\Phi_4 \leq 0$  violates the second law in some cases and thus it is not possible. Similar findings are verified for  $\theta \neq 0$ , but we should note that only neighborhoods with  $\ell^*$  greater than  $\ell - k\theta/(1 - \theta)$  will contribute to the entropy production,  $\sigma = -\sum_{\ell^*}^k \beta_\ell \Phi_\ell$ . For example, for  $k = 20$  and distinct inertia intervals  $3/8 < \theta \leq 7/17$ ,  $7/17 < \theta \leq 4/9$ ,  $\theta > 4/9$ , the corresponding entropy productions read  $\sigma = -\sum_{\ell=14}^k \beta_\ell \Phi_\ell$ ,  $\sigma = -\beta_{16}\Phi_{16} - \beta_{18}\Phi_{18} - \beta_{20}\Phi_{20}$  and  $\sigma = -\beta_{18}\Phi_{18} - \beta_{20}\Phi_{20}$ , such latter one similar to the  $k = 4$  case (but here  $\sum_{\ell=2}^k \Phi_\ell = 0$ ) and once again illustrating that  $\Phi_{\ell^*=18} \leq 0$  and  $\Phi_{k=20} \geq 0$ . We close this section by pointing out that, despite the above non-rigorous argument, the general finding  $\Phi_{\ell^*} \leq 0$  and  $\Phi_k \geq 0$  has been verified in all cases. In contrast, it is not possible to draw general conclusions about intermediate fluxes, in which some change sign as  $f$  increases.

### 3.2.1 Fluctuation theorems

Thermodynamic consistent systems satisfy the detailed fluctuation theorem (DFT) for the entropy production, which gives rise to the stochastic version of the second law. It states that negative fluctuations of the integrated entropy production are exponentially suppressed by the positive counterparts. For a given integration window  $\tau$ , the DFT is asymptotically valid for  $\Sigma = \int_0^\tau \sigma(t)dt$  at the NESS since it is equal to the entropy production:

$$\lim_{\tau \rightarrow \infty} \ln \frac{P_\tau(\Sigma)}{P_\tau(-\Sigma)} = \Sigma, \quad (3.26)$$

where  $P_\tau(\Sigma)$  represents the probability of measuring  $\Sigma$  in a trajectory of length  $\tau$ . This relation holds beyond the long-time limit when the internal change of configuration entropy is considered in addition to the entropy fluxes. Consequence of the above, the integral

fluctuation theorem (IFT) reads

$$\lim_{\tau \rightarrow \infty} \langle e^{-\Sigma} \rangle_{\tau} = 1 \quad (3.27)$$

and is useful for relating the components of  $\Sigma$ , such as in the celebrated Jarzynski equality [94] that relates the statistics of work to free energy differences, bridging equilibrium and nonequilibrium quantities. The feasibility of employing such methods is tightly related to the ability to observe fluctuations in the trajectories, which become rare as  $\tau$  increases. We explore the manifestation of these relations, cornerstones of stochastic thermodynamics, in the MV vote model.

The left panel of Fig. 3.8 shows the convergence of the left-hand side of Eq. (3.26) to its right-hand side as the integration windows get larger for the entropy production evaluated from Eq. (3.22). Observing the DFT becomes an expensive task even for small systems since the negative fluctuations of entropy production become increasingly rare for larger values of  $\tau$ . The right panel shows the left-hand side of the IFT in Eq. (3.27), which converges to one despite the presence of inertia. It is worth mentioning that the convergence is observed from above and from below. Although no general conclusion can be drawn, the behavior of these fluctuation relations might be related to the phase transitions: In the examples, the IFT presents a slower convergence at the vicinity of the phase transition.

### 3.2.2 Heat fluxes at phase transitions

According to Eq. (3.21), every heat flux  $\Phi_{\ell}$  is an ensemble average in similarity with the entropy production and, for this reason, we expect at least the most significant components of the entropy production to behave similarly to  $\sigma$  at the vicinity of a phase transition. As described previously, at discontinuous phase transitions, the curves of entropy production cross at  $f_c$  for distinct system sizes in regular lattices, and a hysteretic branch is present in complex topologies [31]. Thus, a similar behavior might be expected for the most significant heat flux components. These features are promptly verified for the largest fluxes  $\ell = 12, 14$  and  $20$ . For a regular lattice, panels (a)-(c) of Fig. 4.3 display the crossing of the fluxes for different system sizes, and panel (d) shows the quantitative value of each individual flux. For a random-regular network, panels (a)-(c) of Fig. 3.10 show the hysteresis branch while (d) shows individual flux values. The continuous lines in

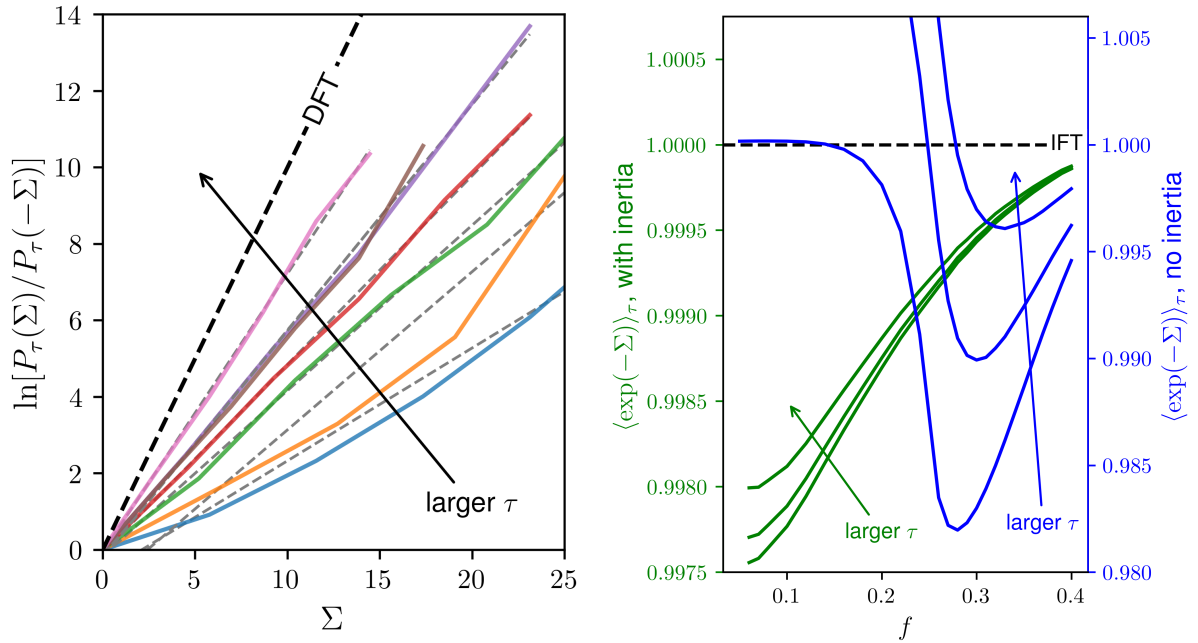


Figure 3.8: *Left*: Convergence to the detailed fluctuation theorem as integration window  $\tau$  increases for a lattice  $L = 6$  and  $f = 0.04$ ; solid lines are simulation results while dashed lines are the respective linear fits. *Right*: Convergence to the integral fluctuation theorem for the case with no inertia (blue) and with inertia  $\theta = 3/8$  (green); additional parameters are  $k = 20$  and  $N = 10^4$ .

panels Fig. 4.3 (a)-(c) are obtained from the bimodal Gaussian description in Eq. (3.15), in good agreement with the simulation results. Remarkably, for both regular and complex topologies, the phase transition can be probed and precisely located from the behavior of any individual flux.

### 3.2.3 Contributions to dissipation

Inspecting of the thermodynamic contribution of individual values of  $\ell$  raises the question of how each type of neighborhood contributes to entropy production, a measure of dissipation. As previously discussed, the second law imposes  $\Phi_{\ell^*} < 0$  and  $\Phi_k > 0$  irrespective of  $f$ , and also local configurations satisfying  $|\ell| < |\ell^*|$  do not dissipate. Taking into account that some intermediate fluxes  $\Phi_\ell$  are non-monotonic in terms of  $f$ , one could expect that they would present a less significant contribution. Inspired by evidence from simulations, we observe the predominance of  $\Phi_{\ell^*}$  and  $\Phi_k$ , hence we introduce the contribution of these two fluxes as  $\sigma_{\ell^*,k} = -\beta_{\ell^*}\Phi_{\ell^*} - \beta_k\Phi_k > 0$ . This represents an approximation but not a bound since the remaining fluxes can change their signs.



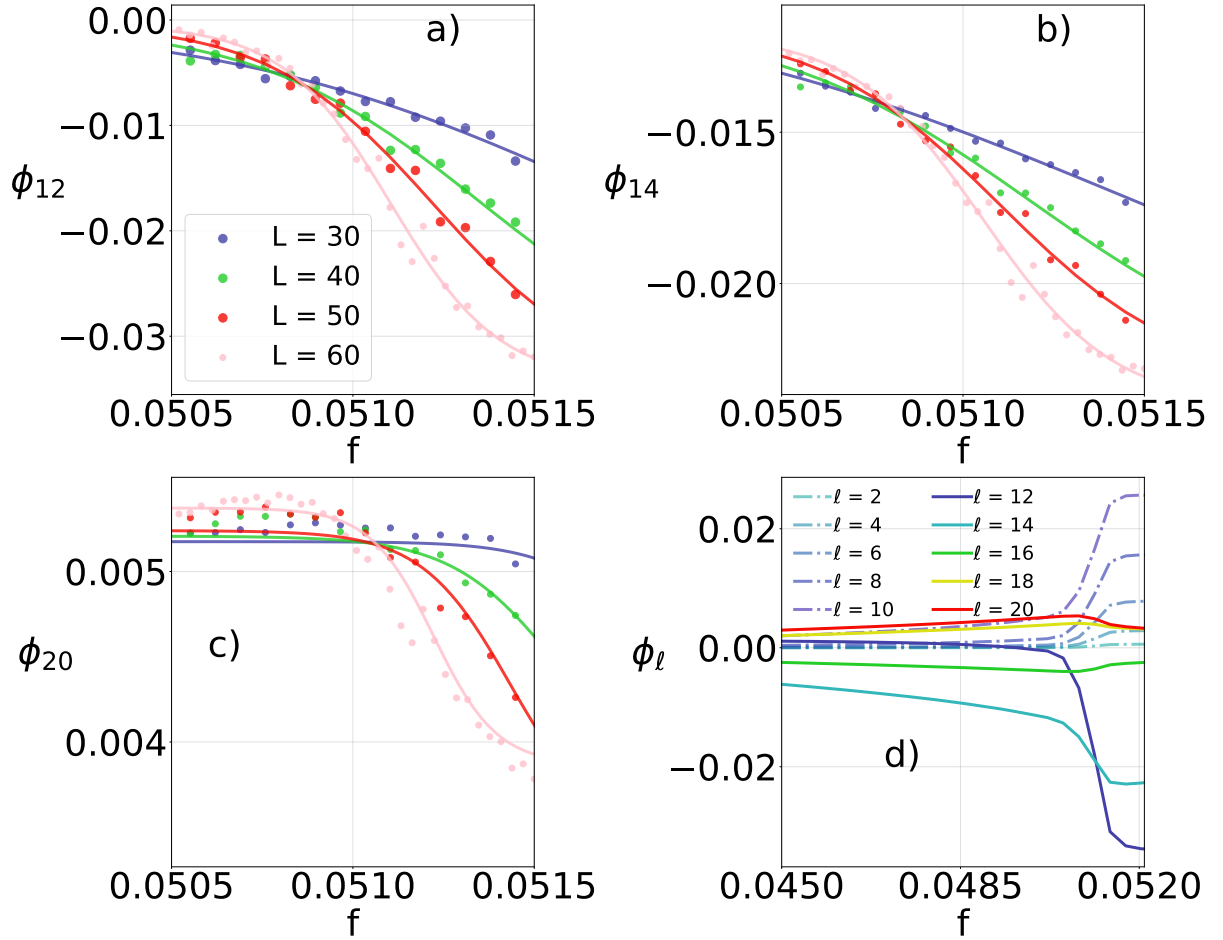


Figure 3.9: For the regular lattice with  $\theta = 3/8$ ,  $k = 20$  and distinct system sizes  $N = L^2$ , panels (a)-(b) depict the most representative (largest absolute values) heat fluxes per particle  $\Phi_\ell$ 's versus control parameter  $f$ . Continuous lines denote correspond to the phenomenological approach according to the ideas of Eq. (3.15). Although the component heat flux panel (c) mildly changes with  $f$ , all curves also cross at  $f_c$ . Panel (d) shows all  $\Phi_\ell$ 's ( $\ell = 2, 4, \dots, k$ ) for  $N = 60^2$ .

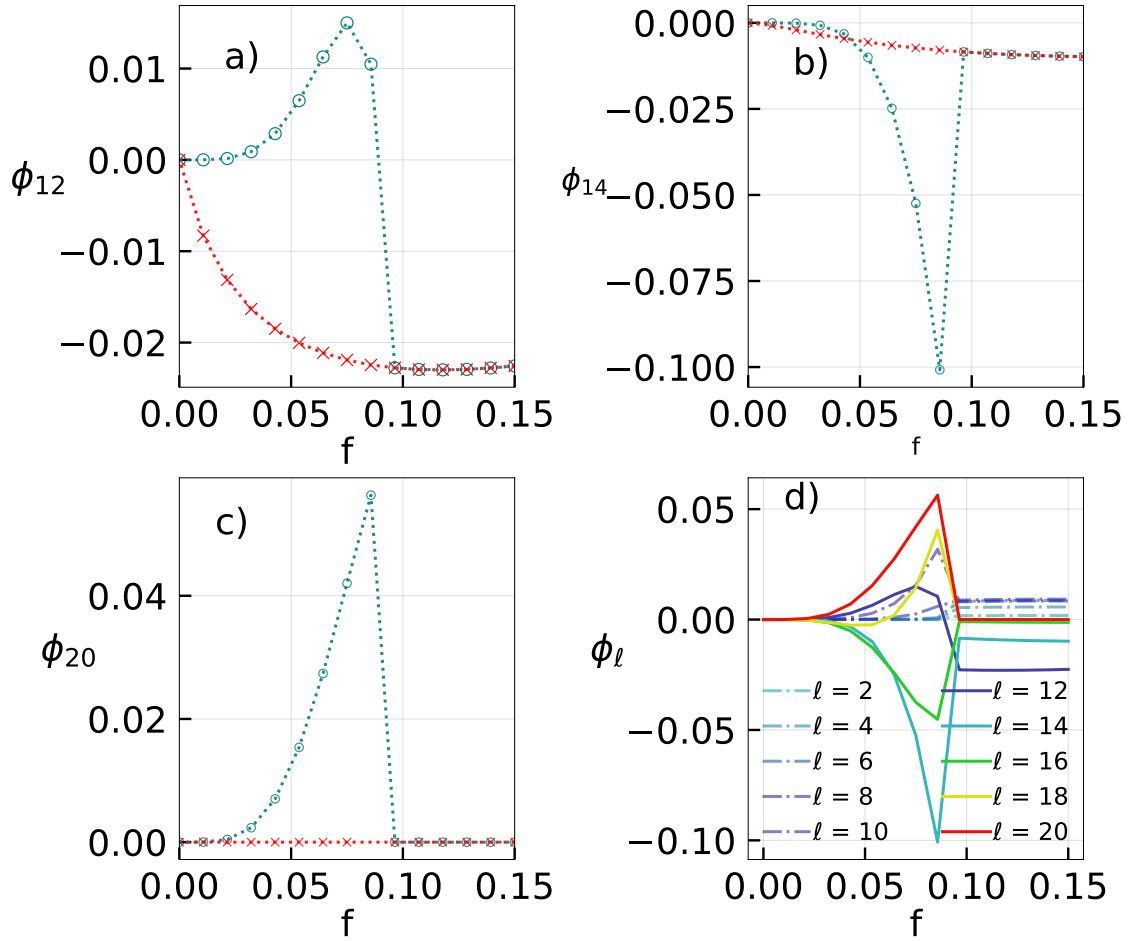


Figure 3.10: For a system of size  $N = 5000$ , the same as before, but for a random-regular structure.

Figure 4.6 compares, for the random-regular and regular lattices,  $\sigma_{\ell^*,k}$  and  $\sigma$  for distinct values of  $\theta$ . In all cases,  $\sigma_{\ell^*,k}$  is not only close to  $\sigma$  but also captures the same qualitative behavior, successfully describing the interplay between the control parameter  $f$ , inertia  $\theta$ , and the dissipation, including a peak located at the vicinity of the phase transition. For larger  $\theta$  the set of dissipating local configurations shrinks, hence the better agreement between both curves.

### 3.2.4 Concluding Remarks

The nonequilibrium thermodynamic theory of the generic majority vote model was presented and thoroughly investigated, encompassing its phase transition. A consistent definition of temperature and the connection between heat fluxes and entropy production were introduced and analyzed in the context of continuous and discontinuous phase transitions.

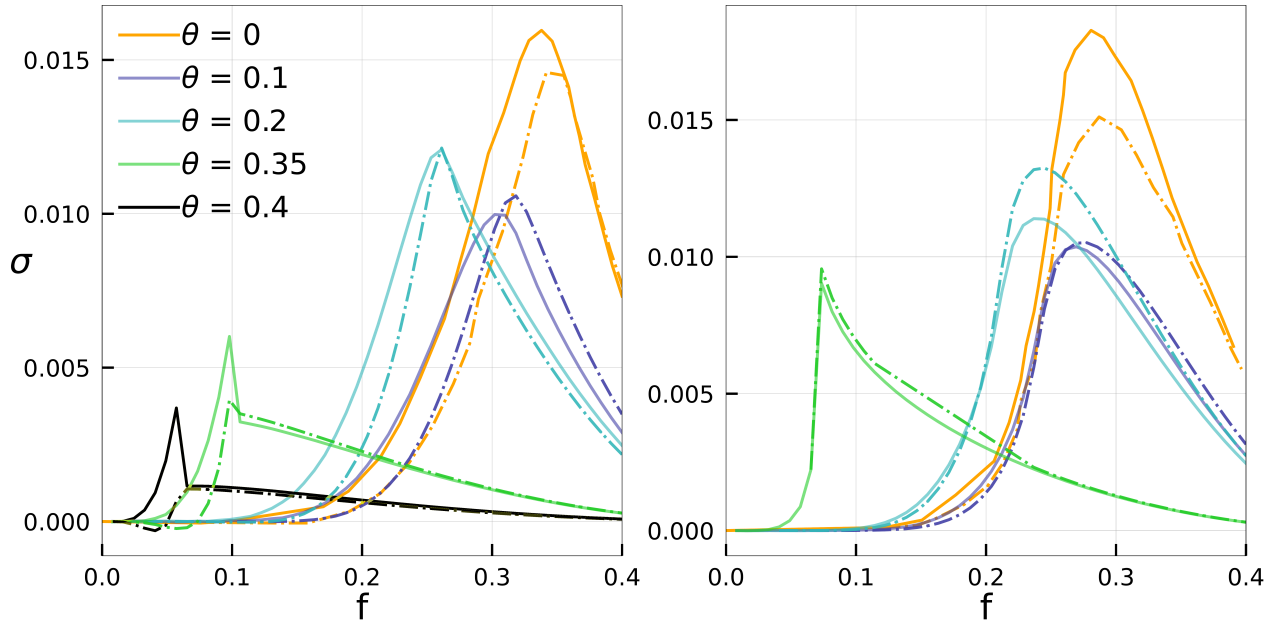


Figure 3.11: For  $k = 20$ , random-regular (left) and regular (right) structures of sizes  $N = 1600$  and  $40^2$ , curves for  $\sigma_{\ell^*,k}$  (dot-dashed) and  $\sigma$  (continuous) are shown in terms of  $f$  for distinct  $\theta$ 's. From top to bottom,  $\ell^* = 2, 4, 6, 12$  and  $14$ .

The present approach for fluxes is thermodynamically consistent and equivalent to the microscopic entropy production definition and satisfies the detailed fluctuation theorem.

We believe that the present framework not only conciliates the thermodynamic aspects of an important class of nonequilibrium systems but also introduces a new kind of nonequilibrium ingredient, based on the idea of a thermal bath associated with the system neighborhood. Such an idea has revealed general for a generic voter-like model with "up-down"  $Z_2$  symmetry. In the presence of inertia, the spin changes induced by some local configurations are reversible, depending on the relation between inertia, neighborhood, and connectivity. Moreover, we explore what are the most relevant neighborhoods driving the system dissipation, including its qualitative features across a phase transition, and how these neighborhoods contribute to the structure of the phase diagram.

Furthermore, it is important to note that while the use of the Ising-like energy associated with the flipping of a spin, and the use of Glauber-like rates to express the transition rates of each local configuration,  $|\ell|$ , may approximate the findings presented here to that of the latter model, the characteristics of the Majority Vote Model, being its out of equilibrium nature and the interaction between inertia and local configuration, are still present in the results. General spin models like the classic Ising model are formulated at equilibrium, and while the connectivity plays a role in phenomena such as ground state

energy, phase transitions and criticality (where the most general mean-field treatment for this model assumes  $k \sim N$ , *i.e.*, all-to-all), and the approach presented here could be also used to describe it (further implying that the approach is general, and not restricted to the M.V.), both the numerical and analytical results presented here from the nonequilibrium thermodynamics of the Majority Vote Model are strictly tied to its characteristic, such as the resulting plateaus on the phase diagrams and the inertia present in the transition rates, whose presence can be seen even in the inverse temperature. For instance, one cannot assume that the estimation of entropy production based on contributing heat fluxes would be valid for an Ising model application, but further investigations may give rise to more general observations of the results of the proposed approach, while the approach itself can be applied to any model [4, 33, 34, 74].

Our findings are valid for a class that describes systems from opinion models to the physics of thermal engines, presenting collective effects that can be leveraged for improved performance. Such potential application raises interesting questions such as the role of lattice topology and even the kind of voter model used (see e.g. Ref. [33] for a comparison between them) in order to optimize the desirable power and efficiency in the presence of a worksource. Such topics should be investigated in the future.

# Chapter 4

## Stochastic Heat Engines

Historically, one of the main goals of thermodynamics has been to optimize the performance of systems such as thermal engines. Afterward, this issue has been extended to the nonequilibrium thermodynamics realm. Given a system and its associated processes, being it purely physical [39–42], biological [95–98], chemical [43, 44], or even applied physics, such as in quantum or nanoscopic technology [45–47], nonequilibrium thermodynamics has always excelled at describing how the system can be optimized when dissipation and fluctuations are presented.

As stated in the introduction, collective effects have recently attracted remarkable interest, not only for their presence in several systems in nature but also for the possibility of being used for the construction of efficient engine setups. Since little is known about the influence of the engine design and most studies are restricted to the simplest cases (e.g. simultaneous contact with two thermal baths), not necessarily constituting a realistic setup implementation, we investigate the collisional/sequential description for a minimal model for collective effects, composed of two interacting nanomachines placed in contact with a distinct thermal reservoir and nonequilibrium worksource at each stage/stroke. Its simplicity enables us to obtain all thermodynamics exactly, irrespective of the model details and to exploit in detail the role of interaction time between the system and reservoir. We investigated two kinds of engines and the influence of the interaction, temperature, period, as well as time asymmetry (*i.e.* a different duration of each stroke).

## 4.1 Minimal Collective Model: 3 states and 2 strokes

Our setup is described as a system composed of two interacting nanomachines. As shall be described in more detail in Sec. 4.3, we are dealing with a system of three states, characterized in terms of the variable  $n$ , accounting for the population of the upper state of each unit. More specifically, states of the system are described as follows: both machines in the lower state ( $n = 0$ ), a single nanomachine in the upper state and the other in the lower state, ( $n = 1$ ), and both on the upper state ( $n = 2$ ). The system is placed in contact with the  $\nu$ -th thermal bath and its respective parameters, specified by transition rates  $\omega_{i,j}^{(\nu)}$ , during the time  $\tau_{\nu-1}$  and  $\tau_{\nu}$ . The only transitions allowed are those consisting of a single "hop" between states,  $n \rightarrow n \pm 1$ , meaning that transitions of the type  $0 \leftrightarrow 2$  are forbidden. An illustration of the model can be seen in Fig. 4.1.

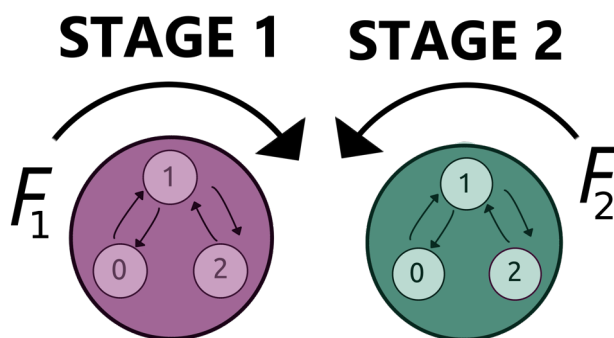


Figure 4.1: Simple illustration of the model for the symmetric case (thermal baths of equal times). In the first stroke, when  $t \leq \tau/2$ , a certain direction of transitions are favoured through the choice of adequate transition rates, either to the presence of a nonconservative driving,  $F_{\nu}$ , as depicted, or a certain interaction energy,  $V^{(\nu)}$ . In the second stroke,  $t > \tau/2$ , the opposite happens. After an entire period is complete, the system returns to the initial reservoir.

Furthermore, given that the system dynamics are temporally constrained to a certain period  $\tau$ , the transition rates during each  $\nu$ -th stroke will be described by that stroke's respective transition matrix,

$$\omega^{(\nu)} = \begin{pmatrix} -\omega_{1,0}^{(\nu)} & \omega_{0,1}^{(\nu)} & 0 \\ \omega_{1,0}^{(\nu)} & -\omega_{0,1}^{(\nu)} - \omega_{2,1}^{(\nu)} & \omega_{1,2}^{(\nu)} \\ 0 & \omega_{2,1}^{(\nu)} & -\omega_{0,1}^{(\nu)} - \omega_{1,2}^{(\nu)} \end{pmatrix} \quad (4.1)$$

In this contribution, we focus solely on the 2 stage application, where the periodic bound-

ary conditions read

$$\mathbf{p}^{(1)}(0) = \mathbf{p}^{(2)}(\tau) \quad (4.2a)$$

$$\mathbf{p}^{(1)}(\tau_1) = \mathbf{p}^{(2)}(\tau_2) \quad (4.2b)$$

The general solution to the master equation (for each stroke) then reads

$$\mathbf{p}^{(\nu)}(t) = \mathbf{p}^{(eq,\nu)} + \sum_{j=1}^2 e^{\lambda_j^{(\nu)}[t-\tau_{\nu-1}]} \Gamma_j^{(\nu)} \mathbf{p}^{(\nu)}(\tau_{\nu-1}), \quad (4.3)$$

where  $\mathbf{p}^{(\nu)}(\tau_{\nu-1})$  is a vector representing the initial conditions for the probability at stage  $\nu$ . To obtain an analytical solution, the equations resulting from the periodic boundary conditions were solved using the software *Mathematica*, and the resulting output was then probed so patterns of combinations (similar sequences of operations, as can be seen in below) of eigenvalues, determinants and products between the matrices  $\Gamma_\mu^{(\nu)}$  were identified. Given that these expressions are quite long, we present the solution for the symmetric case ( $\tau_1 = \tau_2 = \tau/2$ ), the shorter of the two,

$$\begin{aligned} \mathbf{p}^{(1)}(0) = & \\ & - \frac{\left[ e^{\tau\omega^{(1)}/2} + e^{\tau(\lambda_1^{(2)}+\lambda_2^{(2)}+\lambda_1^{(1)}+\lambda_2^{(1)})/2} \right] \mathbf{p}^{(eq,1)}}{\mathcal{Z}} \\ & + \frac{\sum_{\nu,\mu,\mu'} e^{\tau(\lambda_1^{(2)}+\lambda_2^{(2)}+\lambda_\nu^{(1)})/2} \Delta_{\mu,\mu'}^{(1)} \left[ \Gamma_{\mu'+1}^{(2)} \mathbf{p}^{(eq,1)} + e^{-\tau\lambda_{\mu'+1}^{(2)}/2} \mathbf{p}^{(eq,2)} \right]}{\mathcal{Z}}, \end{aligned} \quad (4.4)$$

and

$$\begin{aligned} \mathbf{p}^{(2)}\left(\frac{\tau}{2}\right) = & \\ & - \frac{\left[ e^{\tau\omega^{(1)}/2} + e^{\tau(\lambda_1^{(1)}+\lambda_2^{(1)}+\lambda_1^{(2)}+\lambda_2^{(2)})/2} \right] \mathbf{p}^{(eq,2)}}{\mathcal{Z}} \\ & + \frac{\sum_{\nu,\mu,\mu'} e^{\tau(\lambda_1^{(1)}+\lambda_2^{(1)}+\lambda_\nu^{(2)})/2} \Delta_{\mu,\mu'}^{(2)} \left[ \Gamma_{\mu'+1}^{(1)} \mathbf{p}^{(eq,2)} + e^{-\tau\lambda_{\mu'+1}^{(1)}/2} \mathbf{p}^{(eq,1)} \right]}{\mathcal{Z}}. \end{aligned} \quad (4.5)$$

where

$$\mathcal{Z}/2 = \left( e^{\tau\lambda_1^{(1)}/2} - e^{\tau\lambda_2^{(1)}/2} \right) \left( e^{\tau\lambda_1^{(2)}/2} - e^{\tau\lambda_2^{(2)}/2} \right) \text{Tr}\left\{ \Gamma_2^{(1)} \Gamma_2^{(2)} \right\} - \left( e^{\tau(\lambda_2^{(1)}+\lambda_1^{(2)})/2} - 1 \right) \left( e^{\tau(\lambda_1^{(1)}+\lambda_2^{(2)})/2} - 1 \right),$$

and

$$\Delta_{\mu,\mu'}^{(\nu)} = \text{Tr} \left\{ \Gamma_{\mu}^{(\nu+1)} \Gamma_{\mu'}^{(\nu)} \right\} - \Gamma_{\mu}^{(\nu+1)} \Gamma_{\mu'}^{(\nu)}.$$

By integrating Eqs.(4.4,4.5) over the entire period, one can define the *average probability fluxes*,  $\langle \mathbf{J} \rangle^{(\nu)}$ . For the first reservoir, the fluxes are given by

$$\langle J \rangle_{01}^{(1)} = \frac{1}{\tau} \int_0^{\tau_1} \left\{ \omega_{01}^{(1)} p_1^{(1)}(t) - \omega_{10}^{(1)} p_0^{(1)}(t) \right\} dt, \quad (4.6)$$

$$\langle J \rangle_{21}^{(1)} = \frac{1}{\tau} \int_0^{\tau_1} \left\{ \omega_{21}^{(1)} p_1^{(1)}(t) - \omega_{12}^{(1)} p_2^{(1)}(t) \right\} dt. \quad (4.7)$$

Due to the periodic boundary conditions and normalization of probabilities, the fluxes obey the following equations

$$\sum_{\nu} \langle \mathbf{J} \rangle^{(\nu)} = 0, \quad (4.8a)$$

$$\sum_i \langle \mathbf{J} \rangle_i^{(\nu)} = 0. \quad (4.8b)$$

While the role of the probability fluxes will become more clear in the following section, it's interesting to note its asymptotic behaviors for both short ( $\tau \rightarrow 0$ ) and long ( $\tau \rightarrow \infty$ ) periods,

$$\lim_{\tau \rightarrow 0} \langle \mathbf{J} \rangle^{(\nu)} = \frac{1}{2} \omega^{(\nu)} \tilde{\mathbf{p}}, \quad (4.9a)$$

$$\lim_{\tau \rightarrow \infty} \langle \mathbf{J} \rangle^{(\nu)} = \frac{(-1)^{(\nu+1)}}{\tau} \{ \mathbf{p}^{(eq,1)} - \mathbf{p}^{(eq,2)} \}. \quad (4.9b)$$

In the first limit, the expressions for the probability components of the vector  $\tilde{\mathbf{p}}$  are given by

$$\begin{aligned} \tilde{p}_0 &= \frac{(\omega_{01}^{(1)} + \omega_{01}^{(2)}) (\omega_{12}^{(1)} + \omega_{12}^{(2)})}{(\omega_{01}^{(1)} + \omega_{01}^{(2)}) (\omega_{12}^{(1)} + \omega_{12}^{(2)}) + (\omega_{10}^{(1)} + \omega_{10}^{(2)}) (\omega_{12}^{(1)} + \omega_{12}^{(2)}) + (\omega_{10}^{(1)} + \omega_{10}^{(2)}) (\omega_{21}^{(1)} + \omega_{21}^{(2)})}, \\ \tilde{p}_1 &= \frac{(\omega_{10}^{(1)} + \omega_{10}^{(2)}) (\omega_{12}^{(1)} + \omega_{12}^{(2)})}{(\omega_{01}^{(1)} + \omega_{01}^{(2)}) (\omega_{12}^{(1)} + \omega_{12}^{(2)}) + (\omega_{10}^{(1)} + \omega_{10}^{(2)}) (\omega_{12}^{(1)} + \omega_{12}^{(2)}) + (\omega_{10}^{(1)} + \omega_{10}^{(2)}) (\omega_{21}^{(1)} + \omega_{21}^{(2)})}, \\ \tilde{p}_2 &= \frac{(\omega_{10}^{(1)} + \omega_{10}^{(2)}) (\omega_{21}^{(1)} + \omega_{21}^{(2)})}{(\omega_{01}^{(1)} + \omega_{01}^{(2)}) (\omega_{12}^{(1)} + \omega_{12}^{(2)}) + (\omega_{10}^{(1)} + \omega_{10}^{(2)}) (\omega_{12}^{(1)} + \omega_{12}^{(2)}) + (\omega_{10}^{(1)} + \omega_{10}^{(2)}) (\omega_{21}^{(1)} + \omega_{21}^{(2)})}. \end{aligned}$$



and is the flux is described by exactly *half* of the solution for the case of a system placed in contact with 2 thermal reservoirs, and a single stroke, further explained in Section 4.3.3. With all the necessary ingredients at hand, we are finally in a position to investigate the thermodynamic properties of the model.

## 4.2 General Thermodynamic Properties

Until here, all analyses have been carried out without any thermodynamic consideration. For that, we follow the common approach considered in the literature (see, *e.g.*, Refs. [5, 36, 40, 99, 100]) in which the ratio between transition rates  $\omega_{ij}^{(\nu)}$  and  $\omega_{ji}^{(\nu)}$  is defined according to the local detailed balance,

$$\ln \frac{\omega_{ij}^{(\nu)}}{\omega_{ji}^{(\nu)}} = -\beta_\nu \left[ \tilde{\epsilon}_i^{(\nu)} - \tilde{\epsilon}_j^{(\nu)} + d_{ij}^{(\nu)} F^{(\nu)} \right], \quad (4.10)$$

where  $\tilde{\epsilon}_i^{(\nu)} - \tilde{\epsilon}_j^{(\nu)}$  is the difference between states  $i$  and  $j$ ,  $d_{ji}^{(\nu)} F^{(\nu)}$  accounts to the influence of a driving force, and the element  $d_{ji}^{(\nu)}$  satisfies the anti-symmetric property  $d_{ji}^{(\nu)} = -d_{ij}^{(\nu)}$ .

From Eq.(4.10), we consider the entropy production formula

$$\Pi_\nu(t) = \sum_{i<j} J_{ij}^{(\nu)}(t) \ln \frac{\omega_{ij}^{(\nu)} p_j(t)}{\omega_{ji}^{(\nu)} p_i(t)}, \quad (4.11)$$

whose integration over a complete cycle, together with the previously mentioned boundary conditions, leads to the standard form  $\langle \sigma \rangle = -\sum_\nu \beta^{(\nu)} \langle \dot{Q} \rangle^{(\nu)}$ , where  $\langle \dot{Q} \rangle^{(\nu)}$  is given by

$$\langle \dot{Q} \rangle^{(\nu)} = \frac{1}{\tau} \sum_{i<j} \left[ \tilde{\epsilon}_i^{(\nu)} - \tilde{\epsilon}_j^{(\nu)} + d_{ij}^{(\nu)} F_\nu \right] \langle J \rangle_{ij}^{(\nu)}. \quad (4.12)$$

By expressing Eq. (4.12) in terms of fluxes  $\langle J \rangle_{01}^{(\nu)}$  and  $\langle J \rangle_{21}^{(\nu)}$ , the exchanged heat,  $\langle \dot{Q} \rangle_\nu$ , then reads

$$\langle \dot{Q} \rangle^{(\nu)} = \frac{1}{\tau} \left[ \left( \tilde{\epsilon}_0^{(\nu)} - \tilde{\epsilon}_1^{(\nu)} + d_{01}^{(\nu)} F_\nu \right) \langle J \rangle_{01}^{(\nu)} + \left( \tilde{\epsilon}_2^{(\nu)} - \tilde{\epsilon}_1^{(\nu)} + d_{21}^{(\nu)} F_\nu \right) \langle J \rangle_{21}^{(\nu)} \right]. \quad (4.13)$$

Since the system evolves to a nonequilibrium steady state regime, returning to the initial state after a complete cycle, the first law of thermodynamics establishes that  $\mathcal{P} =$

–  $[\langle \dot{Q} \rangle^{(1)} + \langle \dot{Q} \rangle^{(2)}]$ . Using Eq. (4.12), together with Eq.(4.13), the general expression for power is then given by

$$\langle \mathcal{P} \rangle = - \left[ \sum_i \left( \tilde{\epsilon}_i^{(2)} - \tilde{\epsilon}_i^{(1)} \right) \frac{\left( p_i^{(1)}(\tau_1) - p_i^{(1)}(0) \right)}{\tau} + \sum_{i < j} d_{ij}^{(1)} \left( F^{(1)} \langle J \rangle_{ij}^{(1)} - F^{(2)} \langle J \rangle_{ij}^{(2)} \right) \right], \quad (4.14)$$

Inspection of Eq.(4.14) reveals that the model's power output has two sources. The first term on the right side of Eq.(4.14), conveniently written in terms of the probabilities and energy difference between strokes, pertains to the power output associated with the reservoir switching aspect of the model, meaning that heat dissipated during this dynamic will be reflected as work. The second term on the *R.H.S*, however, can be interpreted as the power output due to the system being forced to an out-of-equilibrium state due to the external non-conservative driving applied to it.

For a consistent analysis throughout the different cases studied with this model, as well as a way to further validate eventual comparisons with the different models presented in the literature [5, 46, 101–103], the second reservoir is defined as being the "hot" reservoir, that is,  $\beta^{(1)} > \beta^{(2)}$ , meaning that the definition for efficiency is simply  $\eta = -\mathcal{P}/\langle \dot{Q} \rangle^{(2)}$ . Given that, in thermodynamics, the maximum value efficiency for a heat engine can achieve is Carnot [1],  $\eta_c = 1 - \beta^{(2)}/\beta^{(1)}$ , it's easy to see that if  $\langle \dot{Q} \rangle^{(2)} > 0$ , part of the extracted heat from the second reservoir will be converted into power output (implying  $\mathcal{P} < 0$ ), and the system will operate as a heat engine. Conversely, in the scenario where  $\langle \dot{Q} \rangle^{(2)} < 0$ , this would imply that  $\mathcal{P} > 0$ , indicating a transition to a heat pump regime, where now the efficiency is bound by  $\eta_c < \eta \leq \infty$ .

Despite the model's simplicity, the appropriate choice of parameters (as will be seen in the two following sections) shows that there's a rich complexity of behaviors where the model can both reproduce previously seen results [5, 101] as well as provide insight into maximum efficiency *and* efficiency at maximum power [104] and contribute to the discourse of relevance of minimal models in the context of stochastic thermodynamics.

### 4.3 Applications

As stated previously, the system is composed of two interacting nanomachines, whose interaction energy depends on their occupations. At each stroke, both are subject to the same temperature in such a way that there is a correspondence between their individual occupation  $\sigma_i$  and the system occupation  $n = \sigma_1 + \sigma_2$ ,

- $n = 0 \rightarrow$  both units are empty,  $\sigma_1 = \sigma_2 = 0$ ,
- $n = 1 \rightarrow$  one unit is occupied (not distinguishable),  $\sigma_\nu \neq \sigma_{\nu'} = 1$ ,
- $n = 2 \rightarrow$  both units are occupied,  $\sigma_1 = \sigma_2 = 1$ .

Such a setup is characterized by the generic energy

$$\tilde{\epsilon}^{(\nu)} = V_\nu[(1 - \sigma_1)\sigma_2 + \sigma_1(1 - \sigma_2)] + U_\nu\sigma_1\sigma_2 + \epsilon_\nu(\sigma_1 + \sigma_2), \quad (4.15)$$

where  $V^{(\nu)}$  and  $U^{(\nu)}$  account for the interaction strength energies provided units are in distinct and the same states, respectively, whereas  $\epsilon^{(\nu)}$  are the individual ones.

We shall consider two approaches for the worksource. First, we consider a case where the units have different energy levels and interaction energies,  $\epsilon^{(\nu)}$  and  $V^{(\nu)}$ , respectively. After, we consider a case where the non-conservative driving changes during strokes,  $F^{(\nu)}$ , and the interaction energy is constant. In both cases, we make a brief description of the effects of period duration and effects of asymmetrical time switchings.

#### 4.3.1 Distinct Interactions between units

##### Main expressions and general findings

Our first approach consists of building a setup via a change of individual and interaction energies at each stroke without non-conservative drivings. Such study has been inspired in recent works [5, 7, 35, 36]. Transition rates  $\omega_{ij}^{(\nu)}$  follow Eq. (4.10) and have been defined in the following form

$$\omega_{10}^{(\nu)} = 2\Gamma \exp \left\{ \frac{-\beta^{(\nu)}}{2} (V^{(\nu)} + \epsilon^{(\nu)}) \right\} \quad (4.16a)$$

$$\omega_{01}^{(\nu)} = \Gamma \exp \left\{ \frac{-\beta^{(\nu)}}{2} (-V^{(\nu)} - \epsilon^{(\nu)}) \right\} \quad (4.16b)$$

$$\omega_{21}^{(\nu)} = \Gamma \exp \left\{ \frac{-\beta^{(\nu)}}{2} (-V^{(\nu)} + \epsilon^{(\nu)}) \right\} \quad (4.16c)$$

$$\omega_{12}^{(\nu)} = 2\Gamma \exp \left\{ \frac{-\beta^{(\nu)}}{2} (V^{(\nu)} - \epsilon^{(\nu)}) \right\} \quad (4.16d)$$

where  $V^{(\nu)}, \epsilon^{(\nu)}$  assume distinct values at each stroke and  $\Gamma$  represents the coupling between the system and the reservoir. From Eq. (4.12), the average heat flux at each stroke is given by

$$\begin{aligned} \langle \dot{Q} \rangle^{(1)} &= - \left[ \langle J \rangle_{01}^{(1)} (V^{(1)} + \epsilon^{(1)}) + \langle J \rangle_{21}^{(1)} (V^{(1)} - \epsilon^{(1)}) \right], \\ \langle \dot{Q} \rangle^{(2)} &= \left[ \langle J \rangle_{01}^{(1)} (V^{(2)} + \epsilon^{(2)}) + \langle J \rangle_{21}^{(1)} (V^{(2)} - \epsilon^{(2)}) \right], \end{aligned} \quad (4.17)$$

whose steady entropy production  $\langle \sigma \rangle$  assumes the generic "fluxes times forces" form  $\bar{\sigma} = J_1 X_1 + J_2 X_2$ , where  $J_1 = \langle J \rangle_{01}^{(1)}$  and  $J_2 = \langle J \rangle_{21}^{(1)}$  with  $X_1$  and  $X_2$  given by

$$X_1 = \frac{V^{(1)} + \epsilon^{(1)}}{T^{(1)}} - \frac{V^{(2)} + \epsilon^{(2)}}{T^{(2)}} \quad (4.18a)$$

$$X_2 = \frac{V^{(1)} - \epsilon^{(1)}}{T^{(1)}} - \frac{V^{(2)} - \epsilon^{(2)}}{T^{(2)}} \quad (4.18b)$$

With this results, the expressions for the power  $\mathcal{P}$  and system efficiency  $\eta$  are then given by

$$\mathcal{P} = [\epsilon^{(1)} - \epsilon^{(2)}] \left[ \langle J \rangle_{01}^{(1)} - \langle J \rangle_{21}^{(1)} \right] + [V^{(1)} - V^{(2)}] \left[ \langle J \rangle_{01}^{(1)} + \langle J \rangle_{21}^{(1)} \right], \quad (4.19)$$

and

$$\eta = - \frac{[\epsilon^{(1)} - \epsilon^{(2)}] \left[ \langle J \rangle_{01}^{(1)} - \langle J \rangle_{21}^{(1)} \right] + [V^{(1)} - V^{(2)}] \left[ \langle J \rangle_{01}^{(1)} + \langle J \rangle_{21}^{(1)} \right]}{\epsilon^{(2)} \left[ \langle J \rangle_{01}^{(1)} - \langle J \rangle_{21}^{(1)} \right] + V^{(2)} \left[ \langle J \rangle_{01}^{(1)} + \langle J \rangle_{21}^{(1)} \right]}, \quad (4.20)$$

respectively. It is important to draw a few comments about these results. First, Eqs. (4.17)-(4.20) are general for the two-stroke case, irrespective of the period, asymmetry and model parameters. Second, in the absence of interactions ( $V^{(1)} \rightarrow 0$  and  $V^{(2)} \rightarrow 0$ ), the system becomes equivalent to the interactionless setup investigated in Refs. [7, 8, 48] for  $\mu_1 = \mu_2 = 0$ . In such cases, Eqs. (4.19) and (4.20) reduce to  $\eta_s = 1 - \epsilon^{(1)}/\epsilon^{(2)}$  and

$\mathcal{P}_s = (\epsilon^{(1)} - \epsilon^{(2)})\langle J \rangle_s$ , respectively, where  $\langle J \rangle_s$  (for  $\tau_1 = \tau/2$ ) reads:

$$\langle J \rangle_s = \frac{\prod_{\mu} \left\{ -1 + \cosh \left[ \tau \cosh \left( \frac{\beta^{(\mu)} \epsilon^{(\mu)}}{2} \right) \right] + \sinh \left[ \tau \cosh \left( \frac{\beta^{(\mu)} \epsilon^{(\mu)}}{2} \right) \right] \right\}}{(e^{\beta^{(1)} \epsilon^{(1)}} - e^{\beta^{(2)} \epsilon^{(2)}})^{-1} \prod_{\mu'} (1 + e^{\beta^{(\mu')} \epsilon^{(\mu')}}) [-1 + \cosh(\tau C) + \sinh(\tau C)]}, \quad (4.21)$$

where

$$C = \cosh \left( \frac{\beta^{(1)} \epsilon^{(1)}}{2} \right) + \cosh \left( \frac{\beta^{(2)} \epsilon^{(2)}}{2} \right)$$

Both  $\eta_s$  and  $\mathcal{P}_s$  can be related through the expression  $\mathcal{P}_s = -\epsilon^{(2)} \eta_s \langle J \rangle_s$ , consistent with the heat engine characterised by  $\langle J \rangle_s > 0$ , since  $\beta^{(1)} \epsilon^{(1)} > \beta^{(2)} \epsilon^{(2)}$ ,  $\langle \mathcal{P}_s \rangle < 0$ ,  $0 < \eta_s < \eta_c$ . Conversely, the pump is characterized by the other way around of conditions  $\langle \bar{J} \rangle < 0$  (since  $\beta^{(1)} \epsilon^{(1)} < \beta^{(2)} \epsilon^{(2)}$ ),  $\mathcal{P}_s > 0$  and  $\eta_c < \eta_s < 1$ .

Third, contrasting with the interactionless case, there are two independent fluxes,  $\langle J \rangle_{01}^{(1)}$  and  $\langle J \rangle_{21}^{(1)}$ , revealing that the interaction between units gives rise to a much richer behavior than the single case [7]. Eqs. (4.17) and (4.19) impose some constraints on the operation of each type of regime. In particular, a quick inspection of the expressions for power and heat reveals that the heat engine occurs when both inequalities

$$[\epsilon^{(2)} - \epsilon^{(1)}] [\langle J \rangle_{01}^{(1)} - \langle J \rangle_{21}^{(1)}] < [V^{(1)} - V^{(2)}] [\langle J \rangle_{01}^{(1)} + \langle J \rangle_{21}^{(1)}], \quad (4.22a)$$

and

$$\epsilon^{(2)} [\langle J \rangle_{21}^{(1)} - \langle J \rangle_{01}^{(1)}] > V^{(2)} [\langle J \rangle_{01}^{(1)} + \langle J \rangle_{21}^{(1)}], \quad (4.22b)$$

are simultaneously satisfied, whereas the pump regime takes place for opposite inequalities.

Fourth, our system will operate more efficiently than the interactionless case ( $\eta > \eta_s$ ) if  $[\epsilon^{(1)} V^{(2)} - \epsilon^{(2)} V^{(1)}] [\langle J \rangle_{01}^{(1)} + \langle J \rangle_{21}^{(1)}] > 0$ . For  $\epsilon^{(1)}/\epsilon^{(2)}$  or  $V^{(1)}/V^{(2)}$  held fixed,  $\eta = \eta_c$  when  $\beta^{(2)} V^{(2)} = \beta^{(1)} V^{(1)}$  and  $\beta^{(2)} \epsilon^{(2)} = \beta^{(1)} \epsilon^{(1)}$ , whose efficiency is given by  $\eta = 1 - V^{(1)}/V^{(2)}$ , akin to the interactionless expression. Conversely, maximum efficiency is lower than Carnot,  $\eta_{ME} < \eta_c$ , if the condition  $\epsilon^{(1)}/\epsilon^{(2)} = V^{(1)}/V^{(2)} = \beta^{(2)}/\beta^{(1)}$  is not satisfied. Fifth and last, the occurrence of the pump regime implies the following relation between parameters

$$[\beta^{(2)} \epsilon^{(2)} - \beta^{(1)} \epsilon^{(1)}] [\langle J \rangle_{21}^{(1)} - \langle J \rangle_{01}^{(1)}] > [\beta^{(2)} V^{(2)} + \beta^{(1)} V^{(1)}] [\langle J \rangle_{21}^{(1)} + \langle J \rangle_{01}^{(1)}]. \quad (4.23)$$

These features are presented in Figs. 4.2, 4.3, and section 4.3.1 contains a phase diagram for the distinct regions of heat engine and pump regimes in the  $\beta^{(\nu)}, V^{(\nu)}, \epsilon^{(\nu)}$  plane.

### Results for symmetric switching times

The analysis will be carried out for the following set of parameters:  $\beta_1 = 10, \beta_2 = 1, \tau = 1$  and  $k_B = 1$ . In order to obtain a first insight into how the interaction between units influences the system performance, Fig. 4.2 depicts the system performance for  $\epsilon_1/\epsilon_2 = 0.6$ , in which the interactionless case operates as an engine with power and efficiency given by  $\mathcal{P}_s = -0.08362$  and  $\eta_s = 0.4$ , respectively.

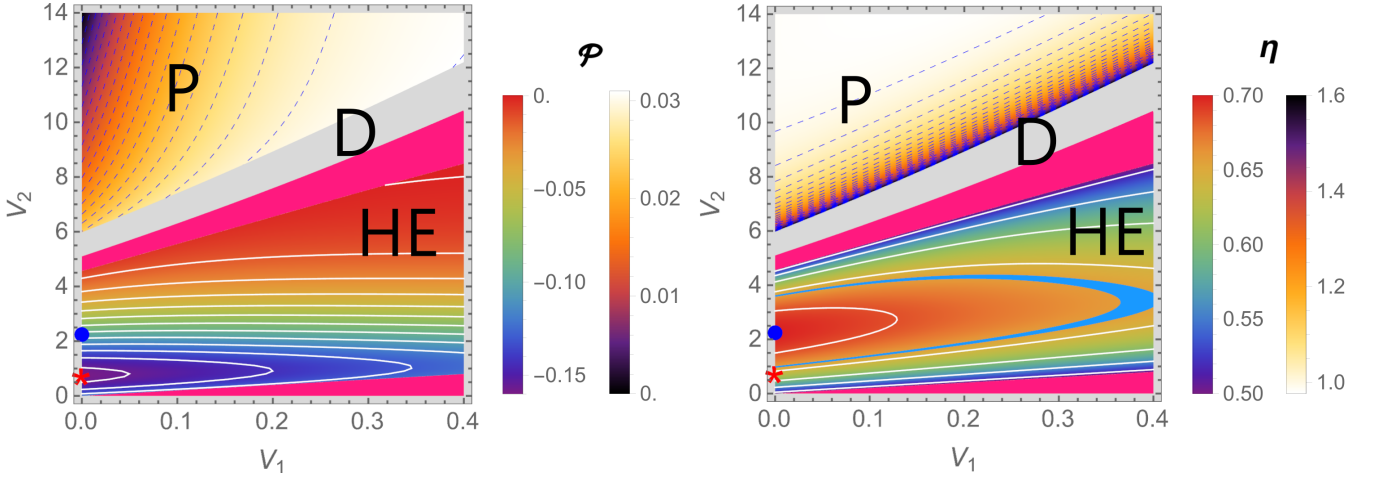


Figure 4.2: The influence of the interaction parameters over the system performance. The top and bottom panels depict the power and efficiency heat maps. The surfaces highlighted by the color pink represent the region in which  $\eta \leq \eta_s$ . Parameters:  $\beta_2 = 1, \beta_1 = 10, \tau = 1$  and  $\epsilon_1/\epsilon_2 = 0.6$ . Symbols HE (left bars) and P (right bars) correspond to the heat engine and pump regimes, respectively, whereas \* and • attempt to the global maximum of  $\mathcal{P}_{mP}$  and  $\eta_{ME}$  in the HE regime. The gray region indicates dud (D) behavior. For this set of parameters  $\eta_{ME} < \eta_c$ , whereas the light blue line in the bottom panel indicates the region in which  $\eta_{mP} = \eta_{CA}$ .

We highlight two remarkable changes coming from the interaction, under suitable choices of  $V^{(1)}(V^{(2)})$  at strokes  $\nu = 1(2)$ . The former is a substantially broader set of parameters, in which  $\eta > \eta_s$  and  $\mathcal{P} > \mathcal{P}_s$ . This also extends the regime of possible distinct operations, giving rise to a pump regime as  $V^{(2)}$  is raised. Similar results are found for distinct  $\beta^{(1)}/\beta^{(2)}$ 's, although the variation of temperatures can favor a given operation regime, as can be seen in Fig. 4.6.

The interplay between the ratio of individual energies,  $\epsilon^{(1)}/\epsilon^{(2)}$  and interactions  $V^{(1)}/V^{(2)}$

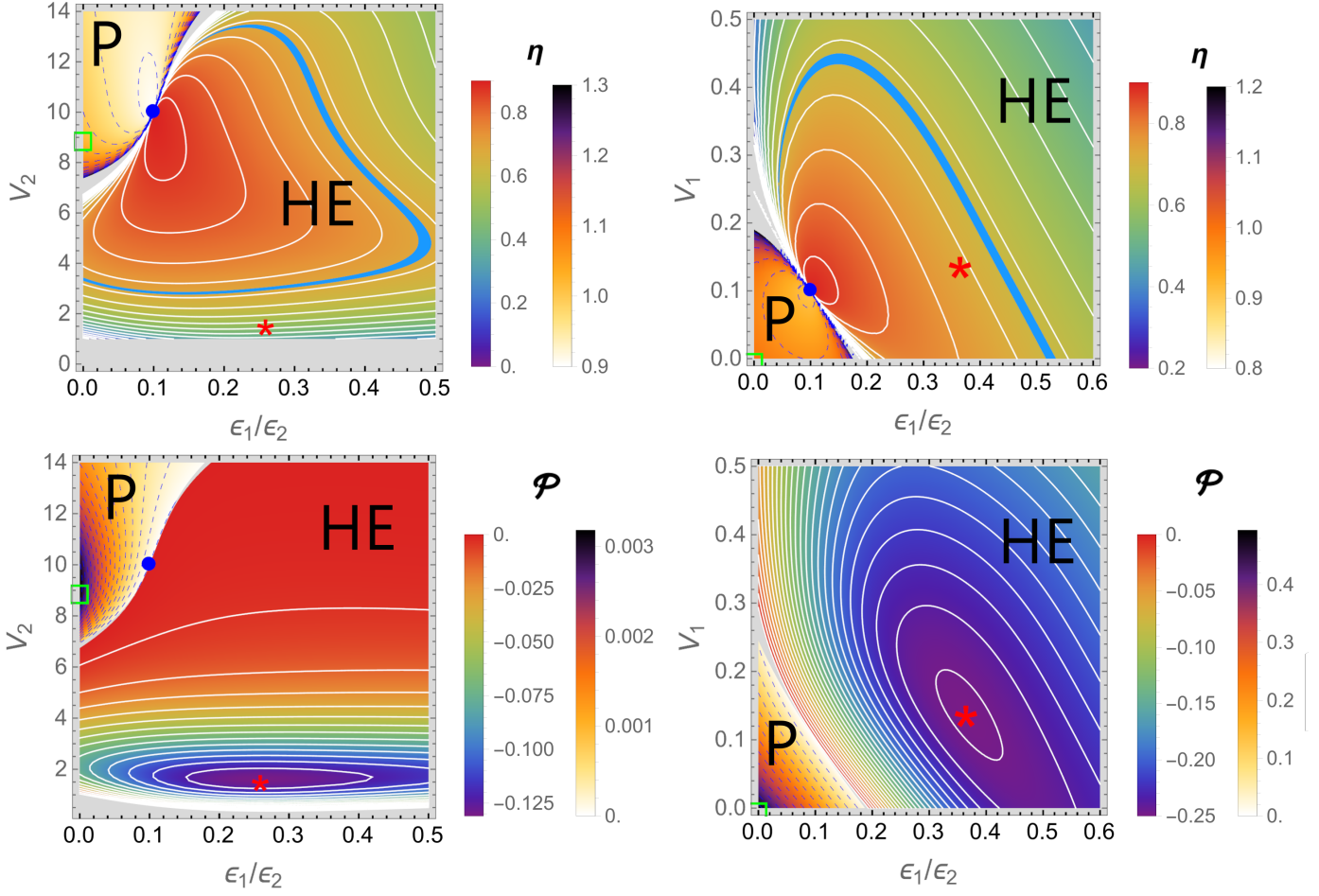


Figure 4.3: The influence of individual energies  $\epsilon^{(1)}/\epsilon^{(2)}$  over the system performance. Left and right panels depict fixed  $V^{(1)}$  and  $V^{(2)}$ , respectively, while top and bottom panels show  $\eta$ 's and  $\mathcal{P}$ 's heat maps, respectively. The left and right bars denote HE and P regimes, respectively. Symbols  $\bullet$ ,  $*$  and  $\square$  attempt to Carnot efficiency  $\eta_c$ , efficiencies at maximum power  $\eta_{mP}$  at the heat engine (HE) and pump (P) regimes, respectively. Light blues in top panels indicate the regions in which  $\eta_{mP} = \eta_{CA}$ . Parameters:  $\beta^{(2)} = 1, \beta^{(1)} = 10, \tau = 1, V^{(2)} = 1$  (right) and  $V^{(1)} = 1$  (left).

energies is depicted in Fig. 4.3, in which  $\eta < \eta_s < \eta_c$  for small  $V_2$ 's. However, increasing the ratios not only extends the heat regime to the region  $0 < \epsilon^{(1)}/\epsilon^{(2)} < \beta^{(2)}/\beta^{(1)}$ , in which the interaction-less case operates as a pump, but also lead to higher efficiencies  $\eta > \eta_s$  as  $V^{(2)}$  increases and presents a maximum value,  $\eta_{ME}$ , at  $V_{ME}^{(2)}$ . As portrayed in Sec. 4.3.1,  $\eta_{ME} < \eta_c$  for  $\epsilon^{(1)}\beta^{(1)} \neq \epsilon^{(2)}\beta^{(2)}$ , and  $\eta_{ME} = \eta_c$  if  $V^{(2)} = V_{ME}^{(2)}$  when  $\epsilon^{(1)}\beta^{(1)} = \epsilon^{(2)}\beta^{(2)}$  (e.g. blue  $\bullet$  in Fig. 4.3). Similarly to  $\eta$ , it is possible to find suitable values of parameters in which  $\mathcal{P} > \mathcal{P}_s$  (from now, we assume the convention of meaning the absolute value of  $\mathcal{P}$ ) as well as optimize it via a suitable choice of  $V_{mP}^{(2)}$ .

As can be seen in Fig. 4.3, the influence of  $V^{(1)}$  ( $V^{(2)}$  held fixed) is remarkably different from the left panels ( $V^{(1)}$  held fixed), whose engine regime and higher efficiencies are

constrained to small values of  $V^{(1)}$ 's (consistent with the general findings from Sec. 4.3.1), hence, indicating that stronger interactions in the second stage are more significant than in the first one. Furthermore,  $\eta > \eta_s$  for a broader set of values of  $V^{(1)}$ . as  $\epsilon^{(1)}/\epsilon^{(2)}$  is increased. The behavior of  $\mathcal{P}$  is akin to the previous one and presents a maximum at a (small)  $V_{1mP}$ 's (fixed  $\epsilon_1/\epsilon_2$ ) as well as an optimal  $\epsilon_1/\epsilon_2$  providing its simultaneous maximization.

As a complementary analysis, it is also possible to compare the efficiencies at maximum power  $\eta_{mP}$  with the Curzon and Ahlborn case,  $\eta_{CA} = 1 - \sqrt{\beta_2/\beta_1}$  [104], which has been verified in distinct systems [36, 105, 106]. Despite not constituting a universal result, it provides a powerful guide about the system operation at finite power, which is more realistic than the ideal case ( $\eta = \eta_c$  and  $\mathcal{P} = 0$ ). In all cases, the interaction among units can also be chosen for providing efficiencies at maximum power  $\eta_{mP} > \eta_{CA}$  for a wide range of parameters (see e.g. light blue lines in Figs. 4.2-4.3 in which  $\eta_{mP} = \eta_{CA}$ ). Depending on the parameters the engine is projected,  $\eta_{mP} < \eta_{CA}$  [Figs. 4.2 and 4.3 (left panel) ] and  $\eta_{mP} > \eta_{CA}$  (right panel of Fig. 4.3) at the simultaneous maximization of power.

In short, the presence of collective effects between two units makes it possible to conveniently choose interaction parameters at each stage, providing higher performances than its interactionless counterpart (for the same values of individual energies), as well as distinct optimization routes, such as the maximization of power and efficiency. Additionally, an extra advantage concerns the possibility of changing the regime operation, from heat engine to pump and vice-versa, by changing the interactions at each stroke.

### **Influence of period $\tau$ and asymmetric switchings**

The influence of period  $\tau$  and the inclusion of a different time duration at each stroke, expressed by the asymmetry  $\kappa = \tau_1/\tau_2 \neq 1$  will be considered in this section. Due to the existence of several distinct parameters, for this section, the set of parameters is fixed at  $\epsilon^{(1)}/\epsilon^{(2)} = 0.6$ ,  $V^{(1)} = 0.2$ ,  $\beta^{(1)} = 10$  and  $\beta^{(2)} = 1$ .

Although  $\mathcal{P}_s$  increases as  $\tau$  is lowered, the period plays a less important role in the interactionless case, in part because  $\eta_s$  is independent of  $J_s$  and  $\tau$  [7, 48]. On the other hand, the existence of two independent fluxes, as a consequence of the interaction between



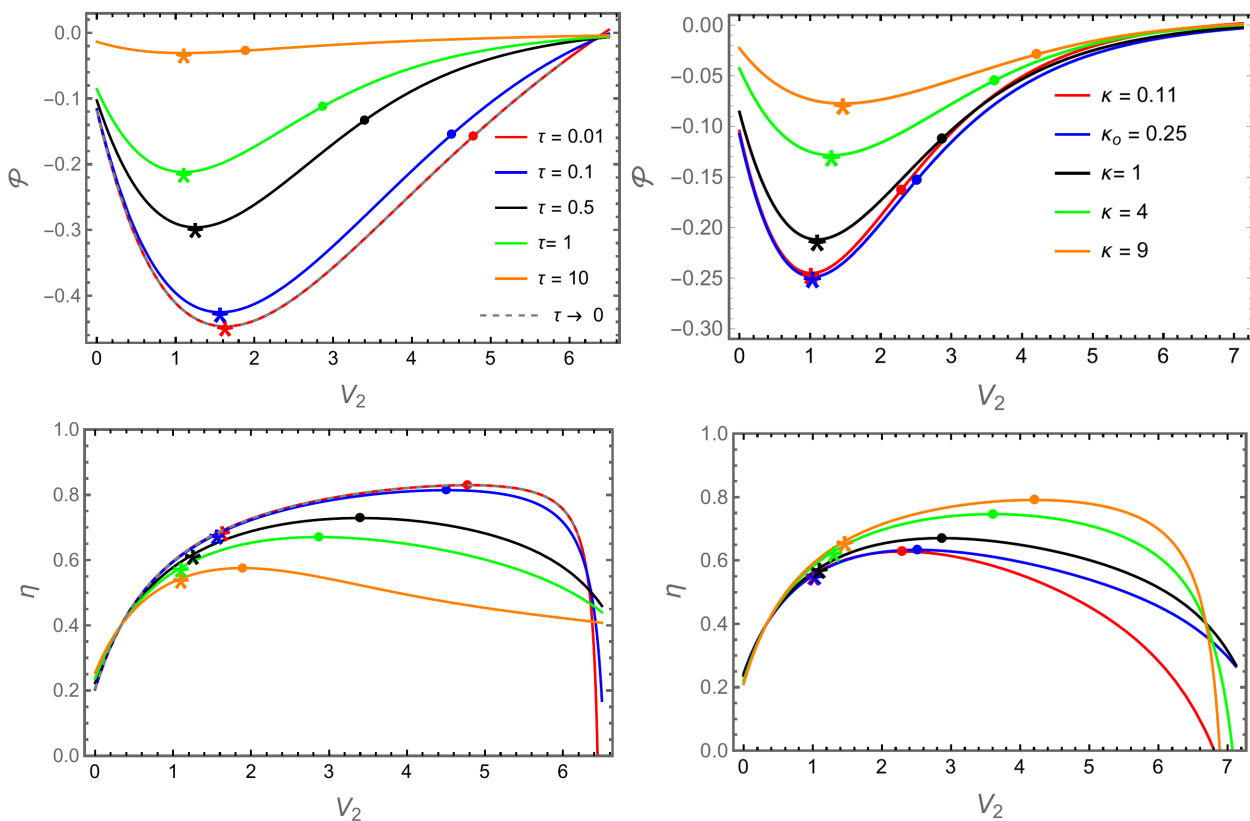


Figure 4.4: Left and right panels depict the influence of period  $\tau$  (for symmetric time switchings) and distinct  $\kappa$ 's (for  $\tau = 1$ ), respectively, for  $\mathcal{P}$  (top) and  $\eta$  (bottom), respectively. Symbols  $*$  and  $\bullet$  denote associate  $\mathcal{P}_{mP}$ 's and  $\eta_{ME}$ 's, respectively. Parameters:  $\beta^{(1)} = 10$ ,  $\beta^{(2)} = 1$ ,  $V^{(1)} = 0.2$ ,  $\epsilon^{(1)}/\epsilon^{(2)} = 0.6$ .

nanomachines, makes the influence of  $\tau$  more revealing. We highlight two aspects regarding the influence of  $\tau$ , as depicted in the left panels of Fig. 4.4. First, it significantly affects the system performance, marking the increase of both  $\mathcal{P}$  (as the interactionless system) and  $\eta$  (unlike the interactionless), with increasing maximum  $\mathcal{P}_{mP}$  and  $\eta_{ME}$  at  $V_{2mP}$  and  $V_{2ME}$ , respectively, as  $\tau$  is decreased toward the limit  $\tau \rightarrow 0$ , in which the system becomes equivalent to the (simultaneous) contact with hot and cold thermal baths (see Eq. 4.21). Second, despite the increase of  $\tau$  reduces  $\mathcal{P}$  and  $\eta$ , it enlarges the heat engine operation. Thus, the period can be conveniently chosen to obtain a desirable compromise between the system performance (power and efficiency) and the range of the operation regime.

A second aspect to be investigated in this section relies on the inclusion of a distinct duration of each stage, measured by the asymmetry  $\kappa = \tau_1/\tau_2$ . This ingredient has been revealed to be a powerful ingredient for improving the system's power in the interactionless case [107] or even both  $\mathcal{P}$  and  $\eta$  in the case of collisional Brownian engines [108] and is depicted in the right panels of Fig. 4.4. Although  $\eta$  typically increases as  $V^{(2)}$  raises and

$\kappa$  (or  $\tau_1$ ) is reduced, consistent with the system placed in contact with the hot thermal bath during a larger interval, there is an optimal  $\kappa_o$  ensuring optimal power  $\mathcal{P}_{mP}$ . Thus, like the interactionless case [107],  $\kappa$  can be conveniently chosen in order to increase the power-output and  $\mathcal{P} > \mathcal{P}_s$ . Since  $\eta > \eta_s$  for a broad range of  $V^{(2)}$ 's and the interaction offers an extra advantage in which  $\kappa$  can be suitably chosen in order to obtain the desired  $\eta$  (greater than  $\eta_s$ ) or even the desired compromise between  $\mathcal{P}$  and  $\eta$ .

### Global phase diagram for distinct interactions at each stroke

In this section, we depict the system phase diagram (top panel) built from inequalities,  $(\epsilon_2 - \epsilon_1)(\bar{J}_{01}^{(1)} - \bar{J}_{21}^{(1)}) < (V_1 - V_2)(\bar{J}_{01}^{(1)} + \bar{J}_{21}^{(1)})$  and  $\epsilon_2(\bar{J}_{21}^{(1)} - \bar{J}_{01}^{(1)}) > V_2(\bar{J}_{01}^{(1)} + \bar{J}_{21}^{(1)})$ , shown in the main text for the heat engine (HE) regime and the other way around for the pump (P). In particular, the crossover between HE and P regimes will be characterized by ideal efficiency provided  $\epsilon_1/\epsilon_2 = V_1/V_2 = \beta_2/\beta_1$  (green symbols). The bottom panels show, for different sets of temperatures, the phase diagram  $V_1/V_2 \times \epsilon_1/\epsilon_2$ . As discussed in the main text, while larger  $\beta_1/\beta_2$  favors the HE regime, its decrease increases the region in which the system operates as a pump.

## 4.3.2 Distinct Non-conservative Drivings

### Main expressions and heat maps

Our second approach encompasses a worksource coming from a non-conservative driving, introduced by means of a bias in order to benefit certain transitions. By following the ideas of Refs.[5, 36, 109], transitions of type  $i \rightarrow i+1$  ( $i \rightarrow i-1$ ) are favored according to whether the system is placed in contact with the cold (hot) thermal baths, leading to an incremental  $\mathcal{P}$  reading  $F_\nu$ , whereas the remaining parameters ( $V$  and  $\epsilon$ ) are held fixed. Our study relies on investigating two important aspects: the role of drivings at each stroke and its relationship with  $V$ , temperatures  $\beta_1/\beta_2$  and the influence of period  $\tau$ . Transition

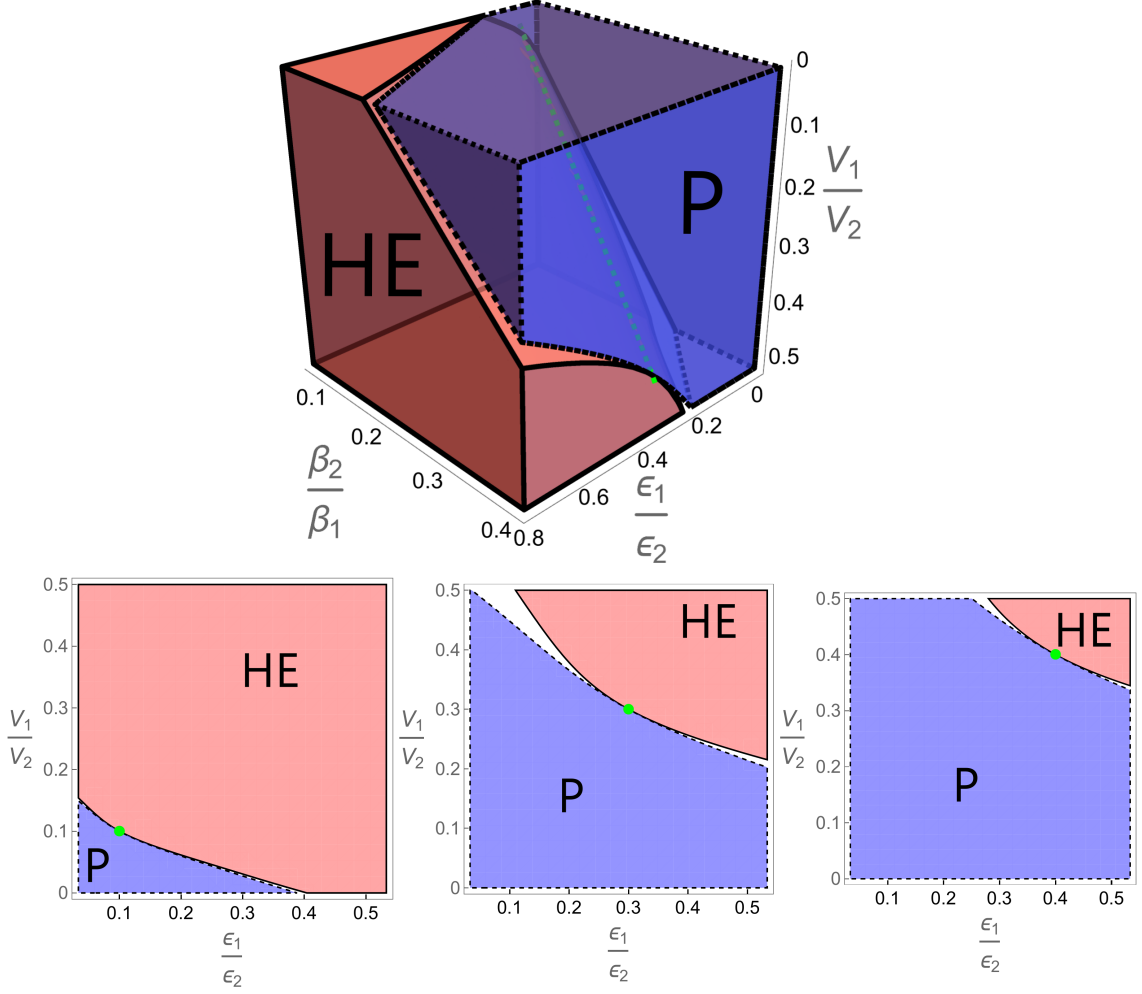


Figure 4.5: Top panel: The phase diagram  $\beta^{(2)}/\beta^{(1)} \times V^{(1)}/V^{(2)} \times \epsilon^{(1)}/\epsilon^{(2)}$ . The green line represents the points where  $\beta^{(2)}/\beta^{(1)} = V^{(1)}/V^{(2)} = \epsilon^{(1)}/\epsilon^{(2)}$ . Bottom panels depict, for  $\beta^{(1)} = 10$  (left),  $\beta^{(1)} = 10/3$  (middle) and  $\beta^{(1)} = 10/4$  (right), the phase diagrams in the  $V^{(1)}/V^{(2)} \times \epsilon^{(1)}/\epsilon^{(2)}$  plane. P and HE denote, respectively, the pump and heat engine regimes. White region attempts to the dud regime, whereas green bullets correspond to the ideal efficiency  $\eta_c$ .

rates  $\omega_{ij}^{(\nu)}$  follow Eq. (4.10) and are listed below

$$\omega_{10}^{(\nu)} = 2\Gamma \exp\left\{-\frac{\beta^{(\nu)}}{2}(E_a + V + \epsilon + (-1)^\nu F_\nu)\right\} \quad (4.24)$$

$$\omega_{01}^{(\nu)} = \Gamma \exp\left\{-\frac{\beta^{(\nu)}}{2}(E_a - V - \epsilon - (-1)^\nu F_\nu)\right\} \quad (4.25)$$

$$\omega_{21}^{(\nu)} = \Gamma \exp\left\{-\frac{\beta^{(\nu)}}{2}(E_a + \epsilon - V + (-1)^\nu F_\nu)\right\} \quad (4.26)$$

$$\omega_{12}^{(\nu)} = 2\Gamma \exp\left\{-\frac{\beta^{(\nu)}}{2}(E_a - \epsilon + V - (-1)^\nu F_\nu)\right\}, \quad (4.27)$$

where  $F_\nu$  assumes distinct values at each stroke. Parameter  $E_a$  attempts to an activation energy and it will be included in order to draw a comparison with previous results [5,

110]. Although our main findings are independent of  $E_a$ , its inclusion makes the heat engine regime more pronounced. From now on, we shall set  $E_a = 1$  in all analyses.

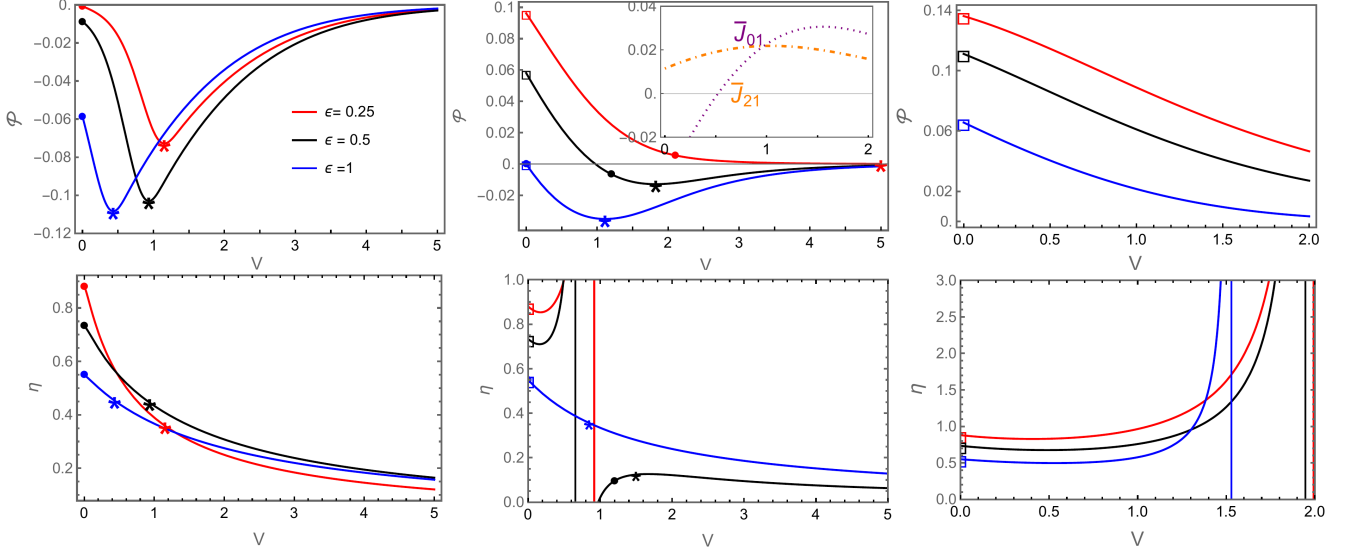


Figure 4.6: Depiction of power  $\mathcal{P}$  (top) and efficiency  $\hat{\eta}$  (bottom) versus  $V$  for distinct  $\beta^{(1)}$ 's. Parameters:  $\beta^{(2)} = 1, E_a = 1, F_2 = 1, F_1 = 0.1$  and  $\tau = 1$  and  $\beta^{(1)} = 10$  (left),  $\beta^{(1)} = 20/9$  (middle) and  $\beta^{(1)} = 3/2$  (right). Stars and squares denote the location of  $\mathcal{P}_{mP}$ 's for heat engine and pump, respectively. Circles and triangles denote the location of maximum efficiencies for the engine ( $0 \leq \eta < \eta_c$ ) and pump ( $\eta_c < \eta \leq \infty$ ) regimes, respectively.

From Eqs. (4.13) and (4.14) and by taking  $V^{(1)} = V^{(2)} = V$  and  $\epsilon^{(1)} = \epsilon^{(2)} = \epsilon$ , the average power and the heat extracted exchanged with the hot bath are given by the following expressions

$$\mathcal{P} = -(F_1 + F_2)(\langle J \rangle_{01}^{(1)} - \langle J \rangle_{21}^{(1)}), \quad (4.28)$$

$$\langle \dot{Q} \rangle^{(2)} = \left[ (V + \epsilon + F_2) \langle J \rangle_{01}^{(1)} + (V - \epsilon - F_2) \langle J \rangle_{21}^{(1)} \right], \quad (4.29)$$

whose system entropy production reads  $\bar{\sigma} = -\beta^{(1)} \langle \dot{Q} \rangle^{(1)} - \beta^{(2)} \langle \dot{Q} \rangle^{(2)}$  and assumes the bilinear form  $\langle \sigma \rangle = J_1 X_1 + J_2 X_2$ , where  $J_1 = \langle J_{01}^{(1)} \rangle$  and  $J_2 = \langle J_{21}^{(1)} \rangle$  with thermodynamic forces  $X_1$  and  $X_2$  given by

$$\begin{aligned} X_1 &= \frac{\epsilon + V + F_2}{T^{(2)}} - \frac{\epsilon + V - F_2}{T^{(1)}}, \\ X_2 &= \frac{\epsilon - V + F_2}{T^{(2)}} - \frac{\epsilon - V - F_2}{T^{(1)}}. \end{aligned} \quad (4.30)$$

The efficiency is given by the ratio between  $\mathcal{P}$  and  $\overline{Q}_2$  given by

$$\eta = \frac{(F_1 + F_2)(\langle J \rangle_{01}^{(1)} - \langle J \rangle_{21}^{(1)})}{(V + \epsilon + F_2)\langle J \rangle_{01}^{(1)} + (V - \epsilon - F_2)\langle J \rangle_{21}^{(1)}}, \quad (4.31)$$

respectively. The existence of the heat engine and pump regimes imposes some constraints in the fluxes, implying that in the former case, parameters have to be adjusted in such a way that  $\langle J \rangle_{01}^{(1)} > \langle J \rangle_{21}^{(1)}$  and  $V(\langle J \rangle_{01}^{(1)} + \langle J \rangle_{21}^{(1)}) > (\epsilon + F_2)(\langle J \rangle_{21}^{(1)} - \langle J \rangle_{01}^{(1)})$ , whereas the latter (pump) implies opposite inequalities.

A first insight about the influence of drivings is depicted in Figs. 4.6 for fixed  $F_1/F_2$ . Efficiency and power curves exhibit an interesting and rich behavior due to the interplay among parameters  $\epsilon, V, \beta^{(1)}/\beta^{(2)}$  and  $\tau$ . While the heat regime is levered by increasing  $\epsilon$  and/or the ratio  $\beta^{(1)}/\beta^{(2)}$  (left and middle panels), the pump regime is favored for lower values of  $\beta^{(1)}/\beta^{(2)}$  (middle and right). The crossover from the heat to the pump regimes gives rise to an intermediate regime in which the system operates dudly (see e.g. middle panels). In such a case, there are optimal interactions  $V_{mP}$  and  $V_{ME}$  marking maximum (absolute) power ( $\mathcal{P}_{mP}$ ) and efficiency ( $\eta_{ME}$ ), respectively. Conversely, only  $\mathcal{P}$  can be optimized when the crossover between the above regimes is marked by the absence of a dud regime (e.g. left and right panels) and  $\eta$  monotonically decreases upon  $V$  being raised. Fig. 4.7 extends the above findings by depicting heat maps for the efficiency and power for distinct ratio  $F_1/F_2$  and fixed  $\epsilon$ . Similarly to systems composed of many interacting units under fixed drivings [36, 110], the power  $\mathcal{P}$  presents a simultaneous maximization (concerning both  $V$  and  $F_1/F_2$ ), whereas  $\eta$  approaches to the ideal regime  $F_2/F_1$  is increased. However, a difference with respect to previous studies concerns the absence of a heat engine as  $F_1 = F_2$ . Unlike Refs. [5, 36, 110], in which the heat engine was investigated for large  $N$ 's, our minimal setup of  $N = 2$  interacting units requires a desirable compromise between  $F_\nu$ 's and parameters for operating properly as a heat engine.

The influence of period is depicted in Fig. 4.8 for the same parameters from Fig. 4.7 (left and right panels). In both cases,  $\mathcal{P}$  is strongly influenced by the period and approaches to the simultaneous contact with baths as  $\tau \rightarrow 0$ , whose expressions were presented in Eq.(4.9a). Also, depending on the parameters the engine is projected (right panels), the increase of  $\tau$  changes the regime operation, from heat engine to pump. In both cases, the behavior of  $\eta$  is more revealing and mildly changes with  $\tau$ . While small

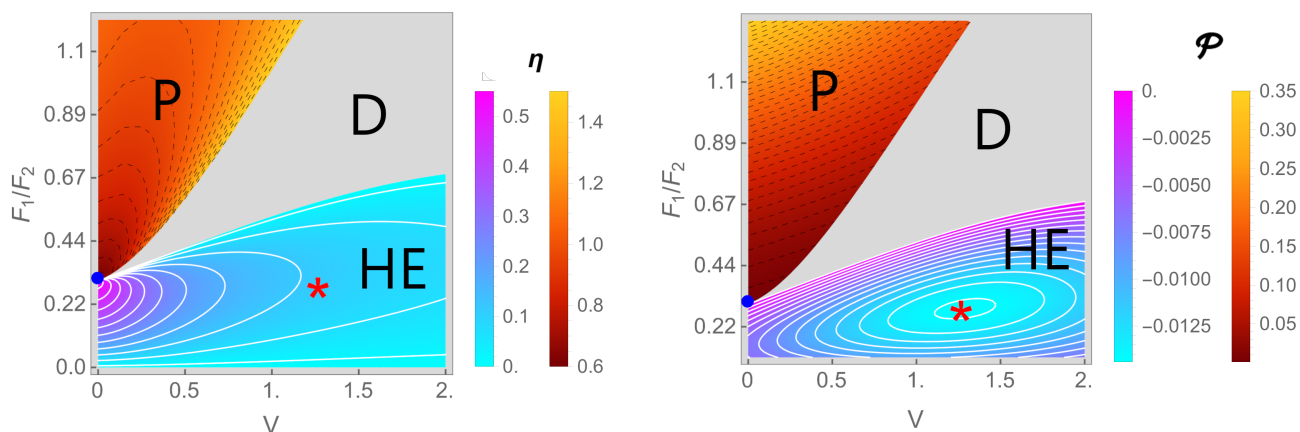


Figure 4.7: The same as in Fig.4.2, but by changing the drivings at each stroke. Parameters:  $\epsilon = 0.5$ ,  $\beta^{(2)} = 1$ ,  $\beta^{(1)} = 20/9$ ,  $E_a = 1$ ,  $\tau = 1$ ,  $F_2 = 0.45$

differences are almost imperceptible in the left panels, a somewhat increase of  $\eta$  as  $\tau$  is lowered is verified. This finding is remarkable, because it may be used for conveniently choosing the period in order to obtain the desirable  $\mathcal{P}$  with a small variation of  $\eta$ .

### Asymmetric time switchings

In the last analysis, we investigate the influence of asymmetric interaction times in the presence of distinct drivings at each stroke, as shown in Fig.4.9. In similarity with Fig. 4.4, the asymmetry can be conveniently chosen for enhancing the power and efficiency or even for obtaining a desirable compromise between them. There is an optimal  $\kappa_o$  leading to simultaneous maximization of power while  $\eta$  always increases as  $\kappa$  is lowered, consistent with the contact with a hot bath for a larger amount of the period. Despite such similarities, the asymmetry seems to be less pronounced than in the previous case, and optimal quantities do not deviate significantly from the symmetric ( $\kappa = 1$ ) case. A possible reason is that power and efficiency exhibit a more intricate dependence on fluxes and changes of energy parameters (former approach) than on driving variations [see e.g. Eqs. (4.19)-(4.28) and (4.20)-(4.31)].

### 4.3.3 The fast time switchings $\tau \rightarrow 0$ and the two reservoirs case

In the regime of fast switching dynamics,  $\tau \rightarrow 0$ , one gets the following expressions for fluxes

$$\lim_{\tau \rightarrow 0} \bar{J}_{01}^{(1)} = \frac{1}{2Z} \left( \omega_{01}^{(1)} \omega_{10}^{(2)} - \omega_{10}^{(1)} \omega_{01}^{(2)} \right) \left( \omega_{12}^{(1)} + \omega_{12}^{(2)} \right), \quad (4.32)$$

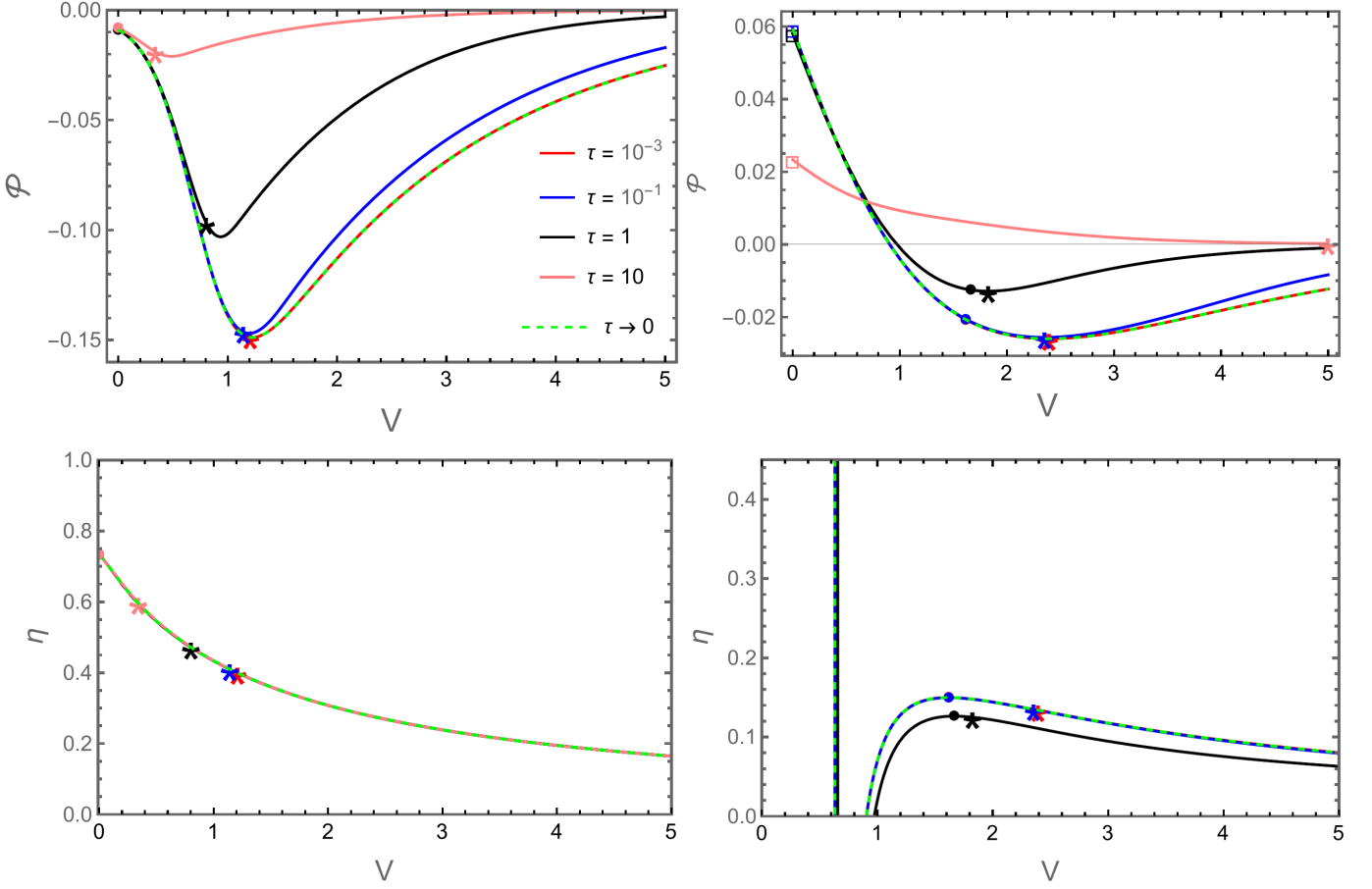


Figure 4.8: The influence of period  $\tau$  over the system performance. Depiction of  $\mathcal{P}$  and  $\eta$  versus  $V$  for distinct  $\tau$ 's for  $\beta^{(1)} = 10$  (left) and  $\beta^{(1)} = 20/9$  (right). Parameters:  $\beta^{(2)} = 1, E_a = 1, \epsilon = 0.5, F_2 = 1, F_1 = 0.1$ .

and

$$\lim_{\tau \rightarrow 0} \bar{J}_{21}^{(1)} = \frac{1}{2Z} \left( \omega_{21}^{(1)} \omega_{12}^{(2)} - \omega_{12}^{(1)} \omega_{21}^{(2)} \right) \left( \omega_{10}^{(1)} + \omega_{10}^{(2)} \right), \quad (4.33)$$

where

$$Z = \left( \omega_{01}^{(1)} + \omega_{01}^{(2)} \right) \left( \omega_{12}^{(1)} + \omega_{12}^{(2)} \right) + \left( \omega_{10}^{(1)} + \omega_{10}^{(2)} \right) \left( \omega_{21}^{(1)} + \omega_{21}^{(2)} \right) + \left( \omega_{01}^{(1)} + \omega_{01}^{(2)} \right) \left( \omega_{21}^{(1)} + \omega_{21}^{(2)} \right) + \left( \omega_{10}^{(1)} + \omega_{10}^{(2)} \right) \left( \omega_{12}^{(1)} + \omega_{12}^{(2)} \right). \quad (4.34)$$

The above expressions can be understood from the fact the system relaxes “infinitely fast” to its steady state at each stroke, allowing to rewrite Eq.(4.3) in the following form  $\dot{p}_i^{(\nu)}(t) = \sum_{j \neq i} \{ \omega_{ji}^{(\nu)} p_i(t) - \omega_{ij}^{(\nu)} p_j(t) \}$ , where  $p_i(t) = p_i^{(1)}(t) + p_i^{(2)}(t)$ . Thus, the fully dynamics is described by  $\dot{p}_i(t) = \sum_{j \neq i} \{ \Omega_{ji} p_i(t) - \Omega_{ij} p_j(t) \}$ , where  $\Omega_{ij} = \omega_{ij}^{(1)} + \omega_{ij}^{(2)}$ , which is equivalent to the simultaneous contact with both thermal reservoirs. A second way of understanding such a limit comes from the time integration of the master Equation over each stage by taking into account the boundary conditions. In such cases, the steady

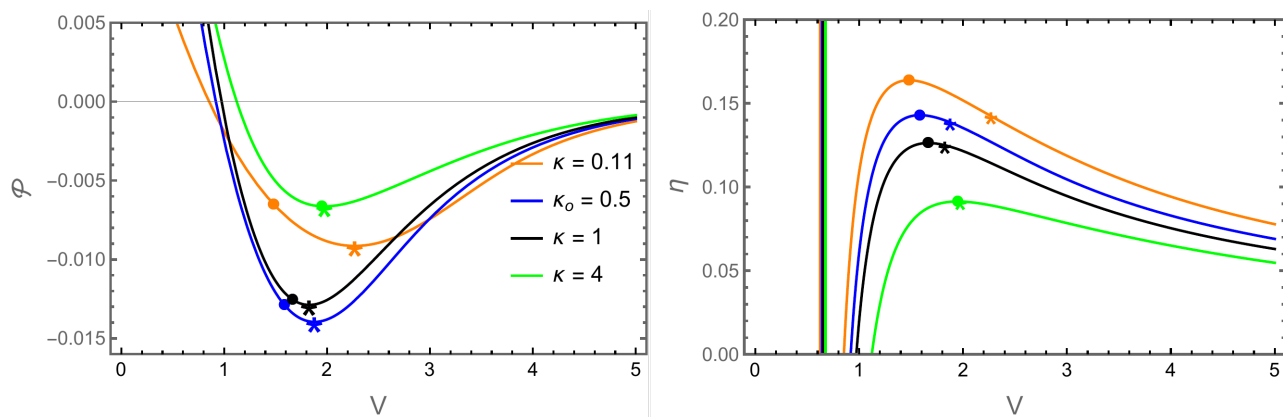


Figure 4.9: Depiction of power  $\mathcal{P}$  and efficiency  $\eta$  versus  $V$  for different  $\kappa$ . Symbols  $\bullet$  and  $*$  denote the maximization of efficiency and power, respectively. Parameters:  $\epsilon = 0.5$ ,  $\beta^{(2)} = 1$ ,  $\beta^{(1)} = 20/9$ ,  $E_a = 1$ ,  $\tau = 1$ ,  $F_1 = 0.1$ ,  $F_2 = 1$ .

state regime is given by the following relations  $(\omega_{01}^{(1)} + \omega_{01}^{(2)})p_1 - (\omega_{10}^{(1)} + \omega_{10}^{(2)})p_0 = 0$  and  $(\omega_{20}^{(1)} + \omega_{20}^{(2)})p_0 + (\omega_{12}^{(1)} + \omega_{12}^{(2)})p_2 - (\omega_{01}^{(1)} + \omega_{01}^{(2)} + \omega_{21}^{(1)} + \omega_{21}^{(2)})p_1 = 0$ . By solving above system of linear equations, together with the condition  $p_0 + p_1 + p_2 = 1$ , one finds the following expressions for the probabilities:

$$p_0 = \frac{1}{Z} (\omega_{01}^{(1)} + \omega_{01}^{(2)}) (\omega_{12}^{(1)} + \omega_{12}^{(2)}),$$

$$p_1 = \frac{1}{Z} (\omega_{10}^{(1)} + \omega_{10}^{(2)}) (\omega_{12}^{(1)} + \omega_{12}^{(2)}), \quad (4.35)$$

$$p_2 = \frac{1}{Z} (\omega_{10}^{(1)} + \omega_{10}^{(2)}) (\omega_{21}^{(1)} + \omega_{21}^{(2)}). \quad (4.36)$$

$$(4.37)$$

It is worth mentioning that  $p_i$ 's can be alternatively obtained via the spanning tree method for  $N = 2$ . From  $p_i$ 's, fluxes are promptly obtained, providing the same results as Eq. (4.32) and (4.33). Thermodynamic quantities are straightforwardly evaluated, whose main expressions for  $\mathcal{P}$ ,  $\langle \dot{Q}_2 \rangle$  and  $\eta$  and have been shown along the main text.

#### 4.3.4 Concluding Remarks

Nanoscale engines operating via collective operation have attracted considerable attention and posed as potential candidates for the construction of reliable setups. However, given that most studies are restricted to fixed thermodynamic forces, little is known about how its construction influences the performance. The present study aimed to fill partially this gap by investigating the thermodynamic quantities of a minimalist collective model



placed sequentially with distinct thermal baths at each stage. Distinct aspects have been addressed, such as different worksources, the role of interactions, the period, and the time durations of each stroke. Results indicate that our minimal approach, together with a suitable choice of parameters, not only can boost the system performance, providing optimal power outputs and efficiencies greater than its interactionless case but also guide the operation regime, including distinct heat engine and pump regimes. Although the ideal regime  $\tau \rightarrow 0$  provides higher performances than for finite  $\tau$ , our contribution sheds light on how the interplay between interaction and individual parameters, together a suitable tuning of the interaction time can optimize both power and efficiency as much as possible under more a realistic context (finite  $\tau$ ). Another remarkable finding concerns that the case of the system simultaneously placed in contact with two thermal reservoirs, previously investigated in various works [5, 7, 101], constitutes a particular case of our framework for fast switchings.

# Chapter 5

## Conclusion

In this work, we investigated, from stochastic thermodynamics, two classes of collective systems. The former was one of the simplest (and most important) opinion models, the majority vote model, displaying the same symmetry as the Ising model. The second model is a prototype of an engine operating collectively.

The idea was to associate, for each local model neighborhood, a distinct thermal reservoir, enabling us to express transition rates according to the local detailed balance and then to associate a well defined temperature. Such an idea has revealed general and it has been considered for distinct opinion models defined by Ising-like variables. The connection between the entropy production and heat was performed together with a detailed analysis of their behaviors in the phase transition regimes, for both regular and complex topologies. Another remarkable aspect of our study relies on the fact that, as the system presents several independent heat fluxes as the neighborhood is large, our framework was able to exploit the most significant ones. With this, we were able to derive a way to estimate entropy production, given a certain upper bound, based on the first and last contributing fluxes. Finally, we were able to further investigate the relationships of said fluxes both at the phase transitions (discontinuous) and with dissipation.

In the second part, we investigated, in detail, distinct approaches for a minimal prototype of a nonequilibrium engine setup. Our results showed that a suited choice of parameters, together with the duration of each stroke, can boost the system performance, leading to efficiencies close to the ideal values, even for an engine composed of two interacting units. Also, despite the model's simplicity and expressions for thermodynamic

quantities being quite cumbersome, our results shed light not only on the collective behavior in a minimal setup but also on how some nonequilibrium projections correspond to particular cases of our implementation.

As potential perspectives of our work, we highlight the usage of voter models as approaches for nonequilibrium engine setups, as well as to optimize the associated power and efficiency. This raises several questions, such as a comparison between opinion models or even the influence of the lattice topology. A question that naturally arises about the second study is an extension for distinct system sizes, in which a phase transition is expected [5], and also possible ramifications of the approach utilized, such as the study of active matter systems as possible worksources, given they also operate out of equilibrium [19, 28]. Another extension of our project concerns the thermodynamics and efficiency of active matter engines [111, 112]. Unlike the engines studied throughout this thesis, active ones operates at the "level of individual particles" and not just by external drivings or difference of temperatures presenting two fundamental ingredients, *i.e.*, self-propulsion and collective dynamics. The so-called "active thermal engines", although less studied in the literature, may present superior performance to classical "non-active" engines as they involve additional degrees of freedom, related to the interactions between particles . In this case, they can operate between temperatures substantially different (effective) and presenting non-conventionally high efficiencies. Such points should be investigated in the future.



# Bibliography

- [1] Herbert B Callen. “Thermodynamics and an Introduction to Thermostatistics”. John Wiley & Sons, New York, (1960).
- [2] R.K. Pathria and Paul D. Beale. Statistical Mechanics. 4th ed. Academic Press, 2021.
- [3] S. R. De Groot and P. Mazur. Non-Equilibrium Thermodynamics. Dover ed. Dover Books on Physics. Dover Publications, (2011).
- [4] Tânia Tomé and Mário J De Oliveira. Stochastic dynamics and irreversibility. Springer, 2015.
- [5] Hadrien Vroylandt, Massimiliano Esposito, and Gatiën Verley. “Collective effects enhancing power and efficiency”. EPL (Europhysics Letters), 120.3 (2017), p. 30009.
- [6] Massimiliano Esposito et al. “Quantum-dot Carnot engine at maximum power”. Physical Review E, 81.4 (2010), p. 041106.
- [7] Alexandre Rosas, Christian Van den Broeck, and Katja Lindenberg. “Stochastic thermodynamics for a periodically driven single-particle pump”. Phys. Rev. E, 96 (5 2017), p. 052135.
- [8] Alexandre Rosas, Christian Van den Broeck, and Katja Lindenberg. “Three-stage stochastic pump: Another type of Onsager-Casimir symmetry and results far from equilibrium”. Phys. Rev. E, 97 (6 2018), p. 062103.
- [9] Bernhard Altaner, Artur Wachtel, and Jürgen Vollmer. “Fluctuating currents in stochastic thermodynamics. II. Energy conversion and nonequilibrium response in kinesin models”. Phys. Rev. E, 92 (4 2015), p. 042133.
- [10] S. Ciliberto. “Experiments in Stochastic Thermodynamics: Short History and Perspectives”. Physical Review X, 7.021051 (2017), p. 1.

## BIBLIOGRAPHY

---

- [11] Yunxin Zhang. “Optimisation of a class of heat engines with explicit solution”. Physica A: Statistical Mechanics and its Applications, 527 (2019), p. 121272. ISSN: 0378-4371.
- [12] T. Schmiedl and U. Seifert. “Efficiency at maximum power: An analytically solvable model for stochastic heat engines”. EPL (Europhysics Letters), 81.2 (2007), p. 20003. ISSN: 1286-4854.
- [13] Massimiliano Esposito, Katja Lindenberg, and Christian Van den Broeck. “Universality of Efficiency at Maximum Power”. Phys. Rev. Lett., 102 (13 2009), p. 130602.
- [14] Michael Bauer, Kay Brandner, and Udo Seifert. “Optimal performance of periodically driven, stochastic heat engines under limited control”. Phys. Rev. E, 93 (4 2016), p. 042112.
- [15] D. Guéry-Odelin et al. “Shortcuts to adiabaticity: Concepts, methods, and applications”. Rev. Mod. Phys., 91 (4 2019), p. 045001.
- [16] Sebastian Deffner and Marcus VS Bonança. “Thermodynamic control—An old paradigm with new applications”. EPL (Europhysics Letters), 131.2 (2020), p. 20001.
- [17] Xiu-Hua Zhao, Zheng-Nan Gong, and Z. C. Tu. “Low-dissipation engines: Microscopic construction via shortcuts to adiabaticity and isothermality, the optimal relation between power and efficiency”. Physical Review E, 106.6 (2022). ISSN: 2470-0053.
- [18] Nicola Pancotti et al. “Speed-Ups to Isothermality: Enhanced Quantum Thermal Machines through Control of the System-Bath Coupling”. Phys. Rev. X, 10 (3 2020), p. 031015.
- [19] Michael E. Cates and Julien Tailleur. “Motility-Induced Phase Separation”. Annual Review of Condensed Matter Physics, 6.1 (2015), pp. 219–244.
- [20] Sherwood Martineau et al. “Enhancing Synchronization by Optimal Correlated Noise”. Physical Review Letters, 128.9 (2022). ISSN: 1079-7114.
- [21] Lynn Frierson Faust. “Natural History and Flash Repertoire of the Synchronous Firefly *Photinus carolinus* (Coleoptera: Lampyridae) in the Great Smoky Mountains National Park”. Florida Entomologist, 93.2 (2010), pp. 208–217.

- [22] Juan A. Acebrón et al. “The Kuramoto model: A simple paradigm for synchronization phenomena”. Rev. Mod. Phys., 77 (1 2005), pp. 137–185.
- [23] Ralf Tönjes, Carlos E Fiore, and Tiago Pereira. “Coherence resonance in influencer networks”. Nature Communications, 12.1 (2021), pp. 1–8.
- [24] Hongbo Zhao, Andrej Košmrlj, and Sujit S. Datta. Chemotactic motility-induced phase separation. 2023. arXiv: [2301.12345](https://arxiv.org/abs/2301.12345) [[physics.bio-ph](https://arxiv.org/archive/physics)].
- [25] H C Berg and D A Brown. “Chemotaxis in Escherichia coli analysed by three-dimensional tracking”. Nature, 239.5374 (1972), pp. 500–504.
- [26] Manfred Schienbein and Hans Gruler. “Langevin equation, Fokker-Planck equation and cell migration”. Bulletin of mathematical biology, 55 (1993), pp. 585–608.
- [27] Tamás Vicsek and Anna Zafeiris. “Collective motion”. Physics Reports, 517.3–4 (2012), pp. 71–140. ISSN: 0370-1573.
- [28] Sriram Ramaswamy. “Active matter”. Journal of Statistical Mechanics: Theory and Experiment, 2017.5 (2017), p. 054002. ISSN: 1742-5468.
- [29] Hanshuang Chen et al. “Critical noise of majority-vote model on complex networks”. Physical Review E, 91.2 (2015).
- [30] Pedro E Harunari, MM de Oliveira, and Carlos Eduardo Fiore. “Partial inertia induces additional phase transition in the majority vote model”. Physical Review E, 96.4 (2017), p. 042305.
- [31] C.E. Fernández Noa et al. “Entropy production as a tool for characterizing nonequilibrium phase transitions”. Physical Review E, 100.1 (2019), p. 012104.
- [32] CE Fernández Noa, William GC Oropesa, and CE Fiore. “Thermodynamics of collisional models for Brownian particles: General properties and efficiency”. Physical Review Research, 2.4 (2020), p. 043016.
- [33] Tânia Tomé, Carlos E Fiore, and Mário J de Oliveira. “Stochastic thermodynamics of opinion dynamics”. arXiv preprint arXiv:2212.07268, (2022).
- [34] Felipe Hawthorne et al. “Nonequilibrium Thermodynamics of the Majority Vote Model”. Entropy, 25.8 (2023). ISSN: 1099-4300.

- [35] Fernando S. Filho et al. “Thermodynamics and efficiency of sequentially collisional Brownian particles: The role of drivings”. Phys. Rev. E, 106 (4 2022), p. 044134.
- [36] Fernando S Filho et al. “Powerful ordered collective heat engines”. arXiv preprint arXiv:2301.06591, (2023).
- [37] Angel L. L. Stable et al. “Thermodynamics of collisional models for Brownian particles: General properties and efficiency”. Physical Review Research, 2.4 (2020).
- [38] Pedro E. Harunari et al. “Maximal power for heat engines: Role of asymmetric interaction times”. Phys. Rev. Research, 3 (2 2021), p. 023194.
- [39] C. Van den Broeck. “Thermodynamic Efficiency at Maximum Power”. Phys. Rev. Lett., 95 (19 2005), p. 190602.
- [40] Udo Seifert. “Stochastic thermodynamics, fluctuation theorems and molecular machines”. Rep. Prog. Phys., 75.12 (2012), p. 126001.
- [41] Shubhashis Rana et al. “Single-particle stochastic heat engine”. Physical review E, 90.4 (2014), p. 042146.
- [42] Ignacio A Martinez et al. “Brownian carnot engine”. Nature physics, 12.1 (2016), pp. 67–70.
- [43] JD Seader. “Thermodynamic efficiency of chemical processes” (1982).
- [44] Massimiliano Esposito et al. “Quantum-dot Carnot engine at maximum power”. Phys. Rev. E, 81 (4 2010), p. 041106.
- [45] Waqar Khan et al. “Efficient and continuous microwave photoconversion in hybrid cavity-semiconductor nanowire double quantum dot diodes”. Nature Communications, 12.1 (2021).
- [46] Karel Proesmans et al. “Brownian duet: a novel tale of thermodynamic efficiency”. Physical Review X, 6.4 (2016), p. 041010.
- [47] N. Golubeva and A. Imparato. “Efficiency at Maximum Power of Interacting Molecular Machines”. Phys. Rev. Lett., 109 (19 2012), p. 190602.
- [48] CE Fernandez Noa et al. “Thermodynamics of a collisional quantum-dot machine: the role of stages”. arXiv e-prints, (2023), arXiv–2305.
- [49] H Vroylandt, M Esposito, and Gatien Verley. “Collective effects enhancing power and efficiency”. EPL (Europhysics Letters), 120.3 (2017), p. 30009.



## BIBLIOGRAPHY

---

- [50] Robert Brown. “A brief account of microscopical observations made in the months of June, July and August, 1827, on the particles contained in the pollen of plants; and on the general existence of active molecules in organic and inorganic bodies”. Philosophical Magazine, 4 (1828), pp. 161–173.
- [51] Paul Langevin. “Sur la théorie du mouvement brownien”. C. R. Acad. Sci. (Paris), 146 (1908), pp. 530–533.
- [52] Don S. Lemons. An Introduction to Stochastic Processes in Physics. Johns Hopkins University Press, (2002).
- [53] Albert Einstein. “Über die von der molekularkinetischen Theorie der Wärme geforderte Bewegung von in ruhenden Flüssigkeiten suspendierten Teilchen”. Annalen der Physik, 322.8 (1905), pp. 549–560.
- [54] H Haken. “"Sociology: A Stochastic Model for the Formation of Public Opinion"”. Synergetics. Springer, (1978).
- [55] Howard C. Berg. Random Walks in Biology. Princeton: Princeton University Press, (1984).
- [56] R B Dickinson and R T Tranquillo. “A stochastic model for adhesion-mediated cell random motility and haptotaxis”. J Math Biol, 31.6 (1993), pp. 563–600.
- [57] James P. Sethna. Statistical Mechanics: Entropy, Order Parameters, and Complexity. 2nd ed. Oxford Master Series in Physics. Oxford University Press, (2021).
- [58] Massimiliano Esposito. “Stochastic thermodynamics under coarse graining”. Physical Review E, 85.4 (2012), p. 041125.
- [59] A. Khrennikov, ed. PQ-QP: Quantum Probability and White Noise Analysis, Volume XIII. Conference held in Växjö, Sweden, 25 November – 1 December 2000. New Jersey, London, Singapore, Hong Kong: World Scientific, (2000).
- [60] Joaquin Marro and Ronald Dickman. Nonequilibrium Phase Transitions in Lattice Models. Collection Alea-Saclay: Monographs and Texts in Statistical Physics. Cambridge University Press, 1999.
- [61] Karel Proesmans, Bart Cleuren, and Christian Van den Broeck. “Power-efficiency-dissipation relations in linear thermodynamics”. Physical review letters, 116.22 (2016), p. 220601.

- [62] JM Encinas et al. “Majority vote model with ancillary noise in complex networks”. Physica A: Statistical Mechanics and its Applications, 516 (2019), pp. 563–570.
- [63] Ronald Dickman. “Numerical analysis of the master equation”. Physical Review E, 65.4 (2002). ISSN: 1095-3787.
- [64] E G D Cohen. “Properties of nonequilibrium steady states: a path integral approach”. Journal of Statistical Mechanics: Theory and Experiment, 2008.07 (2008), P07014. ISSN: 1742-5468.
- [65] José Nahuel Freitas and Massimiliano Esposito. “Emergent second law for non-equilibrium steady states”. Nature Communications, 13.1 (2022). ISSN: 2041-1723.
- [66] Jürgen Schnakenberg. “Network theory of microscopic and macroscopic behavior of master equation systems”. Reviews of Modern physics, 48.4 (1976), p. 571.
- [67] Silvio RA Salinas. “Introduction to Statistical Methods”. Introduction to Statistical Physics. Springer, 2001, pp. 1–17.
- [68] Johannes Roßnagel et al. “A single-atom heat engine”. Science, 352.6283 (2016), pp. 325–329.
- [69] Bart Cleuren and Karel Proesmans. “Stochastic impedance”. Physica A: Statistical Mechanics and its Applications, (2019), p. 122789.
- [70] Carlos E. Fiore and Mário J. de Oliveira. “Entropy production and heat capacity of systems under time-dependent oscillating temperature”. Phys. Rev. E, 99 (5 2019), p. 052131.
- [71] Pedro E Harunari, Carlos E Fiore, and Karel Proesmans. “Exact statistics and thermodynamic uncertainty relations for a periodically driven electron pump”. Journal of Physics A, 53.37 (2020), p. 374001.
- [72] Julia M Yeomans. Statistical mechanics of phase transitions. Clarendon Press, 1992.
- [73] L. D. Landau and E. M. Lifshitz. Statistical Physics. 3rd ed. Butterworth-Heinemann, 1980.
- [74] P. M. Chaikin and T. C. Lubensky. Principles of condensed matter physics. Cambridge: Cambridge University Press, 1995.

## BIBLIOGRAPHY

---

- [75] Leo P. Kadanoff. “More is the Same Phase Transitions and Mean Field Theories”. Journal of Statistical Physics, 137.5-6 (2009), pp. 777–797.
- [76] Tamas Vicsek et al. “Novel type of phase transition in a system of self-driven particles”. Physical Review Letters, 75.6 (1995), p. 1226.
- [77] Francesco Ginelli. “The Physics of the Vicsek model”. The European Physical Journal Special Topics, 225.11-12 (2016), pp. 2099–2117.
- [78] H. Haken. “The maximum entropy principle for non-equilibrium phase transitions: Determination of order parameters, slaved modes, and emerging patterns”. Zeitschrift fur Physik B Condensed Matter, 63.4 (1986), pp. 487–491.
- [79] Jesus M Encinas et al. “Fundamental ingredients for discontinuous phase transitions in the inertial majority vote model”. Scientific reports, 8.1 (2018), pp. 1–9.
- [80] Carlos E Fiore and Mário J de Oliveira. “Entropy production and heat capacity of systems under time-dependent oscillating temperature”. Physical Review E, 99.5 (2019), p. 052131.
- [81] Feng Huang, Hanshuang Chen, and Chuansheng Shen. “Quenched mean-field theory for the majority-vote model on complex networks”. EPL (Europhysics Letters), 120.1 (2017), p. 18003.
- [82] Allan R. Vieira and Nuno Crokidakis. “Phase transitions in the majority-vote model with two types of noises”. Physica A: Statistical Mechanics and its Applications, 450 (2016), pp. 30–36.
- [83] Thomas M. Liggett. Interacting Particle Systems. New York: Springer-Verlag, 1985.
- [84] Pedro E. Harunari, M. M. de Oliveira, and C. E. Fiore. “Partial inertia induces additional phase transition in the majority vote model”. Physical Review E, 96.4 (2017).
- [85] Jesus M. Encinas et al. “Fundamental ingredients for discontinuous phase transitions in the inertial majority vote model”. Scientific Reports, 8.1 (2018).
- [86] J.M. Encinas et al. “Majority vote model with ancillary noise in complex networks”. Physica A: Statistical Mechanics and its Applications, 516 (2019), pp. 563–570.

## BIBLIOGRAPHY

---

- [87] C. E. Fernández Noa et al. “Entropy production as a tool for characterizing nonequilibrium phase transitions”. Physical Review E, 100.1 (2019).
- [88] Hanshuang Chen and Guofeng Li. “Phase transitions in a multistate majority-vote model on complex networks”. Physical Review E, 97.6 (2018).
- [89] David Landau and Kurt Binder.  
A guide to Monte Carlo simulations in statistical physics. Cambridge university press, 2021.
- [90] Peter Hanggi et al. “Bistable systems: Master equation versus Fokker-Planck modeling”. Physical Review A, 29.1 (1984), p. 371.
- [91] C. E. Fiore et al. “Current fluctuations in nonequilibrium discontinuous phase transitions”. Phys. Rev. E, 104 (6 2021), p. 064123.
- [92] Basile Nguyen and Udo Seifert. “Exponential volume dependence of entropy-current fluctuations at first-order phase transitions in chemical reaction networks”. Phys. Rev. E, 102 (2 2020), p. 022101.
- [93] C Van den Broeck and M Esposito. “Ensemble and trajectory thermodynamics: A brief introduction”. Physica A, 418 (2015), pp. 6–16.
- [94] Christopher Jarzynski. “Nonequilibrium equality for free energy differences”. Physical Review Letters, 78.14 (1997), p. 2690.
- [95] Steffen Liepelt and Reinhard Lipowsky. “Kinesin’s Network of Chemomechanical Motor Cycles”. Phys. Rev. Lett., 98 (25 2007), p. 258102.
- [96] S. Liepelt and R. Lipowsky. “Operation modes of the molecular motor kinesin”. Phys. Rev. E, 79 (1 2009), p. 011917.
- [97] Kiriko Terai et al.  
Biological free energy transduction is an Achilles heel of mean-field transport theory. 2022. arXiv: [2210.16654](https://arxiv.org/abs/2210.16654) [[physics.bio-ph](https://arxiv.org/abs/2210.16654)].
- [98] John AC Albay et al. “Shift a laser beam back and forth to exchange heat and work in thermodynamics”. Scientific reports, 11.1 (2021), pp. 1–10.
- [99] Karel Proesmans and Carlos E Fiore. “General linear thermodynamics for periodically driven systems with multiple reservoirs”. Physical Review E, 100.2 (2019), p. 022141.
- [100] Tânia Tomé and Mário J de Oliveira. “Stochastic approach to equilibrium and nonequilibrium thermodynamics”. Physical review E, 91.4 (2015), p. 042140.

## BIBLIOGRAPHY

---

- [101] Hadrien Vroylandt, Karel Proesmans, and Todd R Gingrich. “Isometric uncertainty relations”. Journal of Statistical Physics, 178.4 (2020), pp. 1039–1053.
- [102] Karel Proesmans et al. “Efficiency of single-particle engines”. Physical review E, 92.3 (2015), p. 032105.
- [103] K Proesmans and C Van den Broeck. “The underdamped Brownian duet and stochastic linear irreversible thermodynamics”. Chaos, 27.10 (2017), p. 104601.
- [104] FL Curzon and B Ahlborn. “Efficiency of a Carnot engine at maximum power output”. American Journal of Physics, 43.1 (1975), pp. 22–24.
- [105] II Novikov. “The efficiency of atomic power stations (a review)”. Journal of Nuclear Energy (1954), 7.1-2 (1958), pp. 125–128.
- [106] Christian Van den Broeck. “Thermodynamic efficiency at maximum power”. Physical Review Letters, 95.19 (2005), p. 190602.
- [107] Pedro E. Harunari et al. “Maximal power for heat engines: Role of asymmetric interaction times”. Phys. Rev. Research, 3 (2 2021), p. 023194.
- [108] C. E. Fernández Noa et al. “Efficient asymmetric collisional Brownian particle engines”. Phys. Rev. Research, 3 (4 2021), p. 043152.
- [109] Tim Herpich, Juzar Thingna, and Massimiliano Esposito. “Collective Power: Minimal Model for Thermodynamics of Nonequilibrium Phase Transitions”. Phys. Rev. X, 8 (3 2018), p. 031056.
- [110] Iago N. Mamede, Karel Proesmans, and Carlos E. Fiore. “Thermodynamics of interacting systems: The role of the topology and collective effects”. Phys. Rev. Res., 5 (4 2023), p. 043278.
- [111] Thomas Speck. “Efficiency of isothermal active matter engines: Strong driving beats weak driving”. Physical Review E, 105.1 (2022). ISSN: 2470-0053.
- [112] Patrick Pietzonka et al. “Autonomous Engines Driven by Active Matter: Energetics and Design Principles”. Physical Review X, 9.4 (2019). ISSN: 2160-3308.

# Appendix A

## Finished and submitted Papers

We show the two papers produced from our work, titled "Nonequilibrium Thermodynamics of the Majority Vote Model" and "Thermodynamics of a minimal collective heat engine: Comparison between engine designs". The former was published in *Entropy* **2023**, 25(8), 1230; [doi.org/10.3390/e25081230](https://doi.org/10.3390/e25081230) and the latter (arXiv: <https://doi.org/10.48550/arXiv.2311.18629>) was submitted for publication at *Physical Review E*.

# Nonequilibrium Thermodynamics of the Majority Vote Model

Felipe Hawthorne <sup>1</sup>, Pedro E. Harunari <sup>2</sup>, Mário J. de Oliveira <sup>1</sup> and Carlos E. Fiore <sup>1,\*</sup>

<sup>1</sup> Instituto de Física, Universidade de São Paulo, Rua do Matão, 1371, São Paulo 05508-090, SP, Brazil; felipehgc@gmail.com (F.H.); oliveira@if.usp.br (M.J.d.O.)

<sup>2</sup> Complex Systems and Statistical Mechanics, Department of Physics and Materials Science, University of Luxembourg, L-1511 Luxembourg, Luxembourg; pedroharunari@gmail.com

\* Correspondence: fiore@if.usp.br

**Abstract:** The majority vote model is one of the simplest opinion systems yielding distinct phase transitions and has garnered significant interest in recent years. This model, as well as many other stochastic lattice models, are formulated in terms of stochastic rules with no connection to thermodynamics, precluding the achievement of quantities such as power and heat, as well as their behaviors at phase transition regimes. Here, we circumvent this limitation by introducing the idea of a distinct and well-defined thermal reservoir associated to each local configuration. Thermodynamic properties are derived for a generic majority vote model, irrespective of its neighborhood and lattice topology. The behavior of energy/heat fluxes at phase transitions, whether continuous or discontinuous, in regular and complex topologies, is investigated in detail. Unraveling the contribution of each local configuration explains the nature of the phase diagram and reveals how dissipation arises from the dynamics.

**Keywords:** majority vote models; stochastic thermodynamics; phase transitions and spin systems

## 1. Introduction

Opinion dynamics is a crucial issue in sociophysics, encompassing several topics, such as complex social processes, populational dynamics, decision making, elections and spreading of fake news/rumors and others [1]. In recent years, distinct approaches have been proposed and investigated, aimed at tackling the key aspects of opinion dynamics. Several of them deal with systems presenting phase transitions, marking the existence of two regimes, one of which has a prevailing given opinion.

Among the distinct opinion systems, the majority vote (MV) model is highlighted by its simplicity and for exhibiting universal features of nonequilibrium phase transitions. Its interaction mechanism comprises the agent's tendency to align (follow) its opinion based on the majority opinion of its nearest neighborhood [2–4]. Subsequently, generalizations of the MV model have aroused interest, taking into account the influence of network topology [3,4], the inclusion of distinct noises [5,6], more states per agents [7,8] and more recently, inertial effects [8–10]. In the latter, the presence of inertial terms has revealed a robust mechanism, affecting the classification of phase transitions even for different lattice topologies [10] and in systems subject to temporal disorder [11]. More recently, the main properties of the MV have been extensively studied in terms of entropy production signatures [12,13].

Stochastic thermodynamics [14–17] has become one of the most important topics in the realm of nonequilibrium statistical mechanics and an appropriate framework for describing the thermodynamic properties of Markovian nonequilibrium systems, having as a starting point a suitable definition of production of entropy that is able to discern equilibrium from nonequilibrium systems [18]. It presents intrinsically out of equilibrium results, such as generalizations of the first and second laws, that can be used to describe dynamics in terms of energy exchanges, their fluctuations and limits. Despite previous works investigating the



**Citation:** Hawthorne, F.; Harunari, P.E.; de Oliveira, M.J.; Fiore, C.E. Nonequilibrium Thermodynamics of the Majority Vote Model. *Entropy* **2023**, *25*, 1230. <https://doi.org/10.3390/e25081230>

Academic Editor: Antony N. Beris

Received: 20 June 2023

Revised: 3 August 2023

Accepted: 14 August 2023

Published: 18 August 2023



**Copyright:** © 2023 by the authors. Licensee MDPI, Basel, Switzerland. This article is an open access article distributed under the terms and conditions of the Creative Commons Attribution (CC BY) license (<https://creativecommons.org/licenses/by/4.0/>).

main properties of the MV through the entropy production [12,13], other quantities have to be defined to establish a firm link between voter models and stochastic thermodynamics' own framework. Aimed at overcoming such a drawback, a thermodynamic description for opinion models has been recently proposed [19], in which the idea of a distinct thermal reservoir per neighborhood opinion configuration was introduced. Such a framework not only allows one to associate the dynamics with well-defined temperatures but also reconciles the relationship between entropy production and heat flux.

In this paper, we advance on the aforementioned idea, by thoroughly investigating the thermodynamics of the majority vote model. More concretely, a general and unambiguous temperature definition is derived, providing a way to properly investigate the behavior of entropy production and heat fluxes in distinct phases as well as in continuous and discontinuous transition regimes. The investigation is also aimed at understanding the roles of inertia and distinct topologies (regular and complex), and testing fluctuation theorems. Given that the number of reservoirs and heat fluxes increases with the connectivity, the analysis of their roles and which of them is more representative of entropy production will be addressed and, finally, used to probe its traits across phase transitions.

These introduced thermal reservoirs and their respective temperatures are of an effective nature rather than physical entities. They are introduced to accommodate models that otherwise would not benefit from stochastic thermodynamics' toolbox, thus extending the validity of its results.

This paper is organized as follows: Section 2 introduces the model and its main properties, model thermodynamics are presented in Section 3 and conclusions are drawn in Section 4.

## 2. Majority Vote Model and Phase Transition Behavior

In this section, we present an overview of the majority vote model and its phase transition aspects. It consists of a simple system with  $Z_2$  "up-down" symmetry, in which each microscopic configuration  $\eta$  is set by the collection of  $N$  individuals  $\eta \equiv (\eta_1, \eta_2, \dots, \eta_i, \dots, \eta_N)$ , with  $\eta_i$  being the spin variable of site  $i$  which takes the values  $\pm 1$  according to whether the spin is "up" or "down". With probability  $1 - f$ , the spin  $\eta_i$  tends to align itself with its local neighborhood majority. Conversely, with complementary probability  $f$ , the majority rule is not followed. The inertial version differs from the original one by the inclusion of a term proportional to the local spin competing with the neighborhood. The model dynamics are governed by the following master equation

$$\frac{d}{dt}P(\eta, t) = \sum_{i=1}^N \{w_i(\eta^i)P(\eta^i, t) - w_i(\eta)P(\eta, t)\}, \quad (1)$$

where  $w_i(\eta)$  comprises the transition rate at which each site  $i$  changes its opinion from  $\eta_i$  to  $-\eta_i$ , given by

$$w_i(\eta) = \frac{1}{2} \{1 - (1 - 2f)\eta_i \text{sgn}(X)\}, \quad (2)$$

where  $X = (1 - \theta)\ell + k\theta\eta_i$ ,  $k$  is the connectivity of a site,  $\theta$  is the inertia strength, and  $\text{sgn}(X)$  is the sign function. The term  $\ell$  plays a key role in the following results; it is defined as the sum of a site's neighboring spins,  $\ell := \sum_j \eta_j$ , and we omit the dependence on  $\eta$  for convenience. At a given configuration, all sites with  $\ell$  will become thermodynamically equivalent, defining a thermal reservoir. The system presents two ferromagnetic phases for small  $f$ . Upon raising  $f$ , the system yields an order-disorder phase transition, where the value of the critical point is dependent on the lattice topology and neighborhood [2,3]. Although phase transitions are always continuous for the original model ( $\theta = 0$ ) [4], the inclusion of inertia can shift the phase transition from continuous to discontinuous depending on the lattice topology and the neighborhood [8–10].

Since Equation (2) states that the transition rate depends on the sign of  $X$ , the flip probability (whether  $1 - f$  or  $f$ ) will depend on the interplay between the number of nearest



neighbors  $k$  and  $\theta$ . For example, for  $\eta_i = -1$ , the argument of  $\text{sgn}(X)$  reads  $\ell - \theta(k + \ell)$  implying that the transition  $-1 \rightarrow +1$ , due to a neighborhood with  $\ell/(k + \ell) > \theta$ , occurs with probability  $1 - f$  (similar to the inertialess case), whereas when  $\ell/(k + \ell) < \theta$  the probability is  $f$ . Thus, we define  $\ell^* := -k\theta\eta_i/(1 - \theta)$  as the threshold value splitting the neighborhoods: All values  $|\ell| > |\ell^*|$  yield a transition rate equals to the inertialess case, while  $|\ell| < |\ell^*|$  yield  $w_i(\eta) = f$  regardless of  $\eta_i$ . For completeness, the transition rate is  $1/2$  when both values are the same.

For fixed  $k$ , as in the present case, the phase diagram  $\theta$  versus  $f$  will be characterized by plateaus. If  $\theta$  is increased, the plateaus emerge when  $\ell^*$  has an even integer value, since it marks a regime where one additional neighborhood type  $\ell$  shifts its contribution  $f \leftrightarrow 1 - f$ . The plateaus can be obtained by relation

$$\theta^* = \frac{2m}{k + 2m'}, \quad m \in \mathbb{N}. \tag{3}$$

For instance, when the connectivity is  $k = 20$ , these values are

$$\theta^* = \left\{ \frac{1}{11'}, \frac{1}{6'}, \frac{3}{13'}, \frac{2}{7'}, \frac{1}{3'}, \frac{3}{8'}, \frac{7}{17'}, \frac{4}{9'}, \frac{9}{19'}, \frac{1}{2} \right\}, \tag{4}$$

which are later verified in the phase diagrams obtained by simulations in the first figure in Section 2.2 and the first figure in Section 2.3. They are the same for both regular and random-regular topologies, although the classification of the phase transition is also influenced by the topology, demonstrating that the mechanism behind the appearance of such plateaus is related to sharp shifts of contribution of each neighborhood  $\ell$ .

### 2.1. Entropy Production

The entropy production and its connection with the heat flux is the central issue of this paper. Before relating both of them, we first review the main features of the microscopic entropy production formula. Starting with the entropy definition  $S = -\langle \ln P(\eta) \rangle$  (here and hereafter, we adopt the convention  $k_B = 1$  for the Boltzmann constant) and assuming the system is in contact with a (or multiple) reservoir(s), its time derivative  $dS/dt$  is the difference between two terms:  $dS/dt = \Pi - \sigma$ , where  $\Pi$  and  $\sigma$  are the entropy production and entropy flux rates, given by the generic expressions:

$$\Pi = \frac{1}{2} \sum_{\eta} \sum_i \{w_i(\eta^i)P(\eta^i, t) - w_i(\eta)P(\eta, t)\} \ln \frac{w_i(\eta^i)P(\eta^i, t)}{w_i(\eta)P(\eta, t)} \tag{5}$$

and

$$\sigma = \frac{1}{2} \sum_{\eta} \sum_i \{w_i(\eta^i)P(\eta^i, t) - w_i(\eta)P(\eta, t)\} \ln \frac{w_i(\eta^i)}{w_i(\eta)}. \tag{6}$$

where the one-site dynamics assumption was used. Since  $dS/dt = 0$  in the nonequilibrium steady state (NESS), in which  $P(\eta, t) \rightarrow p^{\text{st}}(\eta)$ , the steady entropy production can be calculated from  $\sigma$ , acquiring the convenient ensemble average form [13]:

$$\sigma = \sum_i \left\langle w_i(\eta) \ln \frac{w_i(\eta)}{w_i(\eta^i)} \right\rangle, \tag{7}$$

In order to evaluate  $\sigma$  from Equation (7) we take the ratio between  $w_i(\eta)$  and its reverse  $w_i(\eta^i)$  given by

$$\frac{w_i(\eta)}{w_i(\eta^i)} = \frac{1 - (1 - 2f)\eta_i \text{sgn}[(1 - \theta)\ell + k\theta\eta_i]}{1 + (1 - 2f)\eta_i \text{sgn}[(1 - \theta)\ell - k\theta\eta_i]}. \tag{8}$$

Inspection of the ratio above reveals that only local configurations where  $|\ell| > |\ell^*|$  will contribute to the entropy production. When  $|\ell| < |\ell^*|$ , the ratio vanishes and therefore these configurations yield reversible transitions. This property is illustrated in Figure 1,

where values of  $\ell^*$  are shown in terms of  $\theta$ . For a given finite  $k$ , the even values of  $\ell$  locate the plateaus in the figure.

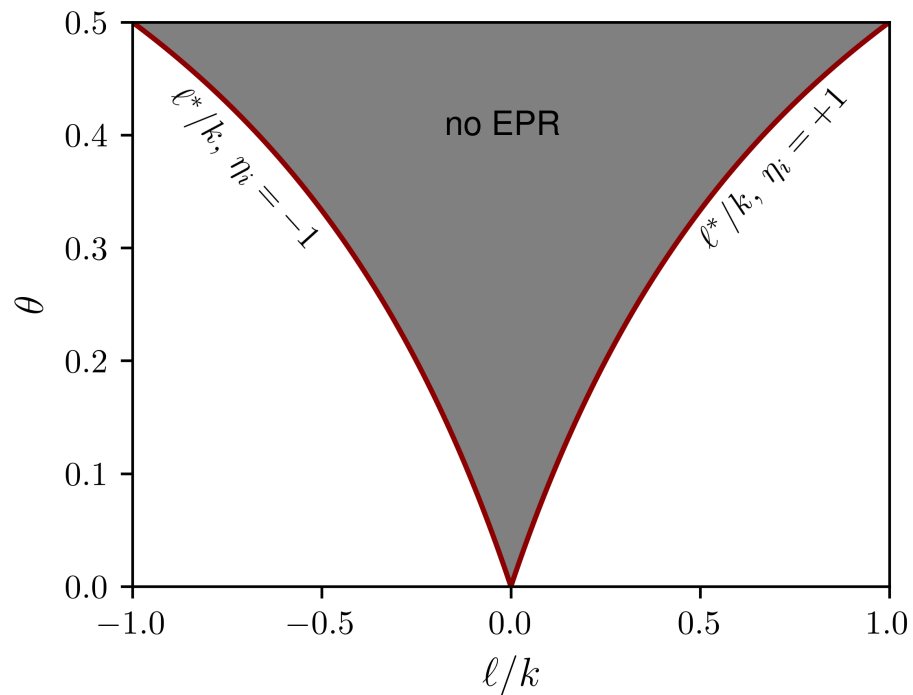


**Figure 1.** Scheme representing the values of  $\ell^*$  for  $\eta_i = \pm 1$  corresponding to the plateaus. In the shaded area, where  $|\ell| < |\ell^*|$ , the neighborhoods do not contribute to the entropy production.

For  $\ell \neq k\theta/(1 - \theta)$ , Equation (8) is conveniently rewritten as

$$\ln \frac{w_i(\eta)}{w_i(\eta^i)} = -\eta_i \text{sgn}(\ell) H \left[ |\ell| - \frac{k\theta}{1 - \theta} \right] \ln \left( \frac{1 - f}{f} \right), \tag{9}$$

where  $H(\bullet)$  is the Heaviside function. However, for  $\ell = k\theta/(1 - \theta)$ , marking the plateau position, Equation (9) acquires a distinct value given by  $\ln(w_i(\eta)/w_i(\eta^i)) = \eta_i \text{sgn}(\ell) \ln(2f)$ .

The above formulae are equivalent by calculating such a ratio only over the subspace of local configurations in which the ratio is different from 1, that is for  $\ell \geq k\theta/(1 - \theta)$  [13]. Thus, when expressed in terms of the misalignment parameter  $f$ , the steady entropy production  $\sigma$  is given by

$$\sigma = \frac{1}{2} \ln \frac{1 - f}{f} \left\{ (1 - 2f) \left\langle \text{sgn}^2(\ell) H \left[ |\ell| - \frac{k\theta}{1 - \theta} \right] \right\rangle - \left\langle \eta_i \text{sgn}(\ell) H \left[ |\ell| - \frac{k\theta}{1 - \theta} \right] \right\rangle \right\}, \tag{10}$$

which only depends on  $f$  and on  $\langle \eta_i \text{sgn}(\ell) H[|\ell| - k\theta/(1 - \theta)] \rangle$  and  $\langle \text{sgn}^2(\ell) H[|\ell| - k\theta/(1 - \theta)] \rangle$ .

### 2.2. Overview about Phase Transitions and Finite-Size Scaling

As stated broadly in the literature, continuous and discontinuous phase transitions become rounded at the vicinity of phase transitions due to finite size effects, whether for equilibrium [20,21] and nonequilibrium systems [22,23]. Despite the order parameter and its moments have been broadly exploited for characterizing nonequilibrium phase transitions, recently, the behavior of entropy production and allied quantities (e.g., its first derivative) has attracted a great deal of attention as their identifiers [12,13,24–27].

According to the finite-size scaling (FSS) theory, at the vicinity of the critical point  $f_c$ , a given quantity  $X$  [ $X \in (|m|, \chi$  and  $\sigma' \equiv d\sigma/df$ )] will behave as  $X = N^{y_x/\nu} f_x(N^{1/\nu}|\epsilon|)$ , where  $f_x$  is a scaling function,  $\epsilon = (f - f_c)/f_c$  is the distance to the criticality and  $y_x$  is the critical exponent obtained from ( $y_x = -\beta, \gamma$  and  $\alpha$ ) [20]. The last exponent is similar to the relationship between the thermal derivative of the entropy,  $S$ , and specific heat,  $C$ , in equilibrium phase transitions (recalling that  $C = N^{\alpha/\nu} f_c(N^{1/\nu}|\epsilon|)$  [20], illustrating that the connection between entropy production and exchanged heat presented here introduces a physical argument for such scaling behavior.

Since the scaling behavior of heat fluxes (and their derivatives) at the criticality was considered previously in [19] we are going to focus on nonequilibrium discontinuous phase transitions in this paper. For a generic ensemble average  $X$ , the starting point consists of assuming a bimodal Gaussian distribution, centered at  $\mu_o$  and  $\mu_d$  (with associated variances  $\chi_o$  and  $\chi_d$ ). In the case of the steady entropy production at the vicinity of  $\epsilon = f - f_c$ , a bimodal entropy production probability distribution centered at  $\mu_o$  and  $\mu_d$  (with associated variances  $\chi_d$  and  $\chi_o$ ) leads to the approximate expression for  $\sigma$ :

$$\sigma \approx \frac{\mu_o + \bar{\alpha}\mu_d e^{-N[(\mu_o - \mu_d)\epsilon]}}{1 + \bar{\alpha}e^{-N[(\mu_o - \mu_d)\epsilon]}} \tag{11}$$

where  $\bar{\alpha} = \sqrt{\chi_d/\chi_o}$ . We note that the ordered and disordered phases are favored as  $\epsilon < 0$  and  $\epsilon > 0$  (assuming that  $\mu_o < \mu_d$ ), respectively, and  $\sigma = (\mu_o + \bar{\alpha}\mu_d)/(1 + \bar{\alpha})$  at  $\epsilon = 0$ , indicating that all entropy production curves, simulated for distinct  $N$ 's, will cross at the transition point  $f_c$ . Having  $\sigma$ , its derivative in respect to  $f$  behaves at the vicinity of  $f_c$  as:

$$\sigma' \approx \frac{N(\mu_o - \mu_d)^2 e^{N(\mu_o - \mu_d)\epsilon}}{\bar{\alpha}(1 + \bar{\alpha}e^{N(\mu_o - \mu_d)\epsilon})^2} \tag{12}$$

showing that  $\sigma'$  scales with  $N$  at the coexistence  $\epsilon = 0$ , in agreement with the above finite size expression for the quantity  $X$ . Alternatively (and analogously), Equation (11) is obtained by resorting to the ideas presented in [28–30], where coexisting phases are treated via a two-state model in which ordered and disordered phases are given by transition rates exhibiting an exponential dependence on the system size  $N$  and proportionality to the distance  $\epsilon$  to the transition point:

$$a \sim k\sqrt{\chi_a}e^{-N(c_0 - c_a\epsilon)}, \quad b \sim k\sqrt{\chi_b}e^{-N(c_0 + c_b\epsilon)}, \tag{13}$$

where  $k, c_0, c_a, c_b > 0$  are constants. ‘‘Ordered’’ and ‘‘disordered’’ probabilities,  $p$  and  $q$ , respectively, are related to rates  $a$  and  $b$  by means of relations  $p = b/(a + b)$  and  $q = 1 - p$ , given by  $p = \sqrt{\chi_b}(\sqrt{\chi_b} + \sqrt{\chi_a}e^{cN\epsilon})^{-1}$ , where  $c = c_a + c_b > 0$ . As shown in Ref. [29], a given ensemble average including the entropy production  $\sigma = \langle \sigma_\tau \rangle / \tau$  averaged over a sufficiently long time  $t \rightarrow \infty$  and over many independent stochastic trajectories given by  $\sigma = \mu_a p + \mu_b q$ , where

$$\sigma \approx \frac{\mu_b\sqrt{\chi_b} + \mu_a\sqrt{\chi_a}e^{cN\epsilon}}{\sqrt{\chi_b} + \sqrt{\chi_a}e^{cN\epsilon}} \tag{14}$$

which has precisely the form of Equation (11).

The main features of discontinuous phase transitions are summarized in Figure 2. From now on we shall consider  $k = 20$  which exhibits a discontinuous phase transition for  $\theta > 1/3$ , as depicted in panel Figure 2a). Aforementioned portraits are exemplified in panels (b) – (d) for  $\theta = 3/8$ . We remark that continuous lines, given by Equation (11), describe very well the behavior of the entropy production and its derivative, the latter presenting a maximum at  $f_c^*$  scaling with  $N^{-1}$ , whose value as  $N \rightarrow \infty$  agrees very well with those obtained from the crossing among curves.

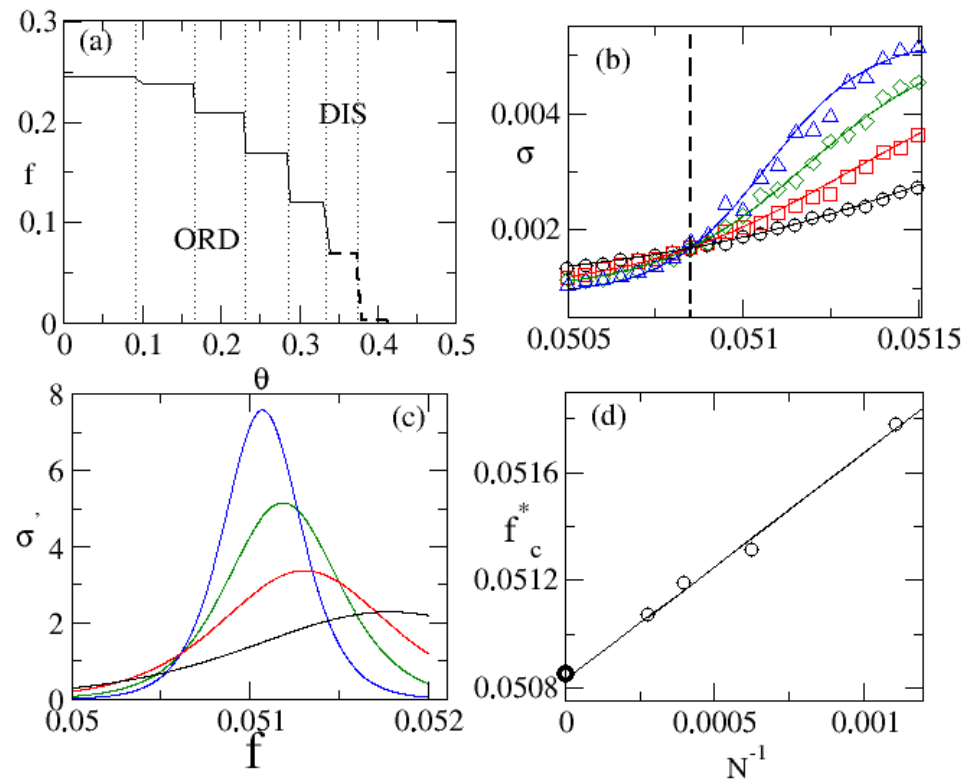


**Figure 2.** In (a), the phase diagram of the inertial majority model for a regular lattice for  $k = 20$ . Vertical lines mark the plateau positions predicted in Equation (3). Panel (b) depicts the entropy production  $\sigma$  for distinct system sizes  $N = L^2$ 's. Continuous lines denote the phenomenological description from Equation (11) and vertical line corresponds to the crossing among entropy production curves at  $f_c = 0.05085(2)$ . In (c), the derivative  $\sigma' \equiv d\sigma/df$  versus  $f$  obtained from continuous lines in (b). Panel (d) show the position  $f_c^*$  of maximum of  $\sigma'$  versus  $N^{-1}$  and its accordance with the crossing among entropy production curves yielding (symbol  $\bullet$ ) as  $N \rightarrow \infty$ .

### 2.3. Discontinuous Phase Transitions in Complex Topologies

The behavior of discontinuous phase transitions in complex topologies is more revealing and it is different for small and large system sizes. In the former case, quantities change smoothly as  $f$  is varied (see e.g., Figure 3c), in similarity with the behavior in regular structures, also characterized by the reduced cumulant  $U_4$  presenting a minimum value increasing with  $N$  (inset) and a maximum behavior of  $\chi$  near the coexistence. Conversely, the behavior becomes akin to the mean-field when  $N$  is large, in which the phase coexistence manifests itself by means of a hysteretic branch, e.g., a region located at  $f_b < f < f_c$  when the dynamics evolve to the ordered (stable for  $f \leq f_b$ ) and disordered (stable for  $f \geq f_c$ ) phases depending on the initial condition. Such changes upon raising  $N$  share some similarities with the metastable behavior observed in the dynamics and thermodynamics of work-to-work transducers, where the system behavior “quickly” approaches the MFT’s [behavior] as  $N$  increases [31].

Here, we describe a brief (nonrigorous) argument about the expected behavior in complex topologies by resorting to the ideas from Ref. [13]. Since spins are independent of each other in the disordered phase, the order parameter behaves as  $\langle \eta_i \rangle \sim N^{-1/2}$  and then a  $n$ -th correlation will behave as  $\langle \eta_i \eta_{i+1} \dots \eta_{i+n} \rangle \approx \langle \eta_i \rangle \langle \eta_{i+1} \rangle \dots \langle \eta_{i+n} \rangle = N^{-n/2}$ . Hence, in the thermodynamic limit, all correlations will vanish and  $\sigma$  will depend solely on control parameters. On the other hand,  $\langle \eta_i \eta_{i+1} \dots \eta_{i+n} \rangle$  is expected to be finite and also  $f$ -dependent in the ordered phase, consistent with  $\sigma$  exhibiting a dependence on the control parameters and correlations. Therefore, the existence of a hysteretic loop for the

order parameter (panel (b)) is also translated to the entropy production behavior (see e.g., panel (d)).

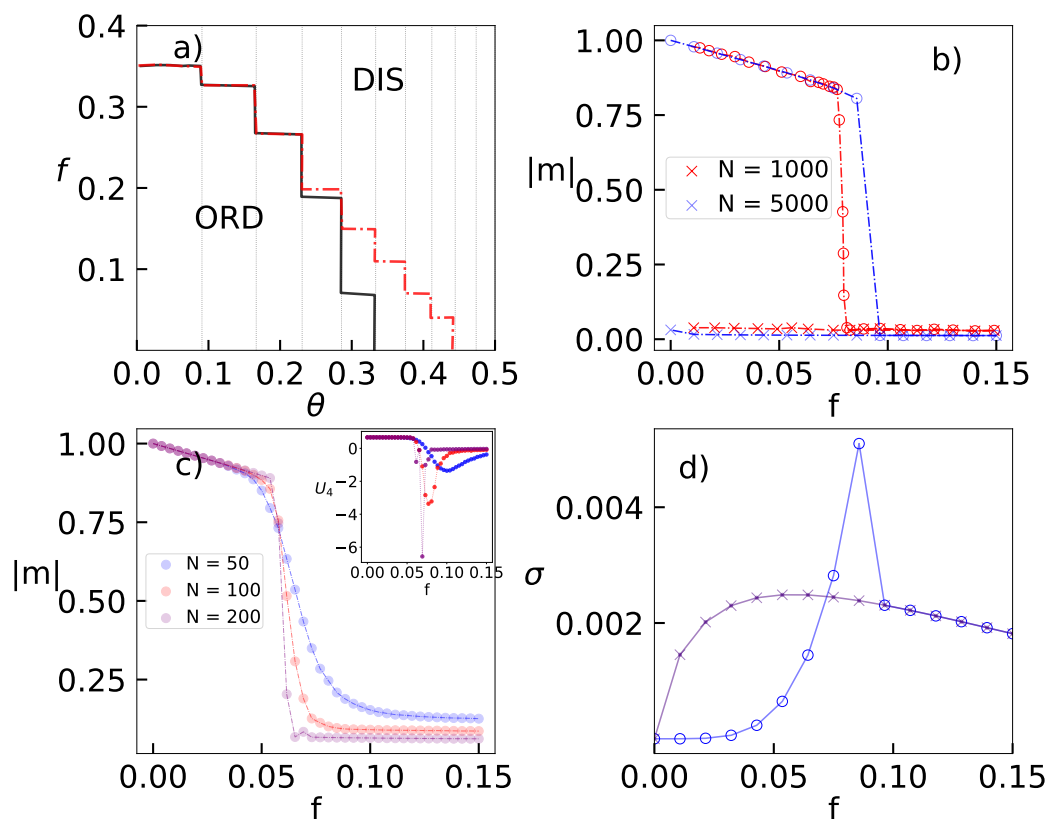


**Figure 3.** Phase transition for the MV in a random-regular topology with connectivity  $k = 20$ . Panel (a) depicts the phase diagram  $\theta$  versus  $f$ . Continuous and dashed lines show, for a system of size  $N = 10^4$ . Note that a hysteretic branch for  $\theta > 3/13$ . Panels (b,c) show, for  $\theta = 3/8$ , the order parameter  $|m|$  versus  $f$  for distinct large and small system sizes  $N$ , respectively. Inset: the reduced cumulant  $U_4$  versus  $f$ . Circles and  $\times$  attempt to the forward and backward “trajectories”, respectively. In (d), its corresponding  $\sigma$ 's for  $N = 5000$ .

### 3. Thermodynamics of the Majority Vote Model

#### 3.1. General Features

In Section 2, the main properties of the majority vote model were analyzed without any thermodynamic consideration. Here, we incorporate the notion of temperatures mediating changes of configuration in order to establish the connection with thermodynamics. Since the stochastic dynamics over the configuration space is fully determined by its transition rates, we shall resort the ideas from Refs. [16,17,32] in which transition rates are defined by assuming the local detailed balance. The central point consists of assuming that the one-site transition rate  $w_i(\eta)$  is decomposed in  $\ell$  distinct (and mutually exclusive) components, each one associated with a given thermal reservoir (reciprocal inverse temperature  $\beta_\ell$ ), given by  $w_i(\eta) = \sum_\ell w_{\ell i}(\eta)$  ( $\ell = 2, 4, \dots, k$ ), where  $w_{\ell i}(\eta)$  assumes the Glauber form:

$$w_{\ell i}(\eta) = \frac{\alpha_\ell}{2} \{1 - \tanh(\beta_\ell \Delta E)\}, \tag{15}$$

where  $\alpha_\ell$  is a constant and  $\Delta E = E(\eta^i) - E(\eta)$  denotes the energy difference between configurations  $\eta$  and  $\eta^i$ . For “up-down”  $Z_2$  symmetry systems, the energy can be generically expressed according to the Ising-like form  $E(\eta) = -J \sum_{(i,j)} \eta_i \eta_j - H \sum_{i=1}^N \eta_i$  [33], where  $J$  represents the interaction energy between spins, and  $H$  is a parameter accounting for the dependence on the local spin  $\eta_i$  (usually the magnetic field). Giving that  $\text{sgn}(\ell) = -\text{sgn}(-\ell)$ ,

one has  $H = 0$  for all values of  $\theta$ . From Equation (15), the ratio  $w_{\ell i}(\eta^i)/w_{\ell i}(\eta)$  is then expressed according to the local detailed balance:

$$\frac{w_{\ell i}(\eta)}{w_{\ell i}(\eta^i)} = e^{-\beta_\ell [E(\eta^i) - E(\eta)]}. \tag{16}$$

We are now in a position to obtain the model’s thermodynamic properties. The time variation of the mean energy  $U = \langle E(\eta) \rangle$  is given by  $dU/dt = \sum_\ell \Phi_\ell$ , where  $\Phi_\ell$  denotes the heat exchanged due to the  $\ell$ -th thermal reservoir, given by

$$\Phi_\ell = \sum_i \langle [E(\eta^i) - E(\eta)] w_{\ell i}(\eta) \rangle, \tag{17}$$

constrained by the first law of thermodynamics,  $\sum_\ell \Phi_\ell = 0$  in the NESS. The entropy production and entropy flux are also decomposed into  $\ell$ -indexed components by replacing  $w_i(\eta) \rightarrow w_{\ell i}(\eta)$  in Equations (5) and (6). In particular, the latter reads

$$\sigma_\ell = \sum_\eta p^{st}(\eta) \sum_i w_{\ell i}(\eta) \ln \frac{w_{\ell i}(\eta)}{w_{\ell i}(\eta^i)}. \tag{18}$$

Since the entropy change vanishes at the NESS,  $dS/dt = \sum_\ell (\Pi_\ell - \sigma_\ell)$ , both entropy production and entropy flux can be identified by Equation (18):  $\Pi = \sum_\ell \Pi_\ell = \sum_\ell \sigma_\ell = \sigma$ . The expressions above are consistent with Refs. [16,32].

Finally, by inserting Equation (16) into Equation (18), each entropy flux component  $\sigma_\ell$  is related with exchanged heat  $\Phi_\ell$  by a Clausius-like form  $\sigma_\ell = -\beta_\ell \Phi_\ell$ , where  $\Phi_\ell$  is given by Equation (17). Alternatively,  $\sigma$  can also be written in the usual thermodynamics form as a sum of thermodynamic fluxes times forces:

$$\sigma = - \sum_\ell \beta_\ell \Phi_\ell \quad \text{or} \quad \sigma = \sum_{\ell \neq 2} X_\ell \Phi_\ell, \tag{19}$$

where the second temperature was set as a reference to define all  $(k/2) - 1$  thermodynamic forces  $X_\ell \equiv \beta_2 - \beta_\ell$ , associated with its respective flux,  $\Phi_\ell$ . For simplicity, we set the Ising interaction parameter to  $J = 1$ . From the expression for  $E(\eta)$ , it follows that  $\Delta E = 2\eta_i \ell$ , which can be rewritten as  $\Delta E = 2\eta_i |\ell| \text{sgn}(\ell)$ . By taking the logarithm of Equation (16), it follows that

$$\ln \frac{w_{\ell i}(\eta)}{w_{\ell i}(\eta^i)} = -2\beta_\ell |\ell| \eta_i \text{sgn}(\ell). \tag{20}$$

Since the transition rates associated with each thermal reservoir are mutually exclusive, a direct comparison with Equation (9) for a given  $\ell$  provides to obtain each (reciprocal inverse) temperature  $\beta_\ell$  given by

$$\beta_\ell = \frac{1}{2|\ell|} H \left[ |\ell| - \frac{k\theta}{1-\theta} \right] \ln \left( \frac{1-f}{f} \right), \tag{21}$$

where  $\beta_2 = 2\beta_4 = 3\beta_6 \dots = k\beta_k/2$  in the inertialess case. We pause to make a few comments. First, Equation (21) comes from the local detailed balance and constitutes one of the main results of this paper. Such temperature relation (see e.g., Equation (15)) provides a clear connection between entropy production and heat fluxes, in which (as shall be discussed later) some of the heat components has to be strictly positive and negative in order to ensure  $\sigma \geq 0$ . Second, Equation (21) extends the calculation of temperatures for a given neighborhood and inertia, and reduces to the expression from Ref. [19] as  $\theta = 0$ . Third,  $\beta_\ell$  vanishes for large enough values of inertia  $\theta > \theta_p$ , illustrating that despite a heat flux

associated with the  $\ell$ -th reservoir being well-defined, it does not produce entropy. Fourth and last, the temperature assumes a different value for  $\theta = \theta_p$  given by

$$\beta_\ell = -\frac{1}{2|\ell|} \ln(2f). \tag{22}$$

This completes our description of the temperature definitions for the MV as well as the influence of inertia. Now we turn to unravel the role of each  $\ell$  to the fluxes of heat and entropy production. Starting with the inertialess case, where  $\beta_2 > \beta_4 > \dots > \beta_k$ , we argue that the heat fluxes associated with the states in contact with the coldest and hottest baths are always positive and negative, respectively:  $\Phi_2 < 0$  and  $\Phi_k > 0$ , whose a (nonrigorous) argument is present as follows. Starting with the two thermal baths case ( $k = 4$ ), it is straightforward to verify that, since  $\sigma$  acquires the simple form  $\sigma = (\beta_2 - \beta_4)\Phi_4 > 0$ . Given that  $\beta_2 - \beta_4 > 0$  (cf. Equation (21)), it follows that  $\Phi_4 \geq 0$  and hence  $\Phi_2 = -\Phi_4 \leq 0$ . The case of more than two reservoirs is more intriguing, since intermediate fluxes can be positive, negative, or even change their sign upon  $f$  being varied (see e.g., the first figure (d) in Section 3.3). For  $k = 6$ , one has  $\sigma = -(\beta_2 - \beta_6)\Phi_2 - (\beta_4 - \beta_6)\Phi_4 \geq 0$  and three possibilities for  $\Phi_2$  and  $\Phi_4$ . The former, in which both are negative, promptly implies  $\sigma \geq 0$ , whereas the second case,  $\Phi_2 \leq 0$  and  $\Phi_4 \geq 0$ , is also consistent since  $-(\beta_2 - \beta_6)\Phi_2 \geq (\beta_4 - \beta_6)\Phi_4$  and hence  $\Phi_6 \geq 0$  (recalling that  $\Phi_6 = -(\Phi_2 + \Phi_4)$ ). The third possibility, in which  $\Phi_2 \geq 0$  and  $\Phi_4 \leq 0$  violates the second law in some cases and thus it is not possible. Similar findings are verified for  $\theta \neq 0$ , but we should note that only neighborhoods with  $\ell^*$  greater than  $\ell - k\theta/(1 - \theta)$  will contribute to the entropy production,  $\sigma = -\sum_{\ell^*}^k \beta_\ell \Phi_\ell$ . For example, for  $k = 20$  and distinct inertia intervals  $3/8 < \theta \leq 7/17$ ,  $7/17 < \theta \leq 4/9$ ,  $\theta > 4/9$ , the corresponding entropy productions read  $\sigma = -\sum_{\ell=14}^k \beta_\ell \Phi_\ell$ ,  $\sigma = -\beta_{16}\Phi_{16} - \beta_{18}\Phi_{18} - \beta_{20}\Phi_{20}$  and  $\sigma = -\beta_{18}\Phi_{18} - \beta_{20}\Phi_{20}$ , such latter one similar to the  $k = 4$  case (but here  $\sum_{\ell=2}^k \Phi_\ell = 0$ ) and once again illustrating that  $\Phi_{\ell^*=18} \leq 0$  and  $\Phi_{k=20} \geq 0$ . We close this section by pointing out that, despite the above nonrigorous argument, the general finding  $\Phi_{\ell^*} \leq 0$  and  $\Phi_k \geq 0$  has been verified in all cases. In contrast, it is not possible to draw general conclusions about intermediate fluxes, in which some change sign as  $f$  increases.

### 3.2. Fluctuation Theorems

Thermodynamic consistent systems satisfy the detailed fluctuation theorem (DFT) for entropy production, which gives rise to the stochastic version of the second law. It states that negative fluctuations of the integrated entropy production are exponentially suppressed by the positive counterparts. For a given integration window  $\tau$ , the DFT is asymptotically valid for  $\Sigma = \int_0^\tau \sigma(t)dt$  at the NESS since it is equal to the entropy production:

$$\lim_{\tau \rightarrow \infty} \ln \frac{P_\tau(\Sigma)}{P_\tau(-\Sigma)} = \Sigma, \tag{23}$$

where  $P_\tau(\Sigma)$  represents the probability of measuring  $\Sigma$  in a trajectory of length  $\tau$ . This relation holds beyond the long-time limit when the internal change of configuration entropy is considered in addition to the entropy fluxes. Consequence of the above, the integral fluctuation theorem (IFT) reads

$$\lim_{\tau \rightarrow \infty} \left\langle e^{-\Sigma} \right\rangle_\tau = 1 \tag{24}$$

and is useful for relating the components of  $\Sigma$ , such as in the celebrated Jarzynski equality [34] that relates the statistics of work to free energy differences, bridging equilibrium and nonequilibrium quantities. The feasibility of employing such methods is tightly related to the ability to observe fluctuations in the trajectories, which become rare as  $\tau$  increases. We explore the manifestation of these relations, cornerstones of stochastic thermodynamics, in the MV vote model.

The left panel of Figure 4 shows the convergence of the left-hand side of Equation (23) to its right-hand side as the integration windows become larger for the entropy production evaluated from Equations (18) and (19). Observing the DFT becomes an expensive task even for small systems since the negative fluctuations of entropy production become increasingly rare for larger values of  $\tau$ . The right panel shows the left-hand side of the IFT in Equation (24), which converges to one despite the presence of inertia. It is worth mentioning that the convergence is observed from above and from below. Although no general conclusion can be drawn, the behavior of these fluctuation relations might be related to the phase transitions: In the examples, the IFT presents a slower convergence at the vicinity of the phase transition.

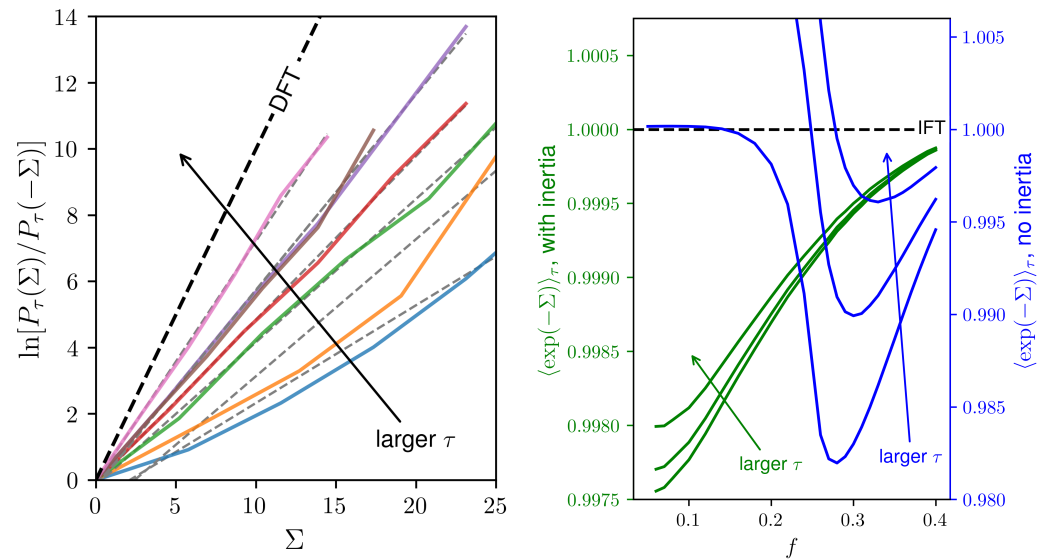


**Figure 4.** (Left) Convergence to the detailed fluctuation theorem as integration window  $\tau$  increases for a lattice  $L = 6$  and  $f = 0.04$ ; solid lines are simulation results while dashed lines are the respective linear fits. (Right) Convergence to the integral fluctuation theorem for the case with no inertia (blue) and with inertia  $\theta = 3/8$  (green); additional parameters are  $k = 20$  and  $N = 10^4$ .

### 3.3. Heat Fluxes at Phase Transitions

According to Equation (17), every heat flux  $\Phi_\ell$  is an ensemble average and, therefore, we expect at least the most significant components of the entropy production to behave similarly to  $\sigma$  at the vicinity of a phase transition. More specifically, at discontinuous phase transitions, the curves of entropy production cross at  $f_c$  for distinct system sizes in regular lattices, and a hysteretic branch is present in complex topologies [13]. These properties are promptly verified for the largest fluxes  $\ell = 12, 14$  and  $20$ . For a regular lattice, panels (a)–(c) of Figure 5 display the crossing of the fluxes for different systems sizes, and panel (d) shows the quantitative value of each individual flux. For a random-regular network, panels (a)–(c) of Figure 6 show the hysteretic branch while (d) shows individual flux values.

The continuous lines in panels Figure 5a–c are obtained from the bimodal Gaussian description in Equation (11), in good agreement with the simulation results. Remarkably, for both regular and complex topologies, the phase transition can be probed and precisely located from the behavior of any individual flux.



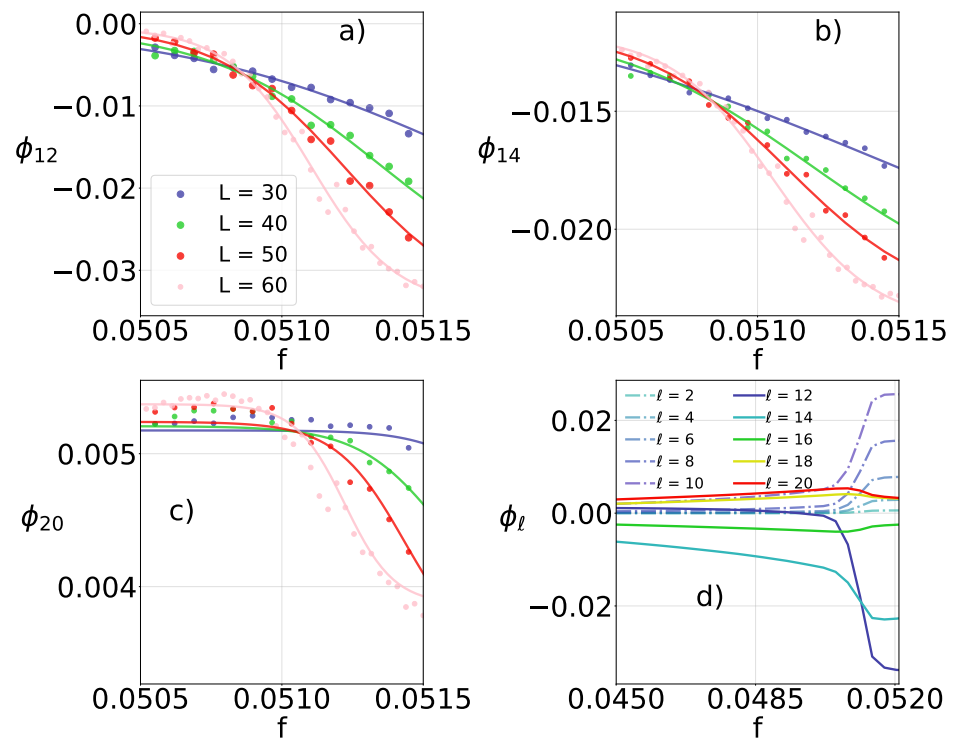


**Figure 5.** For the regular lattice with  $\theta = 3/8$ ,  $k = 20$  and distinct system sizes  $N = L^2$ , panels (a,b) depict the most representative (largest absolute values) heat fluxes per particle  $\Phi_\ell$ 's versus control parameter  $f$ . Continuous lines denote correspond to the phenomenological approach according to the ideas of Equation (11). Although the component heat flux panel (c) mildly changes with  $f$ , all curves also cross at  $f_c$ . Panel (d) shows all  $\Phi_\ell$ 's ( $\ell = 2, 4, \dots, k$ ) for  $N = 60^2$ .

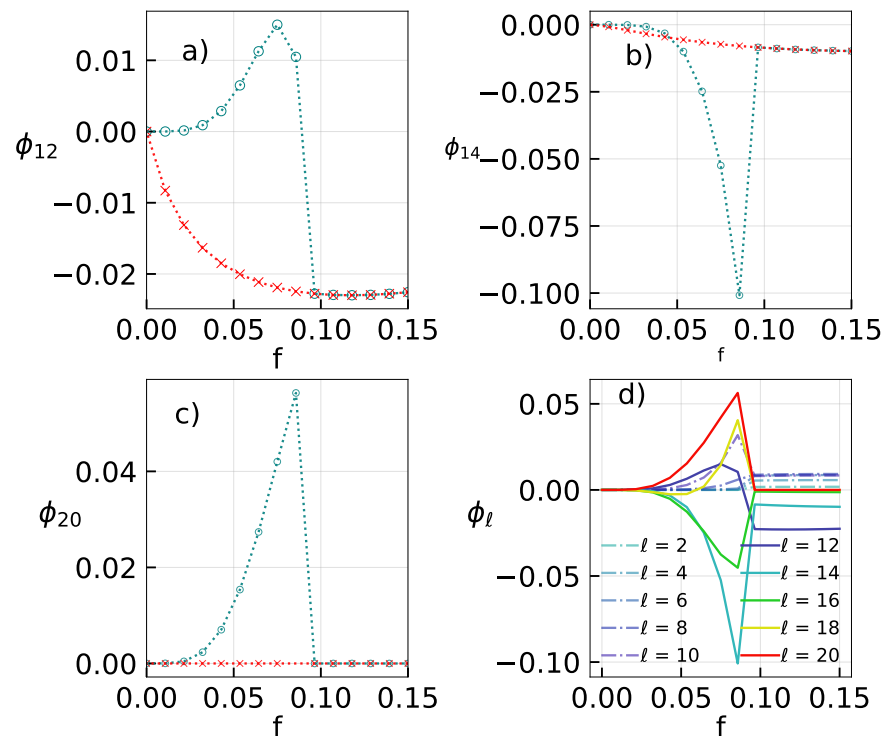


**Figure 6.** For a system of size  $N = 5000$ , (a)–(d) the same as before, but for a random-regular structure.

### 3.4. Contributions to Dissipation

Inspecting the thermodynamic contribution of individual  $\ell$ 's raises the question of how each type of neighborhood contributes to entropy production, a measure of dissipation. As previously discussed, the second law imposes  $\Phi_{\ell^*} < 0$  and  $\Phi_k > 0$  irrespective of  $f$ , and also local configurations satisfying  $|\ell| < |\ell^*|$  do not dissipate. Taking into account that some intermediate fluxes  $\Phi_\ell$  are nonmonotonic in terms of  $f$ , one could expect that they would present a less significant contribution. Inspired by evidence from simulations, we observe the predominance of  $\Phi_{\ell^*}$  and  $\Phi_k$ , hence we introduce the contribution of these two fluxes as  $\sigma_{\ell^*,k} = -\beta_{\ell^*}\Phi_{\ell^*} - \beta_k\Phi_k > 0$ . This represents an approximation but not a bound since the remaining fluxes can change their signs.

Figure 7 compares, for the random-regular and regular lattices,  $\sigma_{\ell^*,k}$  and  $\sigma$  for distinct values of  $\theta$ . In all cases,  $\sigma_{\ell^*,k}$  is not only close to  $\sigma$  but also captures the qualitative behavior, successfully describing the interplay between the control parameter  $f$ , inertia  $\theta$ , and the dissipation, including a peak located at the vicinity of the phase transition. For larger  $\theta$  the set of dissipating local configurations shrinks, hence the better agreement between both curves.

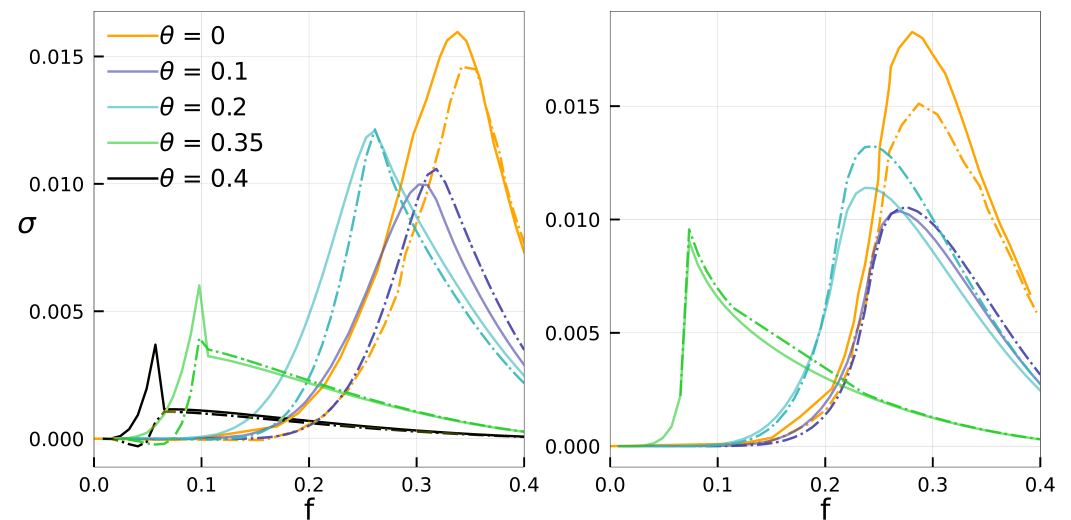


**Figure 7.** For  $k = 20$ , random-regular (left) and regular (right) structures of sizes  $N = 1600$  and  $40^2$ , curves for  $\sigma_{\ell^*,k}$  (dot-dashed) and  $\sigma$  (continuous) are shown in terms of  $f$  for distinct  $\theta$ 's. From top to bottom,  $\ell^* = 2, 4, 6, 12$  and  $14$ .

### 4. Conclusions

The nonequilibrium thermodynamic theory of the generic majority vote model was presented and thoroughly investigated, encompassing its phase transition. A consistent definition of temperature and the connection between heat fluxes and entropy production were introduced and analyzed in the context of continuous and discontinuous phase transitions. The present approach for fluxes is thermodynamically consistent and equivalent to the microscopic entropy production definition and satisfies the detailed fluctuation theorem.

We believe that the present framework not only conciliates the thermodynamic aspects of an important class of nonequilibrium systems but also introduces a new kind of nonequilibrium ingredient, based on the idea of a thermal reservoir associated with the system neighborhood. Such an idea has revealed general for a generic voter-like model with “up-down”  $Z_2$  symmetry. In the presence of inertia, the spin changes induced by some local configurations are reversible. Moreover, we explore what are the most relevant neighborhoods driving the system dissipation, including its qualitative features across a phase transition, and how these neighborhoods contribute to the structure of the phase diagram.

Our findings are valid for a class that describes systems from social dynamics to the physics of thermal engines, presenting collective effects that can be leveraged for improved

performance. Such potential application raises interesting questions such as the role of lattice topology and even the kind of voter model used (see e.g., Ref. [19] for a comparison between them) in order to optimize the desirable power and efficiency. Such topics should be investigated in the future.

**Author Contributions:** Writing—All authors contributed equally for the manuscript writing. All authors have read and agreed to the published version of the manuscript.

**Funding:** This work received the financial support from FAPESP under grant 2021/03372-2, CNPq and CAPES.

**Data Availability Statement:** Not applicable.

**Acknowledgments:** This work has received the financial support from FAPESP under grant 2021/03372-2. The financial supports from Brazilian agencies CAPES and CNPq are also acknowledged.

**Conflicts of Interest:** The authors declare no conflict of interest.

## References

- Castellano, C.; Fortunato, S.; Loreto, V. Statistical physics of social dynamics. *Rev. Mod. Phys.* **2009**, *81*, 591. [CrossRef]
- de Oliveira, M.J. Isotropic majority-vote model on a square lattice. *J. Stat. Phys.* **1992**, *66*, 273–281. [CrossRef]
- Pereira, L.F.; Moreira, F.B. Majority-vote model on random graphs. *Phys. Rev. E* **2005**, *71*, 016123. [CrossRef] [PubMed]
- Chen, H.; Shen, C.; He, G.; Zhang, H.; Hou, Z. Critical noise of majority-vote model on complex networks. *Phys. Rev. E* **2015**, *91*, 022816. [CrossRef]
- Vieira, A.R.; Crokidakis, N. Phase transitions in the majority-vote model with two types of noises. *Phys. A Stat. Mech. Its Appl.* **2016**, *450*, 30–36. [CrossRef]
- Encinas, J.; Chen, H.; de Oliveira, M.M.; Fiore, C.E. Majority vote model with ancillary noise in complex networks. *Phys. A Stat. Mech. Its Appl.* **2019**, *516*, 563–570. [CrossRef]
- Brunstein, A.; Tomé, T. Universal behavior in an irreversible model with  $C_{3v}$  symmetry. *Phys. Rev. E* **1999**, *60*, 3666–3669. [CrossRef]
- Chen, H.; Shen, C.; Zhang, H.; Li, G.; Hou, Z.; Kurths, J. First-order phase transition in a majority-vote model with inertia. *Phys. Rev. E* **2017**, *95*, 042304. [CrossRef]
- Harunari, P.E.; de Oliveira, M.; Fiore, C.E. Partial inertia induces additional phase transition in the majority vote model. *Phys. Rev. E* **2017**, *96*, 042305. [CrossRef]
- Encinas, J.M.; Harunari, P.E.; de Oliveira, M.; Fiore, C.E. Fundamental ingredients for discontinuous phase transitions in the inertial majority vote model. *Sci. Rep.* **2018**, *8*, 9338. [CrossRef]
- Encinas, J.M.; Fiore, C.E. Influence of distinct kinds of temporal disorder in discontinuous phase transitions. *Phys. Rev. E* **2021**, *103*, 032124. [CrossRef] [PubMed]
- Crochik, L.; Tomé, T. Entropy production in the majority-vote model. *Phys. Rev. E* **2005**, *72*, 057103. [CrossRef] [PubMed]
- Noa, C.F.; Harunari, P.E.; de Oliveira, M.; Fiore, C. Entropy production as a tool for characterizing nonequilibrium phase transitions. *Phys. Rev. E* **2019**, *100*, 012104. [CrossRef]
- Tomé, T.; de Oliveira, M.J. Entropy production in irreversible systems described by a Fokker-Planck equation. *Phys. Rev. E* **2010**, *82*, 021120. [CrossRef]
- Esposito, M. Stochastic thermodynamics under coarse graining. *Phys. Rev. E* **2012**, *85*, 041125. [CrossRef] [PubMed]
- Seifert, U. Stochastic thermodynamics, fluctuation theorems and molecular machines. *Rep. Prog. Phys.* **2012**, *75*, 126001. [CrossRef]
- Tomé, T.; de Oliveira, M.J. Stochastic approach to equilibrium and nonequilibrium thermodynamics. *Phys. Rev. E* **2015**, *91*, 042140. [CrossRef]
- Schnakenberg, J. Network theory of microscopic and macroscopic behavior of master equation systems. *Rev. Mod. Phys.* **1976**, *48*, 571. [CrossRef]
- Tomé, T.; Fiore, C.E.; de Oliveira, M.J. Stochastic thermodynamics of opinion dynamics. *Phys. Rev. E* **2023**, *107*, 064135 [CrossRef]
- Landau, D.; Binder, K. *A Guide to Monte Carlo Simulations in Statistical Physics*; Cambridge University Press: Cambridge, UK, 2021.
- Fiore, C.E.; Carneiro, C.E.I. Obtaining pressure versus concentration phase diagrams in spin systems from Monte Carlo simulations. *Phys. Rev. E* **2008**, *76*, 021118. <https://link.aps.org/doi/10.1103/PhysRevE.76.021118>. [CrossRef]
- de Oliveira, M.M.; da Luz, M.G.E.; Fiore, C.E. Generic finite size scaling for discontinuous nonequilibrium phase transitions into absorbing states. *Phys. Rev. E* **2015**, *92*, 062126. [CrossRef] [PubMed]
- de Oliveira, M.M.; da Luz, M.G.E.; Fiore, C.E. Finite-size scaling for discontinuous nonequilibrium phase transitions. *Phys. Rev. E* **2018**, *97*, 060101. [CrossRef] [PubMed]

24. Goes, B.O.; Fiore, C.E.; Landi, G.T. Quantum features of entropy production in driven-dissipative transitions. *Phys. Rev. Res.* **2020**, *2*, 013136. [[CrossRef](#)]
25. Seara, D.S.; Machta, B.B.; Murrell, M.P. Irreversibility in dynamical phases and transitions. *Nat. Commun.* **2021**, *12*, 392. [[CrossRef](#)] [[PubMed](#)]
26. Martynec, T.; Klapp, S.H.; Loos, S.A. Entropy production at criticality in a nonequilibrium Potts model. *New J. Phys.* **2020**, *22*, 093069. [[CrossRef](#)]
27. Aguilera, M.; Moosavi, S.A.; Shimazaki, H. A unifying framework for mean-field theories of asymmetric kinetic Ising systems. *Nat. Commun.* **2021**, *12*, 1197. [[CrossRef](#)]
28. Hanggi, P.; Grabert, H.; Talkner, P.; Thomas, H. Bistable systems: Master equation versus Fokker-Planck modeling. *Phys. Rev. A* **1984**, *29*, 371. [[CrossRef](#)]
29. Fiore, C.E.; Harunari, P.E.; Noa, C.E.F.; Landi, G.T. Current fluctuations in nonequilibrium discontinuous phase transitions. *Phys. Rev. E* **2021**, *104*, 064123. [[CrossRef](#)]
30. Nguyen, B.; Seifert, U. Exponential volume dependence of entropy-current fluctuations at first-order phase transitions in chemical reaction networks. *Phys. Rev. E* **2020**, *102*, 022101. [[CrossRef](#)]
31. Hergich, T.; Thingna, J.; Esposito, M. Collective Power: Minimal Model for Thermodynamics of Nonequilibrium Phase Transitions. *Phys. Rev. X* **2018**, *8*, 031056. [[CrossRef](#)]
32. Van den Broeck, C.; Esposito, M. Ensemble and trajectory thermodynamics: A brief introduction. *Phys. A Stat. Mech. Its Appl.* **2015**, *418*, 6–16. [[CrossRef](#)]
33. Yeomans, J.M. *Statistical Mechanics of Phase Transitions*; Clarendon Press: Oxford, UK, 1992.
34. Jarzynski, C. Nonequilibrium equality for free energy differences. *Phys. Rev. Lett.* **1997**, *78*, 2690. [[CrossRef](#)]

**Disclaimer/Publisher's Note:** The statements, opinions and data contained in all publications are solely those of the individual author(s) and contributor(s) and not of MDPI and/or the editor(s). MDPI and/or the editor(s) disclaim responsibility for any injury to people or property resulting from any ideas, methods, instructions or products referred to in the content.

# Thermodynamics of a minimal collective heat engine: Comparison between engine designs

Felipe Hawthorne,<sup>1</sup> B. Cleuren,<sup>2</sup> and Carlos E. Fiore<sup>1</sup>

<sup>1</sup>*Universidade de São Paulo, Instituto de Física, Rua do Matão, 1371, 05508-090 São Paulo, SP, Brazil*

<sup>2</sup>*UHasselt, Faculty of Sciences, Theory Lab, Agoralaan, 3590 Diepenbeek, Belgium*

(Dated: December 14, 2023)

Collective effects have attracted remarkable recent interest, not only for their presence in several systems in nature but also for the possibility of being used for the construction of efficient engine setups. Notwithstanding, little is known about the influence of the engine design and most studies are restricted to the simplest cases (e.g. simultaneous contact with two thermal baths), not necessarily constituting a realistic setup implementation. Aimed at partially filling this gap, we introduce the collisional/sequential description for a minimal model for collective effects, composed of two interacting nanomachines placed in contact with a distinct thermal reservoir and nonequilibrium worksource at each stage/stroke. Thermodynamic quantities are exactly obtained irrespectively the model details. Distinct kinds of engines are investigated and the influence of the interaction, temperature, period, and time asymmetry have been undertaken. Results show that a careful design of interaction provides a superior performance than the interactionless case, including optimal power outputs and efficiencies at maximum power greater than known bounds or even the system presenting efficiencies close to the ideal (Carnot) limit. We also show that the case of the system simultaneously placed in contact with two thermal reservoirs constitutes a particular case of our framework.

## I. INTRODUCTION

The construction of nanoscopic steady-state heat engines has attracted a great deal of recent attention in the realm of stochastic thermodynamics [1–5], not only for extending the fundamental concept of the energy conversion (from the macroscopic to the nanoscopic scale), but also because it presents three fundamental differences when compared with the equilibrium thermodynamics. First, there is no need for moving parts and pistons since the energy conversion comes from currents of microscopic particles/units. Second, nanoscopic-engineered setups typically operate far from equilibrium and consequently, its performance is expected to be lower than the ideal case. Third, fluctuations of quantities and currents can become important in small-scaled systems. The issues above illustrate the search for the protocol as crucial to ensure its reliability and desired performance.

In the last years, distinct kinds of engines operating far from equilibrium have been proposed and investigated [1, 6–9]. Under a generic point of view, they are grouped out in three categories, stemming from fixed thermodynamic forces [10–16], from the time-periodic variation of external parameters [17–20] and via sequential/collisional approach [21–26], in which at each stroke/stage, the system is subjected to a different condition (held fixed along the stage). Each one has been considered as a reliable approach in distinct contexts, such last one encompassing the presence of distinct drivings over each member of the system, a weak coupling between the system with the reservoir, or even for mimicking the environment for quantum systems [27–29]. While most of the above studies are restricted to setups composed of one unit [18, 19, 23, 24, 30], the thermodynamics of systems exhibiting collective effects has received considerable recent attention as an alternative strategy for improving the system performance. Among the distinct examples, we cite a system of interacting Brownian particles [20], work-to-work transducers [31, 32] and heat engines [15, 16]. All of them are restricted to cases of systems operating at equal temperatures [31, 32],

fixed parameters [15, 16] or sinusoidal drivings [20].

In this contribution, we conciliate the points above by investigating a minimal model for collective effects, formed by two interacting units placed sequentially with distinct thermal baths at each stroke. Previous studies have tackled different versions, such as its all-to-all (mean-field) design [15, 16] and distinct topology of interactions [14], both for fixed thermodynamic forces and a large number of units. Our study will focus on the opposite case, dealing with a minimal collective effect system composed of two interacting units beyond the fixed forces context. Hence, its simplicity constitutes an ideal laboratory for comparing three fundamental aspects of nanoscopic engines: the kind of design (sequential versus fixed thermodynamic forces), distinct approaches for the worksource (not considered previously) and under situations collective effects can improve the system performance when compared with its interactionless version. The former goal has been inspired from previous contributions [24, 30], whereas the different worksources addressed here were considered in Refs. [14–16, 24]. It is worth mentioning that our system shares some similarities with recent studies about a setup composed of two interacting quantum dots under the repeated interactions [33, 34]. Our findings reveal that collective effects, together with a suited design of parameters (energy, period, duration of each stage), can significantly enhance the system's performance. Such remarkable improvement can result in optimal power outputs, efficiencies at maximum power greater than known bounds or even efficiencies approaching to the ideal (Carnot) limit. As a side result, our study shows the simultaneous contact with two thermal baths case [15] as the ideal limit of fast switching times.

This paper is organized as follows. In Sec. II the model and the main expressions for thermodynamic quantities will be presented. In Secs. III and IV we shall analyze in detail two distinct approaches for our engine setup. Conclusions will be drawn in Sec. V.

## II. MODEL AND THERMODYNAMICS

Our minimal model for collective effects is composed of two interacting units sequentially placed into contact with  $N$  distinct reservoirs, each one of duration  $\tau_\nu - \tau_{\nu-1}$ . The total time to complete one cycle being  $\tau$ . At each stroke, occurring between  $\tau_{\nu-1} < t \leq \tau_\nu$ , each unit can be in a lower ( $\sigma_k = 0$ ) or upper ( $\sigma_k = 1$ ) state, with individual energies 0 and  $\epsilon_\nu$ , respectively. The system is connected to the reservoir  $\nu$ , with temperature  $\beta_\nu = 1/(k_B T_\nu)$ , and total energy is given by

$$\tilde{\epsilon}^{(\nu)} = V_\nu[(1-\sigma_1)\sigma_2 + \sigma_1(1-\sigma_2)] + U_\nu\sigma_1\sigma_2 + \epsilon_\nu(\sigma_1 + \sigma_2), \quad (1)$$

where  $U_\nu, V_\nu$  correspond to distinct interaction energies, provided they are in the same and different states, respectively. Throughout this paper, we adopt  $k_B = 1$ . In addition, the system can be subjected to a non-conservative force  $F_\nu$ .

After the time duration  $\tau_\nu$ , it is disconnected and reconnected to the next reservoir with temperature  $\beta_{\nu+1} = 1/T_{\nu+1}$  and subjected to another set of parameters  $\epsilon_{\nu+1}, U_{\nu+1}, V_{\nu+1}$  and  $F_{\nu+1}$ . This process is then repeated until a complete cycle, after the total time  $\tau$ . As in Refs. [14, 15, 35], above system dynamics becomes simpler when characterized by the total particle number  $i$  occupying the upper state, assuming the values  $i = 0, 1$  or 2, according to whether it is empty, having one unit, or having two units, with energies  $\tilde{\epsilon}^{(\nu)} = 0, V_\nu + \epsilon_\nu$  and  $U_\nu + 2\epsilon_\nu$ , respectively. Let  $p_i^{(\nu)}(t)$  be the system's probability at the state  $i$  at the time  $t$  when it is placed in contact with the  $\nu$ -th reservoir, governed by the following master equation

$$\dot{p}_i^{(\nu)}(t) = \sum_{j \neq i} J_{ij}^{(\nu)}, \quad (2)$$

where  $J_{ij}^{(\nu)} \equiv \omega_{ij}^{(\nu)} p_j^{(\nu)} - \omega_{ji}^{(\nu)} p_i^{(\nu)}$  and  $\omega_{ij}^{(\nu)}$  accounts to the transition rate from state  $j$  to  $i$ , satisfying the condition  $\sum_i \omega_{ij}^{(\nu)} = 0$  for every strokes.

We shall restrict our analysis to the simplest case  $N = 2$ , as sketched in Fig. 1, in which the time duration of the first and second strokes read  $\tau_1$  and  $\tau_2 = \tau - \tau_1$ , respectively. Note that one has the symmetric time operation when  $\tau_1 = \tau/2$ . Given that the probability distribution is continuous, it should satisfy the following boundary conditions for  $p_i^{(\nu)}(t)$  (for all  $i = 0, 1$  and 2):

$$p_i^{(1)}(\tau_1) = p_i^{(2)}(\tau_1), \quad p_i^{(1)}(0) = p_i^{(2)}(\tau). \quad (3)$$

By resorting to the eigendecomposition of Eq. (2) along with the periodic boundary conditions given by Eq. (3), it is possible to obtain the expression for the probability component  $p_i^{(\nu)}(t)$  at the  $\nu$ -th stage:

$$p_i^{(\nu)}(t) = p_i^{(eq,\nu)} + \sum_{j=1}^2 e^{\lambda_j^{(\nu)}[t-\tau_{\nu-1}]} \Gamma_j^{(\nu)} \mathbf{p}^{(\nu)}(\tau_{\nu-1}), \quad (4)$$

where  $\mathbf{p}^{(eq,\nu)}$  is the probability vector associated with  $\lambda_0 = 0$ ,  $\lambda_j^{(\nu)} < 0$  is the  $j$ -th non-zero eigenvalue,  $\Gamma_j^{(\nu)} = \psi_j^{(\nu)} \phi_j^{(\nu)}$  is the

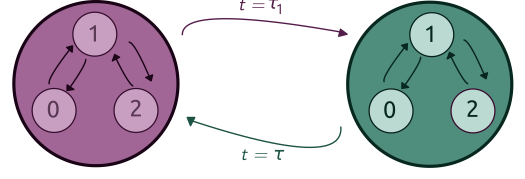


FIG. 1. Sketch of the setup, composed of two coupled nanomachines, characterized by a three-state system specified by the variable  $i$  accounting to the occupation of the upper level. At each stage (with duration  $\tau_1$  and  $\tau - \tau_1$ ) the system is placed in contact with a distinct thermal bath and parameters, specified by the purple and green colors. The stroke change occurs at  $t = \tau_1$  and the system returns to its initial state at  $t = \tau$ .

matrix associated with the product of the  $j$ -th right and left eigenvectors and  $\mathbf{p}_i^{(\nu)}$  is the initial condition vector at the start of each stroke, obtained from the above boundary conditions. Despite being exact, expressions for  $\mathbf{p}_i^{(\nu)}$  are quite cumbersome. In Appendix A, we list them for the particular case  $\tau_1 = \tau/2$ .

Once the probability distribution, all thermodynamic quantities can be obtained. By integrating Eq. (2) over a complete cycle and by summing them, one has that  $\sum_{j \neq i} \bar{J}_{ij}^{(1)} = -\sum_{j \neq i} \bar{J}_{ij}^{(2)}$ , where  $\bar{J}_{ij}^{(1)} = \int_0^{\tau_1} J_{ij}^{(1)} dt/\tau$ ,  $\bar{J}_{ij}^{(2)} = \int_{\tau_1}^{\tau} J_{ij}^{(2)} dt/\tau$  and Eq. (3) was used. At each time, only transitions  $i \rightarrow i \pm 1$  are allowed, implying that a transition of type  $0 \leftrightarrow 2$  is forbidden and hence the system presents only two independent fluxes, namely  $\bar{J}_{01}^{(1)}$  and  $\bar{J}_{21}^{(1)}$ , whose expressions are given by

$$\bar{J}_{01}^{(1)} = \frac{1}{\tau} \int_0^{\tau_1} \{ \omega_{01}^{(1)} p_1^{(1)}(t) - \omega_{10}^{(1)} p_0^{(1)}(t) \} dt \quad (5a)$$

$$\bar{J}_{21}^{(1)} = \frac{1}{\tau} \int_0^{\tau_1} \{ \omega_{21}^{(1)} p_1^{(1)}(t) - \omega_{12}^{(1)} p_2^{(1)}(t) \} dt, \quad (5b)$$

respectively. We pause to make a few comments about fluxes  $\bar{J}_{ij}^{(1)}$ 's. Firstly, in the regime of fast switchings  $\tau \rightarrow 0$ , where each stroke relaxes infinitely fast to the steady state, each flux  $\bar{J}_{ij}^{(\nu)}$  acquires a simpler form listed in Appendix B. They can be alternatively obtained by assuming the system relaxes “infinitely fast” to the steady state in such a way that

$$\bar{J}_{ij}^{(\nu)} \rightarrow \frac{1}{2} \{ \omega_{ij}^{(\nu)} p_j - \omega_{ji}^{(\nu)} p_i \}, \quad (6)$$

for  $j = 1$  and  $i \in \{0, 2\}$ , where  $p_i = p_i^{(1)} + p_i^{(2)}$ , whose expressions for  $p_i$  are listed in Appendix B and are equivalent to the system simultaneously placed in contact with both thermal baths. Secondly, in the regime of slow switchings,  $\tau \gg 1$ ,

$$\bar{J}_{ij}^{(\nu)} \rightarrow \frac{(-1)^{(\nu+1)}}{\tau} \{ p_i^{(eq,1)} - p_i^{(eq,2)} \}, \quad (7)$$

which vanishes as  $\tau \rightarrow \infty$ , consistent with the case of the system being placed in contact with a single thermal reservoir.

Until here, all analyses have been carried out without any thermodynamic consideration. For that, we follow the common approach considered in the literature (see, *e.g.*, Refs. [1, 15, 16, 36, 37]) in which the ratio between transition rates  $\omega_{ij}^{(v)}$  and  $\omega_{ji}^{(v)}$  are defined according to the local detailed balance:

$$\ln \frac{\omega_{ij}^{(v)}}{\omega_{ji}^{(v)}} = -\beta_v [\tilde{\epsilon}_i^{(v)} - \tilde{\epsilon}_j^{(v)} + d_{ij}^{(v)} F_v], \quad (8)$$

where  $\tilde{\epsilon}_i^{(v)} - \tilde{\epsilon}_j^{(v)}$  is the difference between states  $i$  and  $j$  and  $d_{ij}^{(v)} F_v$  accounts to the influence of a driving force, where element  $d_{ji}^{(v)}$  satisfies the anti-symmetric property  $d_{ji}^{(v)} = -d_{ij}^{(v)}$ .

From Eq.(8) we consider the entropy production formula

$$\Pi_v(t) = \sum_{i<j} J_{ij}^{(v)}(t) \ln \frac{\omega_{ij}^{(v)} p_j(t)}{\omega_{ji}^{(v)} p_i(t)}, \quad (9)$$

whose integration over a complete cycle, together with the previously mentioned boundary conditions leads to the standard form  $\bar{\sigma} = -\sum_v \beta_v \bar{Q}_v$ , where  $\bar{Q}_v$  is given by

$$\bar{Q}_v = \sum_{i<j} [\tilde{\epsilon}_i^{(v)} - \tilde{\epsilon}_j^{(v)} + d_{ij}^{(v)} F_v] \bar{J}_{ij}^{(v)}. \quad (10)$$

By expressing Eq. (10) in terms of fluxes  $\bar{J}_{01}^{(v)}$  and  $\bar{J}_{21}^{(v)}$ , the exchanged heat  $\bar{Q}_v$  then reads

$$\bar{Q}_v = \left[ (\tilde{\epsilon}_0^{(v)} - \tilde{\epsilon}_1^{(v)} + d_{01}^{(v)} F_v) \bar{J}_{01}^{(v)} + (\tilde{\epsilon}_2^{(v)} - \tilde{\epsilon}_1^{(v)} + d_{21}^{(v)} F_v) \bar{J}_{21}^{(v)} \right]. \quad (11)$$

Since the system evolves to a nonequilibrium steady state regime returning to the initial state after a complete cycle, the first law of thermodynamics establishes that  $\mathcal{P} = -(\bar{Q}_1 + \bar{Q}_2)$ , and hence the expression for  $\mathcal{P}$  is given by

$$\mathcal{P} = -\left[ \sum_i (\tilde{\epsilon}_i^{(2)} - \tilde{\epsilon}_i^{(1)}) \frac{(p_i^{(1)}(\tau_1) - p_i^{(1)}(0))}{\tau} + \sum_{i<j} d_{ij}^{(1)} (F_1 \bar{J}_{ij}^{(1)} - F_2 \bar{J}_{ij}^{(2)}) \right], \quad (12)$$

where Eqs. (3) and (11) were used, together the properties:  $d_{ij}^{(1)} = -d_{ij}^{(2)}$ ,  $d_{ij}^{(v)} = -d_{ji}^{(v)}$  and  $\bar{J}_{ij}^{(v)} = -\bar{J}_{ji}^{(v)}$ . Above equation states that the power output comes from two work-sources: the former, from the time variation of energies (first term) after each stroke and the latter from non-conservative forces (second term). By expressing in terms of independent fluxes, Eq. (12) reads  $\mathcal{P} = \left[ (\tilde{\epsilon}_0^{(2)} - \tilde{\epsilon}_1^{(2)}) - (\tilde{\epsilon}_0^{(1)} - \tilde{\epsilon}_1^{(1)}) \right] \bar{J}_{01}^{(1)} + \left[ (\tilde{\epsilon}_2^{(2)} - \tilde{\epsilon}_1^{(2)}) - (\tilde{\epsilon}_2^{(1)} - \tilde{\epsilon}_1^{(1)}) \right] \bar{J}_{21}^{(1)} - (d_{01}^{(1)} \bar{J}_{01}^{(1)} + d_{21}^{(1)} \bar{J}_{21}^{(1)}) (F_1 + F_2)$ .

Finally, by defining the second stage as the hot reservoir and choosing parameters properly, an amount of heat extracted from the hot bath  $\bar{Q}_2 > 0$  can be partially converted into power output  $\mathcal{P} < 0$  ( $\bar{Q}_2 = -\mathcal{P} - \bar{Q}_1$ ), consistent to the heat engine operation. Conversely, the pump regime is characterized by an

amount of power required for delivering heat or particles from the cold to the hot reservoir, implying that  $\mathcal{P} = -\bar{Q}_1 - \bar{Q}_2$  with  $\mathcal{P} > 0$  and  $\bar{Q}_2 < 0$ . In both cases, we adopted the efficiency definition  $\eta = -\mathcal{P}/\bar{Q}_2$ , implying that the former and latter regimes have efficiencies constrained according to  $0 \leq \eta < \eta_c$  and  $\eta_c < \eta \leq \infty$ , respectively, where  $\eta_c = 1 - \beta_2/\beta_1$  denotes Carnot efficiency.

Despite the simplicity, the model presents a great number of parameters ( $\beta_v, \epsilon_v, V_v, U_v, F_v$ ) and one of our main goals is to draw a comparison with previous results [15, 35] in which solely units in distinct states interact with each other. For this reason, we shall curb ourselves to the case  $U_v = 0$ .

### III. DISTINCT INTERACTIONS AT EACH STROKE

#### A. Main expressions and general findings

Our first approach consists of building a setup via change of individual and interaction energies at each stroke without non-conservative drivings. Transition rates  $\omega_{ij}^{(v)}$  follow Eq. (8) and have been defined in the following form

$$\omega_{10}^{(v)} = 2\Gamma \exp\left\{\frac{-\beta_v}{2}(V_v + \epsilon_v)\right\}, \quad (13)$$

$$\omega_{01}^{(v)} = \Gamma \exp\left\{\frac{-\beta_v}{2}(-V_v - \epsilon_v)\right\}, \quad (14)$$

$$\omega_{21}^{(v)} = \Gamma \exp\left\{\frac{-\beta_v}{2}(-V_v + \epsilon_v)\right\}, \quad \text{and} \quad (15)$$

$$\omega_{12}^{(v)} = 2\Gamma \exp\left\{\frac{-\beta_v}{2}(V_v - \epsilon_v)\right\} \quad (16)$$

where  $V_v, \epsilon_v$  assume distinct values at each stroke and  $\Gamma$  expresses the coupling between the system and the reservoir. From Eq. (10), the average heat flux at each stroke is given by

$$\begin{aligned} \bar{Q}_1 &= -\left[ \bar{J}_{01}^{(1)}(V_1 + \epsilon_1) + \bar{J}_{21}^{(1)}(V_1 - \epsilon_1) \right], \\ \bar{Q}_2 &= \left[ \bar{J}_{01}^{(1)}(V_2 + \epsilon_2) + \bar{J}_{21}^{(1)}(V_2 - \epsilon_2) \right], \end{aligned} \quad (17)$$

whose steady entropy production  $\bar{\sigma}$  assumes the generic "fluxes times forces" form  $\bar{\sigma} = J_1 X_1 + J_2 X_2$ , where  $J_1 = \bar{J}_{01}^{(1)}$  and  $J_2 = \bar{J}_{21}^{(1)}$  with  $X_1$  and  $X_2$  given by

$$\begin{aligned} X_1 &= \frac{V_1 + \epsilon_1}{T_1} - \frac{V_2 + \epsilon_2}{T_2}, \\ X_2 &= \frac{V_1 - \epsilon_1}{T_1} - \frac{V_2 - \epsilon_2}{T_2}. \end{aligned} \quad (18)$$

Expressions for the power  $\mathcal{P}$  and system efficiency  $\eta$  are given by

$$\mathcal{P} = (\epsilon_1 - \epsilon_2)(\bar{J}_{01}^{(1)} - \bar{J}_{21}^{(1)}) + (V_1 - V_2)(\bar{J}_{01}^{(1)} + \bar{J}_{21}^{(1)}), \quad (19)$$

and

$$\eta = -\frac{(\epsilon_1 - \epsilon_2)(\bar{J}_{01}^{(1)} - \bar{J}_{21}^{(1)}) + (V_1 - V_2)(\bar{J}_{01}^{(1)} + \bar{J}_{21}^{(1)})}{\epsilon_2(\bar{J}_{01}^{(1)} - \bar{J}_{21}^{(1)}) + V_2(\bar{J}_{01}^{(1)} + \bar{J}_{21}^{(1)})}, \quad (20)$$

respectively. We pause again to make a few comments. First, Eqs. (17)-(20) are general for the two-stroke case, irrespective of the period, asymmetry and model parameters. Second, in the absence of interactions ( $V_1 \rightarrow 0$  and  $V_2 \rightarrow 0$ ), the system becomes equivalent to the interactionless setup investigated in Refs. [24, 25, 38] for  $\mu_1 = \mu_2 = 0$ . In such cases, Eqs. (19) and (20) reduce to  $\eta_s = 1 - \epsilon_1/\epsilon_2$  and  $\mathcal{P}_s = (\epsilon_1 - \epsilon_2)\bar{J}_s$ , respectively, where  $\bar{J}_s$  (for  $\tau_1 = \tau/2$ ) reads:

$$\bar{J}_s = \frac{\prod_{\mu} \left\{ -1 + \cosh \left[ \tau \cosh \left( \frac{\beta_{\mu} \epsilon_{\mu}}{2} \right) \right] + \sinh \left[ \tau \cosh \left( \frac{\beta_{\mu} \epsilon_{\mu}}{2} \right) \right] \right\}}{(e^{\beta_1 \epsilon_1} - e^{\beta_2 \epsilon_2})^{-1} \prod_{\mu'} (1 + e^{\beta_{\mu'} \epsilon_{\mu'}}) [-1 + \cosh(\tau X) + \sinh(\tau X)]}, \quad (21)$$

where  $X = \cosh(\beta_1 \epsilon_1/2) + \cosh(\beta_2 \epsilon_2/2)$ . Both  $\eta_s$  and  $\mathcal{P}_s$  can be related through expression  $\mathcal{P}_s = -\epsilon_2 \eta_s \bar{J}_s$ , consistent to heat engine characterized by  $\bar{J}_s > 0$  (since  $\beta_1 \epsilon_1 > \beta_2 \epsilon_2$ ),  $\mathcal{P}_s < 0$ ,  $0 \leq \eta_s \leq \eta_c$ . Conversely, the pump is characterized by the other way around of conditions  $\bar{J}_s < 0$  (since  $\beta_1 \epsilon_1 < \beta_2 \epsilon_2$ ),  $\mathcal{P}_s > 0$  and  $\eta_c < \eta_s \leq 1$ . Third, contrasting with the interactionless case, there are two independent fluxes,  $\bar{J}_{01}^{(1)}$  and  $\bar{J}_{21}^{(1)}$ , revealing that the interaction between units gives rise to a much richer behavior than the single case [24]. Eqs. (17) and (19) impose some constraints on the operation regime. In particular, the heat engine occurs when both inequalities  $(\epsilon_2 - \epsilon_1)(\bar{J}_{01}^{(1)} - \bar{J}_{21}^{(1)}) < (V_1 - V_2)(\bar{J}_{01}^{(1)} + \bar{J}_{21}^{(1)})$  and  $\epsilon_2(\bar{J}_{21}^{(1)} - \bar{J}_{01}^{(1)}) > V_2(\bar{J}_{01}^{(1)} + \bar{J}_{21}^{(1)})$  are simultaneously satisfied, whereas the pump regime takes place for opposite inequalities. Fourth, our system will operate more efficiently than the interactionless case ( $\eta > \eta_s$ ) if  $(\epsilon_1 V_2 - \epsilon_2 V_1)(\bar{J}_{01}^{(1)} + \bar{J}_{21}^{(1)}) > 0$ . The ideal regime operation yields when  $\bar{J}_{01}^{(1)}, \bar{J}_{21}^{(1)} \rightarrow 0$ . For  $\epsilon_1/\epsilon_2$  or  $V_1/V_2$  held fixed,  $\eta = \eta_c$  when  $\beta_2 V_2 = \beta_1 V_1$  and  $\beta_2 \epsilon_2 = \beta_1 \epsilon_1$ , respectively, whose efficiency is given by  $\eta = 1 - V_1/V_2$ , akin to the interactionless expression. Conversely, maximum efficiencies  $\eta_{ME} < \eta_c$  if the condition  $\epsilon_1/\epsilon_2 = V_1/V_2 = \beta_2/\beta_1$  is not satisfied. Fifth and last, the occurrence of the pump regime implies at the following relation between parameters  $(\beta_2 \epsilon_2 - \beta_1 \epsilon_1)(\bar{J}_{21}^{(1)} - \bar{J}_{01}^{(1)}) > (\beta_2 V_2 + \beta_1 V_1)(\bar{J}_{21}^{(1)} + \bar{J}_{01}^{(1)})$ . Figs. 2, 3 and Appendix C illustrate all above features.

## B. System behavior and heat maps for equal switching times

$$\tau_1 = \tau/2$$

Once introduced the main expressions, we are now in a position to depict the system behavior and main results. We chose units in such a way that  $\beta_{\nu} V_{\nu}$  and  $\beta_{\nu} \epsilon_{\nu}$  are dimensionless. The analysis will be carried out for the following set of parameters:  $\beta_1 = 10, \beta_2 = 1, \tau = 1$ . In order to obtain a first insight into how the interaction between units influences the system performance, Fig. 2 depicts the system performance for  $\epsilon_1/\epsilon_2 = 0.5$ , in which the interactionless case operates as an engine with power and efficiency given by  $\mathcal{P}_s = -0.1477$  and  $\eta_s = 0.5$ , respectively.

We highlight two remarkable changes coming from the interaction, under suitable choices of  $V_1(V_2)$  at strokes  $\nu = 1(2)$ .

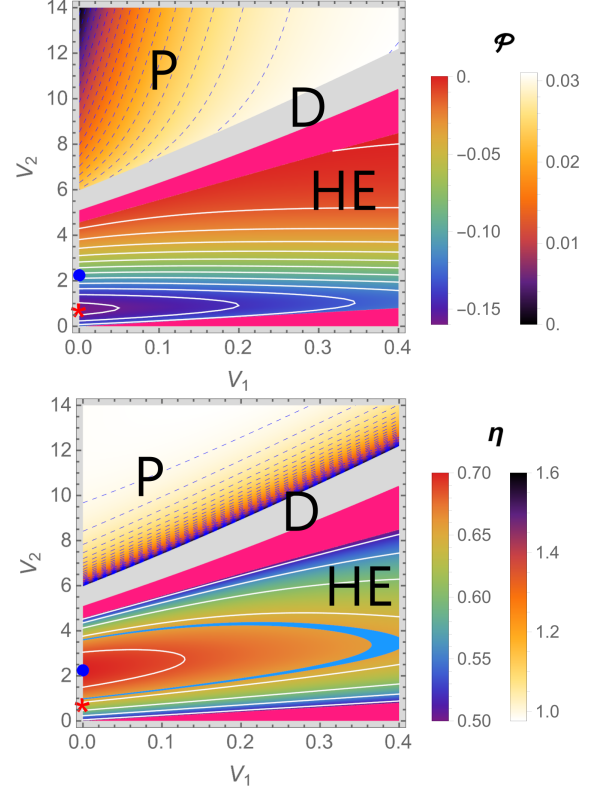


FIG. 2. The influence of the interaction parameters over the system performance. Top and bottom panels depict the power and efficiency heat maps. The surfaces highlighted by the color pink represent the region in which  $\eta \leq \eta_s$ . Parameters:  $\beta_2 = 1, \beta_1 = 10, \tau = 1$  and  $\epsilon_1/\epsilon_2 = 0.5$ . Symbols HE (left bars) and P (right bars) correspond to the heat engine and pump regimes, respectively, whereas \* and • attempt to the global maximum of  $\mathcal{P}_{mP}$  and  $\eta_{ME}$  in the HE regime. The gray region indicates dud (D) behavior. For this set of parameters  $\eta_{ME} < \eta_c$ , whereas the light blue line in the bottom panel indicates the region in which  $\eta_{mP} = \eta_{CA}$ .

The former is a broad set of parameters, in which  $\eta > \eta_s$  and  $\mathcal{P} > \mathcal{P}_s$ . The inclusion of interactions also extends the regime of operation, giving rise to a pump regime as  $V_2$  is raised. Similar results are found for distinct  $\beta_1/\beta_2$ 's, although the variation of temperatures can favor a given operation regime (see e.g. Appendix C).

The interplay between individual  $\epsilon_1/\epsilon_2$  and interaction  $V_1/V_2$  energies is depicted in Fig. 3, in which  $\eta < \eta_s < \eta_c$  for small  $V_2$ 's. However, its increase not only extends the heat regime to the region  $0 < \epsilon_1/\epsilon_2 < \beta_2/\beta_1$ , in which the interactionless case operates as a pump, but also leads to higher efficiencies  $\eta > \eta_s$  as  $V_2$  increases and a maximum value  $\eta_{ME}$  at  $V_{2ME}$ . As portrayed in Sec. III A,  $\eta_{ME} < \eta_c$  for  $\epsilon_1 \beta_1 \neq \epsilon_2 \beta_2$  and  $\eta_{ME} = \eta_c$  at  $V_2 = V_{2ME}$  when  $\epsilon_1 \beta_1 = \epsilon_2 \beta_2$  (e.g. blue • in Fig. 3) and the interactionless case is efficient in such latter case. Similarly to  $\eta$ , it is possible to find suitable values of parameters in which  $\mathcal{P} > \mathcal{P}_s$  (from now on meaning the absolute value of  $\mathcal{P}$ ) as well as optimize it via a suitable choice of  $V_{2mP}$ . However, there is a remarkable difference with re-



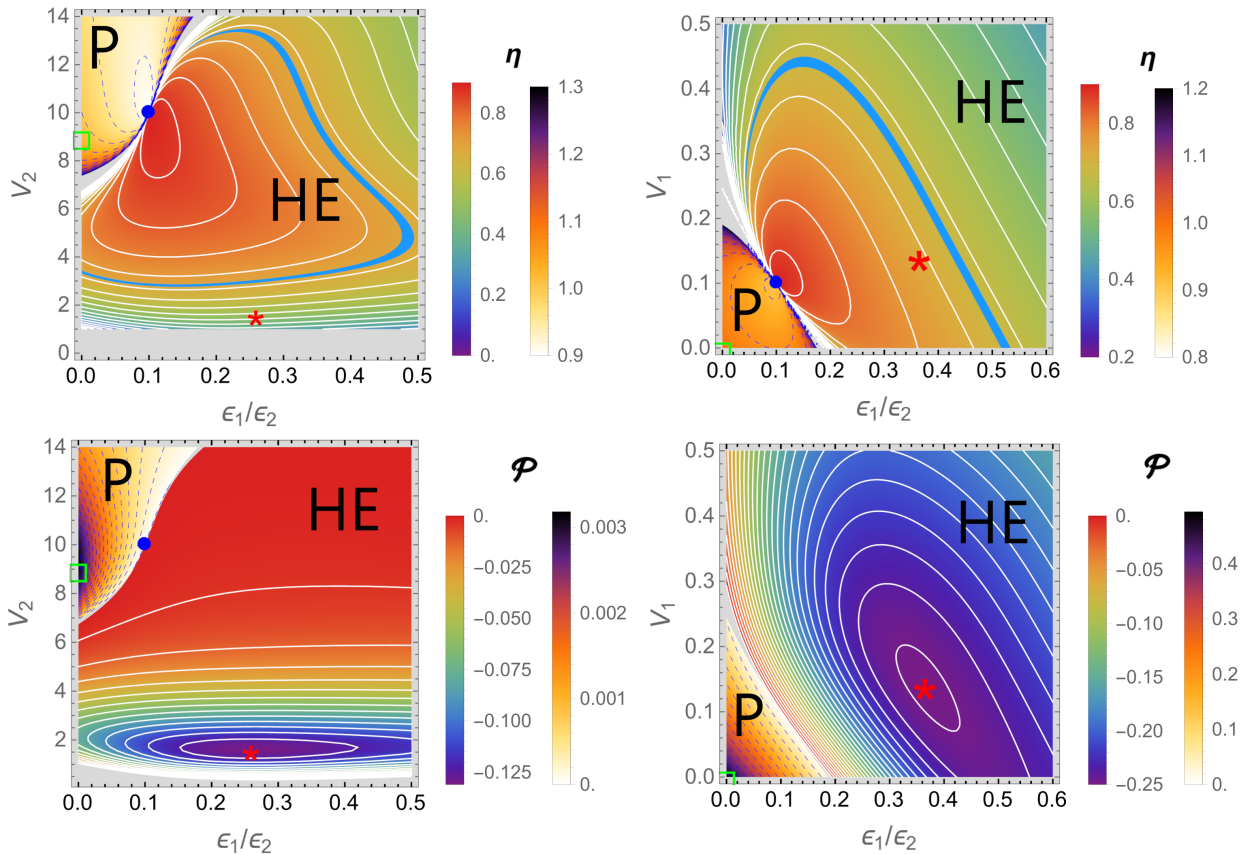


FIG. 3. The influence of individual energies  $\epsilon_1/\epsilon_2$  over the system performance. Left and right panels depict fixed  $V_1$  and  $V_2$ , respectively, while top and bottom panels show  $\eta$ 's and  $\mathcal{P}$ 's heat maps, respectively. Left and right bars denote HE and P regimes, respectively. Symbols  $\bullet$ ,  $*$  and  $\square$  attempt to Carnot efficiency  $\eta_c$ , efficiencies at maximum power  $\eta_{mp}$  at the heat engine (HE) and pump (P) regimes, respectively. Light blues in top panels indicate the regions in which  $\eta_{mp} = \eta_{CA}$ . Parameters:  $\beta_2 = 1, \beta_1 = 10, \tau = 1, V_2 = 1$  (right) and  $V_1 = 1$  (left).

spect to  $\eta$ , the existence of an optimal set of  $\epsilon_1/\epsilon_2$  and  $V_2$  in which (the absolute)  $\mathcal{P}$  is simultaneously maximized (see e.g. symbol  $*$  in bottom heat maps).

The influence of  $V_1$  ( $V_2$  held fixed) is remarkably different from left panels ( $V_1$  held fixed), and the engine regime and higher efficiencies are constrained to small values of  $V_1$ 's (consistent with the general findings from Sec. III A), hence pointing us out that stronger interactions in the second stage are more significant than in the first one (second stage operating as the hot thermal bath). Also,  $\eta > \eta_s$  for a broader set of values of  $V_1$  as  $\epsilon_1/\epsilon_2$  is large. The behavior of  $\mathcal{P}$  is akin to the previous one and presents a maximum at a (small)  $V_{1mp}$ 's (fixed  $\epsilon_1/\epsilon_2$ ) as well as an optimal  $\epsilon_1/\epsilon_2$  providing its simultaneous maximization.

As a side analysis, we compare efficiencies at maximum power  $\eta_{mp}$  with Curzon and Ahlborn bound  $\eta_{CA} = 1 - \sqrt{\beta_2/\beta_1}$  [39], which has been verified in distinct systems [2, 16, 40]. Despite not constituting a universal result, it provides a powerful guide about the system operation at finite power, which is more realistic than the ideal case ( $\eta = \eta_c$  and  $\mathcal{P} = 0$ ). In all cases, the interaction among units can also be chosen for providing efficiencies at maximum power  $\eta_{mp} > \eta_{CA}$  for a wide range of parameters (see e.g. light blue lines in Figs. 2-3

in which  $\eta_{mp} = \eta_{CA}$ ). Depending on the parameters the engine is projected,  $\eta_{mp} < \eta_{CA}$  [Figs. 2 and 3 (left panel)] and  $\eta_{mp} > \eta_{CA}$  (right panel of Fig. 3) at the simultaneous maximization of power.

Summarizing our findings, the presence of collective effects between two units makes it possible to conveniently choose interaction parameters at each stage, providing higher performances than its interactionless counterpart (for the same values of individual energies), as well as distinct optimization routes, such as the maximization of power and efficiency. Additionally, an extra advantage concerns the possibility of changing the regime operation, from heat engine to pump and vice-versa, by changing the interactions at each stroke.

### C. Influence of period $\tau$ and asymmetric switchings

The influence of period  $\tau$  and the inclusion of a different time duration at each stroke, expressed by  $\kappa = \tau_1/\tau_2 \neq 1$  will be considered in this section. Due to the existence of several distinct parameters, we shall focus on parameters  $\epsilon_1/\epsilon_2 = 0.6, V_1 = 0.2, \beta_1 = 10$  and  $\beta_2 = 1$ .

Although  $\mathcal{P}_s$  increases as  $\tau$  is lowered, the period plays a

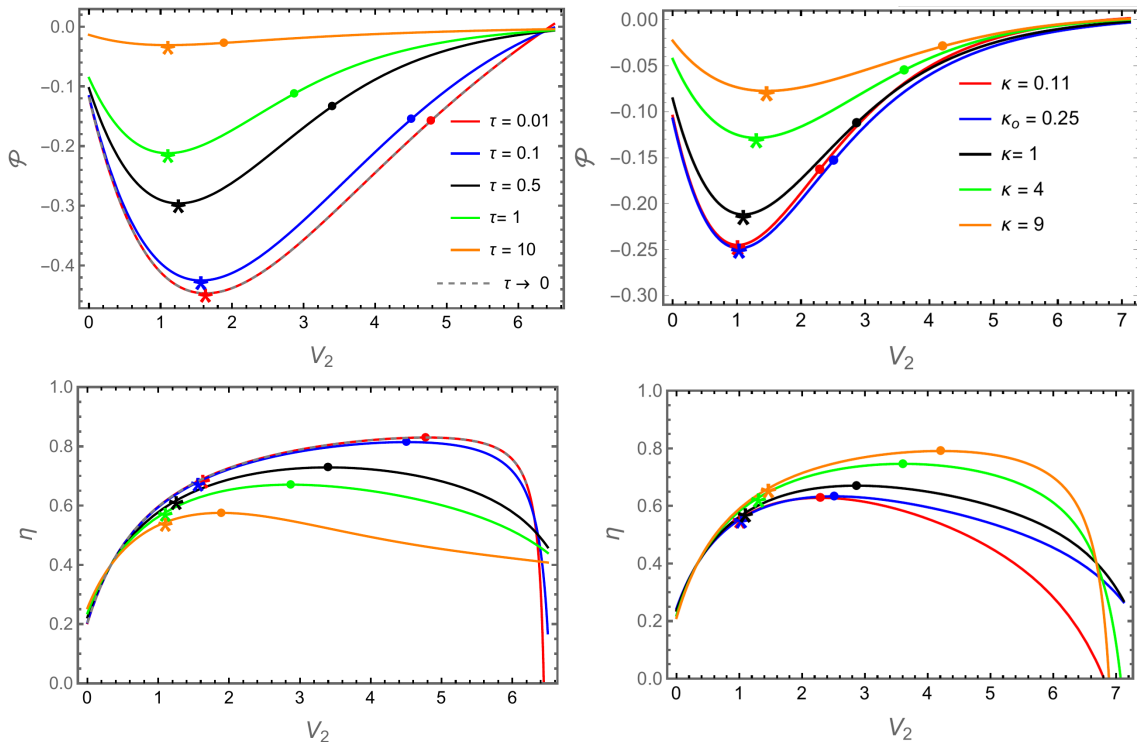


FIG. 4. Left and right panels depict the influence of period  $\tau$  (for symmetric time switchings) and distinct  $\kappa$ 's (for  $\tau = 1$ ), respectively, for  $\mathcal{P}$  (top) and  $\eta$  (bottom), respectively. Symbols \* and • denote associate  $\mathcal{P}_{mP}$ 's and  $\eta_{ME}$ 's, respectively. Parameters:  $\beta_1 = 10, \beta_2 = 1, V_1 = 0.2, \epsilon_1/\epsilon_2 = 0.6$ .

less important role in the interactionless case, in part because  $\eta_s$  is independent of  $J_s$  and  $\tau$  [24, 38]. On the other hand, the existence of two independent fluxes, as a consequence of the interaction between nanomachines makes the influence of  $\tau$  more revealing. We highlight two aspects regarding the influence of  $\tau$ , as depicted in the left panels of Fig. 4. First, it significantly affects the system performance, marking the increase of both  $\mathcal{P}$  (as the interactionless system) and  $\eta$  (unlike the interactionless), with increasing maximum  $\mathcal{P}_{mP}$  and  $\eta_{ME}$  at  $V_{2mP}$  and  $V_{2ME}$ , respectively, as  $\tau$  is decreased toward the limit  $\tau \rightarrow 0$ , in which the system becomes equivalent to the (simultaneous) contact with hot and cold thermal baths (see e.g. Appendix B). Second, despite the increase of  $\tau$  reduces  $\mathcal{P}$  and  $\eta$ , it enlarges the heat engine operation. Thus, the period can be conveniently chosen to obtain a desirable compromise between the system performance (power and efficiency) and the range of the operation regime.

A second aspect to be investigated in this section relies on the inclusion of a distinct duration of each stage, measured by the asymmetry  $\kappa$ . This ingredient has been revealed to be a powerful ingredient for improving the system power in the interactionless case [30] or even both  $\mathcal{P}$  and  $\eta$  in the case of collisional Brownian engines [22] and is depicted in the right panels of Fig. 4. Although  $\eta$  typically increases as  $V_2$  raises and  $\kappa$  (or  $\tau_1$ ) is reduced, consistent with the system placed in contact with the hot thermal bath during a larger interval, there is an optimal  $\kappa_o$  ensuring optimal power  $\mathcal{P}_{mP}$ . Thus, like

the interactionless case [30],  $\kappa$  can be conveniently chosen in order to increase the power-output and  $\mathcal{P} > \mathcal{P}_s$ . Since  $\eta > \eta_s$  for a broad range of  $V_2$ 's, the interaction offers an extra advantage in which  $\kappa$  can be suitably chosen in order to obtain the desired  $\eta$  (greater than  $\eta_s$ ) or even the desired compromise between  $\mathcal{P}$  and  $\eta$ .

#### IV. COLLISIONAL MACHINE UNDER NON CONSERVATIVE DRIVINGS

##### A. Main expressions and heat maps

Our second approach encompasses a worksource coming from a non-conservative driving, introduced by means of a bias in order to benefit certain transitions. By following the ideas of Refs.[15, 16, 31], transitions of type  $i \rightarrow i + 1$  ( $i \rightarrow i - 1$ ) are favored according to whether the system is placed in contact with the cold (hot) thermal baths, leading to an incremental  $\mathcal{P}$  reading  $F_v$ , whereas the remaining parameters ( $V$  and  $\epsilon$ ) are held fixed. Our study relies on investigating two important aspects: the role of drivings at each stroke and its relationship with  $V$ , temperatures  $\beta_1/\beta_2$  and the influence of period  $\tau$ . Transition rates  $\omega_{ij}^{(v)}$  follow Eq. (8) and are listed

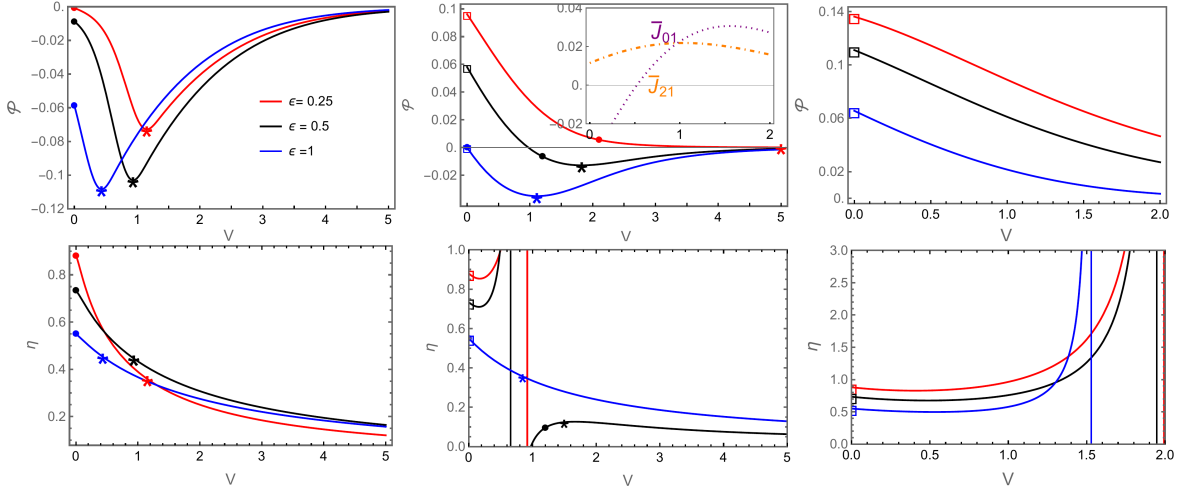


FIG. 5. Depiction of power  $\mathcal{P}$  (top) and efficiency  $\hat{\eta}$  (bottom) versus  $V$  for distinct  $\beta_1$ 's. Parameters:  $\beta_2 = 1, E_a = 1, F_2 = 1, F_1 = 0.1$  and  $\tau = 1$  and  $\beta_1 = 10$  (left),  $\beta_1 = 20/9$  (middle) and  $\beta_1 = 3/2$  (right). Stars and squares denote the location of  $\mathcal{P}_{mP}$ 's for heat engine and pump, respectively. Circles denote the location of maximum efficiencies for the engine ( $0 \leq \eta < \eta_c$  regime).

below

$$\omega_{10}^{(v)} = 2\Gamma \exp\left\{\frac{-\beta_v}{2}(E_a + V + \epsilon + (-1)^v F_v)\right\} \quad (22)$$

$$\omega_{01}^{(v)} = \Gamma \exp\left\{\frac{-\beta_v}{2}(E_a - V - \epsilon - (-1)^v F_v)\right\} \quad (23)$$

$$\omega_{21}^{(v)} = \Gamma \exp\left\{\frac{-\beta_v}{2}(E_a + \epsilon - V + (-1)^v F_v)\right\} \quad (24)$$

$$\omega_{12}^{(v)} = 2\Gamma \exp\left\{\frac{-\beta_v}{2}(E_a - \epsilon + V - (-1)^v F_v)\right\}, \quad (25)$$

where  $F_v$  assumes distinct values at each stroke. Parameter  $E_a$  attempts to an activation energy and it will be included in order to draw a comparison with previous results [14, 15]. Although our main findings are independent of  $E_a$ , its inclusion makes the heat engine regime more pronounced. From now on, we shall set  $E_a = 1$  in all analyses.

From Eqs. (11) and (12) and by taking  $V_1 = V_2 = V$  and  $\epsilon_1 = \epsilon_2 = \epsilon$ , the average power and the heat extracted exchanged with the hot bath are given by the following expressions

$$\begin{aligned} \mathcal{P} &= -(F_1 + F_2)(\bar{J}_{01}^{(1)} - \bar{J}_{21}^{(1)}), \\ \bar{Q}_2 &= \left[(V + \epsilon + F_2)\bar{J}_{01}^{(1)} + (V - \epsilon - F_2)\bar{J}_{21}^{(1)}\right], \end{aligned} \quad (26)$$

whose system entropy production reads  $\bar{\sigma} = -\beta_1 \bar{Q}_1 - \beta_2 \bar{Q}_2$  and assumes the bilinear form  $\bar{\sigma} = J_1 X_1 + J_2 X_2$ , where  $J_1 = \bar{J}_{01}^{(1)}$  and  $J_2 = \bar{J}_{21}^{(1)}$  (as in Sec. III) with thermodynamic forces  $X_1$  and  $X_2$  given by

$$\begin{aligned} X_1 &= \frac{\epsilon + V + F_2}{T_2} - \frac{\epsilon + V - F_1}{T_1}, \\ X_2 &= \frac{\epsilon - V + F_2}{T_2} - \frac{\epsilon - V - F_1}{T_1}. \end{aligned} \quad (27)$$

The efficiency is given by the ratio between  $\mathcal{P}$  and  $\bar{Q}_2$  given

by

$$\eta = \frac{(F_1 + F_2)(\bar{J}_{01}^{(1)} - \bar{J}_{21}^{(1)})}{(V + \epsilon + F_2)\bar{J}_{01}^{(1)} + (V - \epsilon - F_2)\bar{J}_{21}^{(1)}}, \quad (28)$$

respectively. The existence of the heat engine and pump regimes imposes some constraints in the fluxes, implying that in the former case parameters have to be adjusted in such a way that  $\bar{J}_{01}^{(1)} > \bar{J}_{21}^{(1)}$  and  $V(\bar{J}_{01}^{(1)} + \bar{J}_{21}^{(1)}) > (\epsilon + F_2)(\bar{J}_{21}^{(1)} - \bar{J}_{01}^{(1)})$ , whereas the latter (pump) implies opposite inequalities.

A first insight about the influence of drivings is depicted in Figs. 5 for fixed  $F_1/F_2$ . Efficiency and power curves exhibit an interesting and rich behavior due to the interplay among parameters  $\epsilon, V, \beta_1/\beta_2$  and  $\tau$ . While the heat regime is levered by increasing  $\epsilon$  and/or the ratio  $\beta_1/\beta_2$  (left and middle panels), the pump regime is favored for lower values of  $\beta_1/\beta_2$  (middle and right). The crossover from the heat to the pump regimes gives rise to an intermediate regime in which the system operates dudly (see e.g. middle panels). In such a case, there are optimal interactions  $V_{mP}$  and  $V_{ME}$  marking maximum (absolute) power ( $\mathcal{P}_{mP}$ ) and efficiency ( $\eta_{ME}$ ), respectively. Conversely, only  $\mathcal{P}$  can be optimized when the crossover between the above regimes is marked by the absence of a dud regime (e.g. left and right panels) and  $\eta$  monotonically decreases upon  $V$  being raised. Fig. 6 extends above findings by depicting heat maps for the efficiency and power for distinct ratio  $F_1/F_2$  and fixed  $\epsilon$ . Similarly to systems composed of many interacting units under fixed drivings [14, 16] and results from Sec. III, the power  $\mathcal{P}$  presents a simultaneous maximization (concerning both  $V$  and  $F_1/F_2$ ), whereas  $\eta$  approaches to the ideal regime  $F_2/F_1$  is increased. However, a difference with respect to previous studies concerns the absence of heat engine as  $F_1 = F_2$ . Unlike Refs. [14–16], in which the heat engine was investigated for large  $N$ 's, our minimal setup of  $N = 2$  interacting units requires a desirable compromise between  $F_v$ 's and parameters for operating properly as a heat

engine.

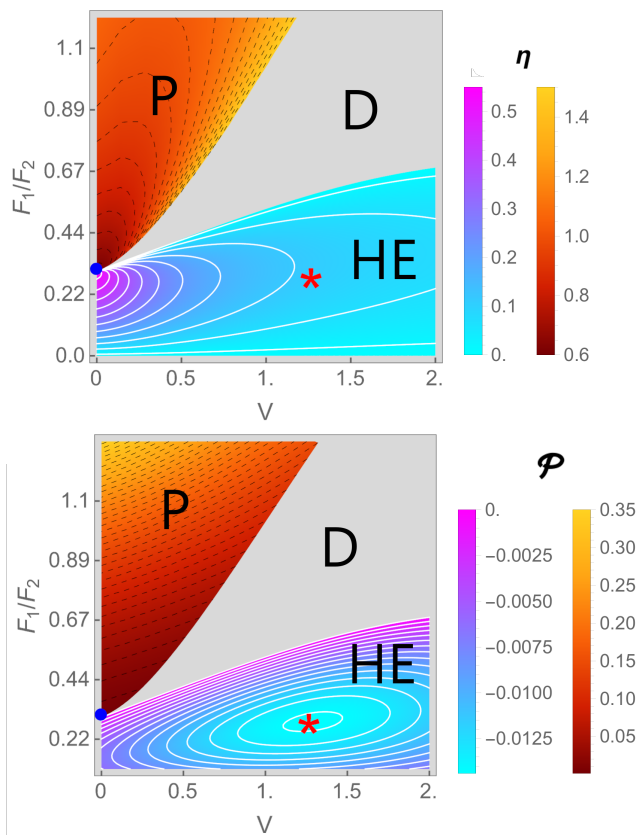


FIG. 6. The same as in Fig. 2, but by changing the drivings at each stroke. Parameters:  $\epsilon = 0.5, \beta_2 = 1, \beta_1 = 20/9, E_a = 1, \tau = 1, F_1 = 0.1, F_2 = 0.45$

The influence of period is depicted in Fig. 7 for the same parameters from Fig. 6 (left and right panels). In both cases,  $\mathcal{P}$  is strongly influenced by the period and approaches to the simultaneous contact with baths as  $\tau \rightarrow 0$ , whose expressions are evaluated via Appendix B. Also, depending on the parameters the engine is projected (right panels), the increase of  $\tau$  changes the regime operation, from heat engine to pump. In both cases, the behavior of  $\eta$  is more revealing and mildly changes with  $\tau$ . While small differences are almost imperceptible in the left panels, a somewhat increase of  $\eta$  as  $\tau$  is lowered is verified. This finding is remarkable, because it may be used for conveniently choosing the period in order to obtain the desirable  $\mathcal{P}$  with a small variation of  $\eta$ .

### B. Asymmetric time switchings

In the last analysis, we investigate the influence of asymmetric interaction times in the presence of distinct drivings at each stroke, as shown in Fig. 8.

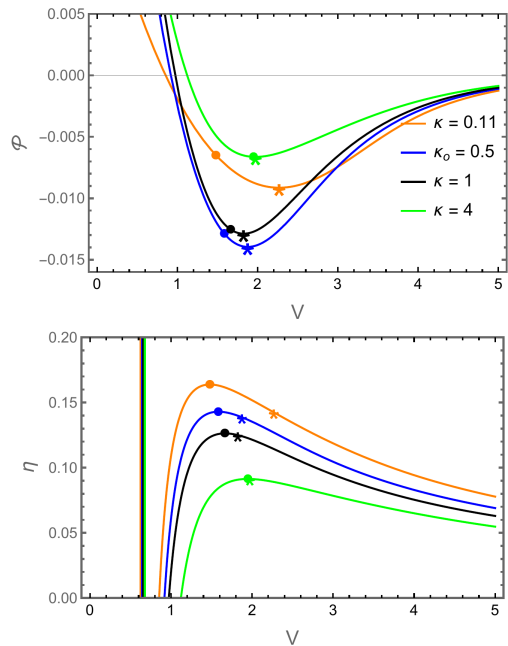


FIG. 8. Depiction of power  $\mathcal{P}$  and efficiency  $\eta$  versus  $V$  for different  $\kappa$ . Symbols  $\bullet$  and  $*$  denote the maximization of efficiency and power, respectively. Parameters:  $\epsilon = 0.5, \beta_2 = 1, \beta_1 = 20/9, E_a = 1, \tau = 1, F_1 = 0.1, F_2 = 1$ .

In similarity with Fig. 4, the asymmetry can be conveniently chosen for enhancing the power and efficiency or even for obtaining a desirable compromise between them. There is an optimal  $\kappa_o$  leading to simultaneous maximization of power while  $\eta$  always increases as  $\kappa$  is lowered, consistent with the contact with hot bath for a larger amount of the period. Despite such similarities, the asymmetry seems to be less pronounced than in the previous case, and optimal quantities do not deviate significantly from the symmetric ( $\kappa = 1$ ) case. A possible reason is that power and efficiency exhibit a more intricate dependence on fluxes and changes of energy parameters (former approach) than on driving variations [see e.g. Eqs. (19)-(26) and (20)-(28)].

## V. CONCLUSIONS

Nanoscale engines operating via collective operation have attracted considerable attention and posed as potential candidates for the construction of reliable setups. However, given that most studies are restricted to fixed thermodynamic forces, little is known about how its construction influences the performance. The present study aimed to fill partially this gap by investigating the thermodynamic quantities of a minimalist collective model placed sequentially with distinct thermal baths at each stage. Distinct aspects have been addressed, such as different worksources, the role of interactions, the period and the time durations of each stroke. Results indicate that our minimal approach, together with a suitable choice of parameters, not only can boost the system performance, providing optimal power outputs and efficiencies greater than its

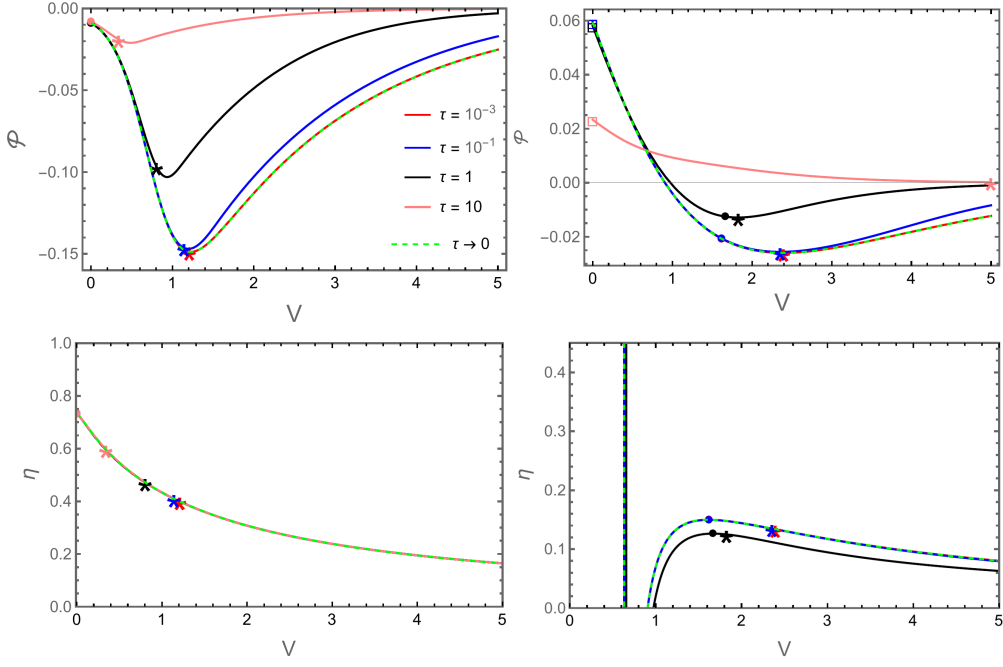


FIG. 7. The influence of period  $\tau$  over the system performance. Depiction of  $\mathcal{P}$  and  $\eta$  versus  $V$  for distinct  $\tau$ 's for  $\beta_1 = 10$  (left) and  $\beta_1 = 20/9$  (right). Parameters:  $\beta_2 = 1, E_a = 1, \epsilon = 0.5, F_2 = 1, F_1 = 0.1$ .

interactionless case, but also guide the operation regime, including distinct heat engine and pump regimes. Although the ideal regime  $\tau \rightarrow 0$  provides higher performances than for finite  $\tau$ 's, the present contribution sheds light on how the interplay between interaction and individual parameters, together a suitable tuning of the interaction time can optimize both power and efficiency as much as possible under more a realistic context (finite  $\tau$ ). Another remarkable finding concerns that the case of the system simultaneously placed in contact with two thermal reservoirs, previously investigated in various works [15, 20, 35], constitutes a particular case of our framework for fast switchings. As future extensions of our paper,

it might be interesting to extend our sequential framework to setups composed of a larger number of nanomachines as well as drawing a comparison among their interactions.

## VI. ACKNOWLEDGMENTS

This study was supported by the Special Research Fund (BOF) of Hasselt University under Grant No. BOF23BL14. We acknowledge the financial support from CAPES and FAPESP under grants 88887.816488/2023-00 and 2021/03372-2, respectively. The financial support from CNPq is also acknowledged.

### Appendix A: Obtaining the exact solution for the boundary conditions

As described in the main text, by resorting to the eigendecomposition of the evolution matrix, together above boundary conditions, we arrive at the following expression for the probability component  $p_i^{(v)}(t)$  at the  $v$ -th stroke:

$$p_i^{(v)}(t) = p_i^{(eq,v)} + \sum_{j=1}^2 e^{\lambda_j^{(v)} [t - (v-1)\frac{\tau}{2}]} \Gamma_j^{(v)} \mathbf{p}^{(v)}((v-1)\frac{\tau}{2}), \quad (\text{A1})$$

where  $\mathbf{p}^{(eq,v)}$  is the stationary state probability associated with  $\lambda_0 = 0$  and  $\lambda_j^{(v)}$  is the  $j$ -th non-zero eigenvalue and  $\Gamma_j^{(v)} = \psi_j^{(v)} \phi_j^{(v)}$  is the matrix associated with the product of the  $j$ -th right and left eigenvectors and  $\mathbf{p}^{(v)}((v-1)\frac{\tau}{2})$  is the vector at each stroke given by

$$\mathbf{p}^{(1)}(0) = \frac{-\left[ e^{\tau\omega^{(1)}/2} + e^{\tau(\lambda_1^{(2)} + \lambda_2^{(2)} + \lambda_1^{(1)} + \lambda_2^{(1)})/2} \right] \mathbf{p}^{(eq,1)} + \sum_{\nu, \mu, \mu'} e^{\tau(\lambda_1^{(2)} + \lambda_2^{(2)} + \lambda_\nu^{(1)})/2} \Delta_{\mu, \mu'}^{(1)} \left[ \Gamma_{\mu'+1}^{(2)} \mathbf{p}^{(eq,1)} + e^{-\tau\lambda_{\mu'+1}^{(2)}/2} \mathbf{p}^{(eq,2)} \right]}{2 \left[ \left( e^{\tau\lambda_1^{(1)}/2} - e^{\tau\lambda_2^{(1)}/2} \right) \left( e^{\tau\lambda_1^{(2)}/2} - e^{\tau\lambda_2^{(2)}/2} \right) \text{Tr} \left\{ \Gamma_2^{(1)} \Gamma_2^{(2)} \right\} - \left( e^{\tau(\lambda_2^{(1)} + \lambda_1^{(2)})/2} - 1 \right) \left( e^{\tau(\lambda_1^{(1)} + \lambda_2^{(2)})/2} - 1 \right) \right]} \quad (\text{A2})$$

$$\mathbf{p}^{(2)}\left(\frac{\tau}{2}\right) = \frac{-\left[e^{\tau\omega^{(1)}/2} + e^{\tau(\lambda_1^{(1)}+\lambda_2^{(1)}+\lambda_1^{(2)}+\lambda_2^{(2)})/2}\right]\mathbf{p}^{(eq,2)} + \sum_{\nu,\mu,\mu'} e^{\tau(\lambda_1^{(1)}+\lambda_2^{(1)}+\lambda_\nu^{(2)})/2}\Delta_{\mu,\mu'}^{(2)}\left[\Gamma_{\mu'+1}^{(1)}\mathbf{p}^{(eq,2)} + e^{-\tau\lambda_{\mu'+1}^{(1)}/2}\mathbf{p}^{(eq,1)}\right]}{2\left[\left(e^{\tau\lambda_1^{(1)}/2} - e^{\tau\lambda_2^{(1)}/2}\right)\left(e^{\tau\lambda_1^{(2)}/2} - e^{\tau\lambda_2^{(2)}/2}\right)\text{Tr}\{\Gamma_2^{(1)}\Gamma_2^{(2)}\} - \left(e^{\tau(\lambda_2^{(1)}+\lambda_1^{(2)})/2} - 1\right)\left(e^{\tau(\lambda_1^{(1)}+\lambda_2^{(2)})/2} - 1\right)\right]} \quad (\text{A3})$$

where

$$\Delta_{\mu,\mu'}^{(\nu)} = \text{Tr}\{\Gamma_\mu^{(\nu+1)}\Gamma_{\mu'}^{(\nu)}\} - \Gamma_\mu^{(\nu+1)}\Gamma_{\mu'}^{(\nu)}$$

### Appendix B: The fast time switchings $\tau \rightarrow 0$ and the two reservoirs case

In the regime of fast switching dynamics,  $\tau \rightarrow 0$ , one gets the following expressions for fluxes

$$\lim_{\tau \rightarrow 0} \bar{J}_{01}^{(1)} = \frac{1}{2Z} \left( \omega_{01}^{(1)}\omega_{10}^{(2)} - \omega_{10}^{(1)}\omega_{01}^{(2)} \right) \left( \omega_{12}^{(1)} + \omega_{12}^{(2)} \right), \quad (\text{B1})$$

and

$$\lim_{\tau \rightarrow 0} \bar{J}_{21}^{(1)} = \frac{1}{2Z} \left( \omega_{21}^{(1)}\omega_{12}^{(2)} - \omega_{12}^{(1)}\omega_{21}^{(2)} \right) \left( \omega_{10}^{(1)} + \omega_{10}^{(2)} \right), \quad (\text{B2})$$

where  $Z = (\omega_{01}^{(1)} + \omega_{01}^{(2)}) (\omega_{12}^{(1)} + \omega_{12}^{(2)}) + (\omega_{10}^{(1)} + \omega_{10}^{(2)}) (\omega_{12}^{(1)} + \omega_{12}^{(2)}) + (\omega_{10}^{(1)} + \omega_{10}^{(2)}) (\omega_{21}^{(1)} + \omega_{21}^{(2)})$ . The above expressions can be understood from the fact the system relaxes ‘‘infinitely fast’’ to its steady state at each stroke, allowing to rewrite Eq.(2) in the following form  $\dot{p}_i^{(v)}(t) = \sum_{j \neq i} \{\omega_{ji}^{(v)} p_j(t) - \omega_{ij}^{(v)} p_i(t)\}$ , where  $p_i(t) = p_i^{(1)}(t) + p_i^{(2)}(t)$ . Thus, the fully dynamics is described by  $\dot{p}_i(t) = \sum_{j \neq i} \{\Omega_{ji} p_j(t) - \Omega_{ij} p_i(t)\}$ , where  $\Omega_{ij} = \omega_{ij}^{(1)} + \omega_{ij}^{(2)}$ , which is equivalent to the simultaneous contact with both thermal reservoirs. A second way of understanding such a limit comes from the time integration of Eq. (2) over each stage by taking into account the boundary conditions from Eq. (3). In such cases, the steady state regime is given by the following relations  $(\omega_{01}^{(1)} + \omega_{01}^{(2)})p_1 - (\omega_{10}^{(1)} + \omega_{10}^{(2)})p_0 = 0$  and  $(\omega_{20}^{(1)} + \omega_{20}^{(2)})p_0 + (\omega_{12}^{(1)} + \omega_{12}^{(2)})p_2 - (\omega_{01}^{(1)} + \omega_{01}^{(2)} + \omega_{21}^{(1)} + \omega_{21}^{(2)})p_1 = 0$ . By solving above system of linear equations, together with the condition  $p_0 + p_1 + p_2 = 1$ , one finds the following expressions for the probabilities:

$$p_0 = \frac{1}{Z} \left( \omega_{01}^{(1)} + \omega_{01}^{(2)} \right) \left( \omega_{12}^{(1)} + \omega_{12}^{(2)} \right),$$

$$p_1 = \frac{1}{Z} \left( \omega_{10}^{(1)} + \omega_{10}^{(2)} \right) \left( \omega_{12}^{(1)} + \omega_{12}^{(2)} \right), \quad (\text{B3})$$

$$p_2 = \frac{1}{Z} \left( \omega_{10}^{(1)} + \omega_{10}^{(2)} \right) \left( \omega_{21}^{(1)} + \omega_{21}^{(2)} \right). \quad (\text{B4})$$

$$(\text{B5})$$

It is worth mentioning that  $p_i$ 's can be alternatively obtained via the spanning tree method for  $N = 2$ . From  $p_i$ 's, fluxes are promptly obtained, providing the same results as Eq. (B1) and (B2). Thermodynamic quantities are straightforwardly evaluated, whose main expressions for  $\mathcal{P}$ ,  $\bar{Q}_2$  and  $\eta$  and have been shown along the main text.

We close this section by pointing out above expressions are general and hold valid in both Secs. III and IV when  $\tau \rightarrow 0$ .

### Appendix C: Global phase diagram for distinct interactions at each stroke

In this section, we depict the system phase diagram (top panel) built from inequalities,  $(\epsilon_2 - \epsilon_1)(\bar{J}_{01}^{(1)} - \bar{J}_{21}^{(1)}) < (V_1 - V_2)(\bar{J}_{01}^{(1)} + \bar{J}_{21}^{(1)})$  and  $\epsilon_2(\bar{J}_{21}^{(1)} - \bar{J}_{01}^{(1)}) > V_2(\bar{J}_{01}^{(1)} + \bar{J}_{21}^{(1)})$ , shown in the main text for the heat engine (HE) regime and the other way around for the pump (P). In particular, the crossover between HE and P regimes will be characterized by ideal efficiency provided  $\epsilon_1/\epsilon_2 = V_1/V_2 = \beta_2/\beta_1$  (green symbols). The bottom panels show, for different sets of temperatures, the phase diagram  $V_1/V_2 \times \epsilon_1/\epsilon_2$ . As discussed in the main text, while larger  $\beta_1/\beta_2$  favors the HE regime, its decrease increases the region in which the system operates as a pump.

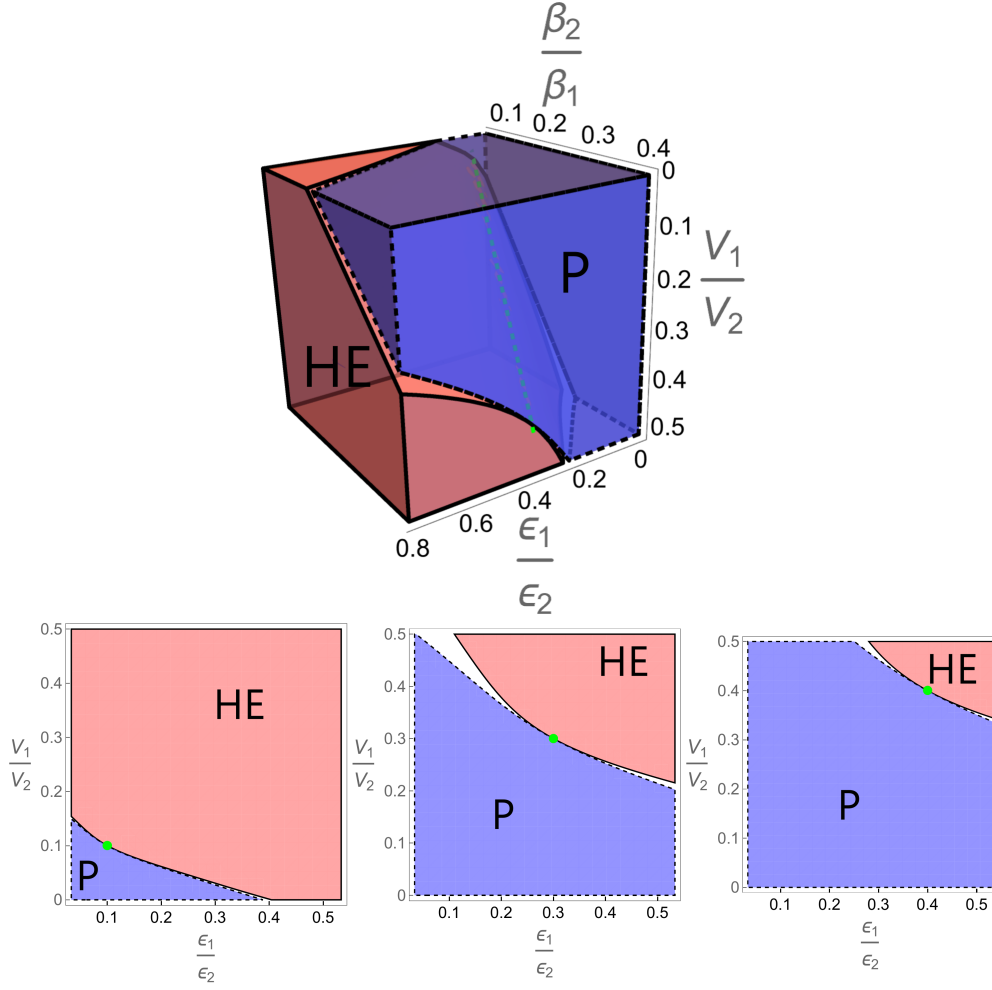


FIG. 9. Top panel: The phase diagram  $\beta_2/\beta_1 \times V_1/V_2 \times \epsilon_1/\epsilon_2$ . The green line represents the points where  $\beta_2/\beta_1 = V_1/V_2 = \epsilon_1/\epsilon_2$ . Bottom panels depict, for  $\beta_1 = 10$  (left),  $\beta_1 = 10/3$  (middle) and  $\beta_1 = 10/4$  (right), the phase diagrams in the  $V_1/V_2 \times \epsilon_1/\epsilon_2$  plane. P and HE denote, respectively, the pump and heat engine regimes. White region attempts to the dud regime, whereas green bullets correspond to the ideal efficiency  $\eta_c$ .

- 
- [1] U. Seifert, *Rep. Prog. Phys.* **75**, 126001 (2012).  
[2] C. Van den Broeck, *Physical Review Letters* **95**, 190602 (2005).  
[3] H. B. Callen, John Wiley & Sons, New York (1960).  
[4] S. V. Moreira, P. Samuelsson, and P. P. Potts, “Stochastic thermodynamics of a quantum dot coupled to a finite-size reservoir,” (2023), [arXiv:2307.06679](https://arxiv.org/abs/2307.06679) [[cond-mat.stat-mech](https://arxiv.org/abs/2307.06679)].  
[5] J. H. Fritz, B. Nguyen, and U. Seifert, *The Journal of Chemical Physics* **152** (2020), 10.1063/5.0006115.  
[6] T. F. F. Santos, F. Tacchino, D. Gerace, M. Campisi, and M. F. Santos, *Physical Review A* **103** (2021), 10.1103/physreva.103.062225.  
[7] D. Zhao, “A stochastic heat engine based on prandtl-tomlinson model,” (2021), [arXiv:2112.12536](https://arxiv.org/abs/2112.12536) [[physics.class-ph](https://arxiv.org/abs/2112.12536)].  
[8] R. Fu, O. M. Miangolarra, A. Taghvaei, Y. Chen, and T. T. Georgiou, “Stochastic thermodynamic engines under time-varying temperature profile,” (2022), [arXiv:2207.05069](https://arxiv.org/abs/2207.05069) [[cond-mat.stat-mech](https://arxiv.org/abs/2207.05069)].  
[9] A. Kumari, M. Samsuzzaman, A. Saha, and S. Lahiri, “Stochastic heat engine using multiple interacting active particles,” (2023), [arXiv:2304.11867](https://arxiv.org/abs/2304.11867) [[cond-mat.stat-mech](https://arxiv.org/abs/2304.11867)].  
[10] H. Ge, M. Qian, and H. Qian, *Physics Reports* **510**, 87 (2012).  
[11] S. Liepelt and R. Lipowsky, *Phys. Rev. Lett.* **98**, 258102 (2007).  
[12] S. Liepelt and R. Lipowsky, *Phys. Rev. E* **79**, 011917 (2009).  
[13] D. M. Busiello and C. Fiore, *Journal of Physics A: Mathematical and Theoretical* **55**, 485004 (2022).  
[14] I. N. Mamede, K. Proesmans, and C. E. Fiore, *arXiv preprint arXiv:2308.02255* (2023).  
[15] H. Vroylandt, M. Esposito, and G. Verley, *EPL (Europhysics Letters)* **120**, 30009 (2017).  
[16] F. S. Filho, G. A. L. Forão, D. M. Busiello, B. Cleuren, and C. E. Fiore, *Phys. Rev. Res.* **5**, 043067 (2023).

- [17] K. Proesmans, C. Driesen, B. Cleuren, and C. Van den Broeck, *Physical review E* **92**, 032105 (2015).
- [18] K. Proesmans, Y. Dreher, M. Gavrilov, J. Bechhoefer, and C. Van den Broeck, *Physical Review X* **6**, 041010 (2016).
- [19] K. Proesmans and C. Van den Broeck, *Chaos: An Interdisciplinary Journal of Nonlinear Science* **27**, 104601 (2017).
- [20] I. N. Mamede, P. E. Harunari, B. A. N. Akasaki, K. Proesmans, and C. E. Fiore, *Phys. Rev. E* **105**, 024106 (2022).
- [21] C. F. Noa, W. G. Oropesa, and C. Fiore, *Physical Review Research* **2**, 043016 (2020).
- [22] C. E. F. Noa, A. L. L. Stable, W. G. C. Oropesa, A. Rosas, and C. E. Fiore, *Phys. Rev. Research* **3**, 043152 (2021).
- [23] I. N. Mamede, A. L. L. Stable, and C. E. Fiore, *Phys. Rev. E* **106**, 064125 (2022).
- [24] A. Rosas, C. Van den Broeck, and K. Lindenberg, *Phys. Rev. E* **96**, 052135 (2017).
- [25] A. Rosas, C. Van den Broeck, and K. Lindenberg, *Phys. Rev. E* **97**, 062103 (2018).
- [26] S. Ray and A. C. Barato, *Phys. Rev. E* **96**, 052120 (2017).
- [27] C. H. Bennett, *International Journal of Theoretical Physics* **21**, 905 (1982).
- [28] T. Sagawa, *Journal of Statistical Mechanics: Theory and Experiment* **2014**, P03025 (2014).
- [29] V. Giovannetti and G. M. Palma, *Phys. Rev. Lett.* **108**, 040401 (2012).
- [30] P. E. Harunari, F. S. Filho, C. E. Fiore, and A. Rosas, *Phys. Rev. Research* **3**, 023194 (2021).
- [31] T. Herpich, J. Thingna, and M. Esposito, *Phys. Rev. X* **8**, 031056 (2018).
- [32] T. Herpich and M. Esposito, *Phys. Rev. E* **99**, 022135 (2019).
- [33] L. P. Bettmann, M. J. Kewming, and J. Goold, *Phys. Rev. E* **107**, 044102 (2023).
- [34] K. Prech, P. Johansson, E. Nyholm, G. T. Landi, C. Verdozzi, P. Samuelsson, and P. P. Potts, *Phys. Rev. Res.* **5**, 023155 (2023).
- [35] H. Vroylandt, K. Proesmans, and T. R. Gingrich, *Journal of Statistical Physics* **178**, 1039 (2020).
- [36] K. Proesmans and C. E. Fiore, *Physical Review E* **100**, 022141 (2019).
- [37] T. Tomé and M. J. de Oliveira, *Physical review E* **91**, 042140 (2015).
- [38] C. Fernandez Noa, C. Fiore, B. Wijns, B. Cleuren, *et al.*, arXiv e-prints, arXiv (2023).
- [39] F. Curzon and B. Ahlborn, *American Journal of Physics* **43**, 22 (1975).
- [40] I. Novikov, *Journal of Nuclear Energy (1954)* **7**, 125 (1958).